Direct Laser Writing of Metal and Metal Oxide Patterns for Flexible and Memristive Electronic Components

by

Joshua Jones

A thesis

presented to the University of Waterloo

in fulfillment of the

thesis requirement for the degree of

Master of Applied Science

in

Mechanical and Mechatronics Engineering

Waterloo, Ontario, Canada, 2023

Author’s Declaration

I hereby declare that I am the sole author of this thesis. This is a true copy of the thesis, including any required final revisions, as accepted by my examiners.

I understand that my thesis may be made electronically available to the public.

Abstract

Growing interest in the fields of flexible electronics and AI are leading the development of new manufacturing techniques able to make computer hardware devices that can suite their unique needs. Research into these areas is stalled by the high cost of manufacturing putting rapid and low-cost manufacturing methods in high demand. Direct Laser Writing, as a novel manufacturing technique, has been shown to be able to produce flexible electronic devices rapidly and with the use of inexpensive raw materials. It works by treating a substrate coated in a metal ion precursor with focused laser irradiation. Where the laser interacts with the precursor organic reduction agents within the precursor are able to reduce the metal ions which then form nanoparticles that are then sintered to form interconnected nanoparticle networks.

In this work direct laser writing is utilized to develop a manufacturing technique of novel flexible electronics for neuromorphic computing hardware. Direct laser writing of copper and copper patterns is used to study the relationship between applied laser energy and electrical properties of deposited patterns. Other metals are also studied. Anodic metals are not able to be fully reduced and are deposited as metal oxides. Cathodic metals are easily reduced and deposited as metals. Metals with intermediate reduction potentials can selectively be deposited as either metals or metal oxides. Deposition of metal alloys with homogenous composition is also demonstrated through the deposition of copper-nickel alloys.

Memristor devices fabricated from Cu/Cu2O/Cu patterns are produced using direct laser writing. Planar patterns are fabricated and shown to have a high sensitivity to changing laser settings used to print the oxide region. Bipolar resistive switching is observed with setting and resetting occurring near +/- 0.7V, and ratios between the high and low resistance states being as high as 102 are achieved. Fabricated devices are shown to flexible and stable over long periods of time.

Memristor based logic structures Including Boolean “And” and “Or” gates are fabricated in planar patterns from memristor pairs. Logic gates show signal processing in times as short as 300ns. Moderate signal degradation from the logic gates are noted at 9% and 21% in the “Or” gate and “And” gate respectively. Memristor crossbar arrays are also fabricated from Cu/Cu2O/Cu and Ag/Cu2O/Cu patterns. Their multiple resistance states are programmed and performances are compared.

In summary Direct laser writing is demonstrated as a process that has promise as a method for producing flexible novel computer hardware. Further work is recommended to focus on identifying combinations of materials and laser settings that can further improve the consistency and performance of the direct laser writing fabricated memristor devices.

Acknowledgements

First and Foremost, I would like to thank my Supervisor Professor Peng Peng. His unwavering support and advice helped guide and lead me for the past several years. I would also like to extend my gratitude towards all the members of my research group, and the many members of CAMJ. Through working alongside a great group of talented and motivated people I have learned so many skills and life lessons. Finally I would like to thank my friends.

Dedication

To my Mother Patti, My Father Alex, and my Step Father David. Your unwavering support has given me the confidence to pursue my dreams. To my partner Danika, for standing by my side for all the highs and lows.

Table of Contents

List of Figures

List of Tables

Chapter 1
Introduction

1.1 Background

The methods used to fabricate electronics largely define the scope and applications of computer based technologies[1]. For the past several decades developments in electronics manufacturing have mostly focused around reducing the size of fundamental computing logic devices, in an attempt to increase computing density, and thusly computing power[2]. As the computing power grows there is interest in expanding the roles of computers in everyday life. As the roles of computers expand into unique and demanding applications the techniques used to fabricate the electronics must also adapt to provide components suitable to the new application[3].

One such growing field is that of flexible electronics[4]. Flexible electronics has been an area of growing interest as it increases the ability for electronic devices to be applied in a variety of physical scenarios such as medicine and wearable devices. These applications necessarily need unique fabrication techniques capable of producing suitable devices.

Another growing field of computer science is that of Artificial intelligence and Machine learning. These applications promise to dramatically expand the roles that computers play in everyday life. However they utilize software techniques that demand exorbitant amounts of energy. A such new devices that are able to reduce the energy consumption of computer logic are desired[5].

Traditionally manufacturing techniques used to fabricate electronics are complex and high cost procedures[6]. This acts as a barrier to development of new novel electronic devices, as designing new devices that deviate from conventional designs incur a high cost. Therefor there is a growing field of research focusing on developing manufacturing techniques of electronics that are inexpensive and simple[7]. In this work we will be exploring a novel technique of direct laser writing, that has been shown to have potential as a low cost and easily accessible method of fabricating flexible electronic devices.

1.1.1 Flexible Electronics

The field of flexible electronics has been proliferating in recent years[4] due to interest in a variety of applications, such as wearable electronics[8], healthcare and medical sciences[9], automotive[10], and aerospace[11]. Currently, in many consumer applications, fabricating flexible electronics relies on

established semiconductor fabrication methods designed to create thin components so they can be integrated into flexible substrates[7]. While these methods see some success, they are limited to components that are not inherently flexible, which limits the usefulness of the devices as they tend to suffer due to bending strains leading to a high rate of malfunction and low reliability[12]. Recently, Oh et al. demonstrated intrinsically flexible semiconductor polymers as candidate materials for flexible electronics; however, the materials are limited by their stability and limited electrical properties[13]. This information highlights the need for manufacturing methods of flexible electronics that produce inherently flexible components with high-performance electrical properties. Current methods for producing flexible electronic components typically rely on expensive raw materials, such as pre-synthesized nanoparticles[14] or nanowires[15]. Additionally, they tend to be complex multi-step processes with low throughput. As such, there is a desire for novel manufacturing processes capable of producing flexible electronics at low cost and with the potential for high production rates.

1.1.2 Analog Computing Hardware

Computers and automation have become ingrained in many daily activities and are critical to the functioning of practically all modernized industrial processes. Recently the advent of new computer technologies that rely on neural networks, such as Artificial intelligence (AI) and Machine Learning (ML), promise to overhaul many aspects of modern life such as commerce[16], manufacturing[17], healthcare[18], and many more[19]–[21]. This proliferation of advanced computing applications has dramatically increased the energy demands of computing globally. By 2030 it is anticipated that twenty percent of the globe's total energy production will be used towards computer and IT applications[22]. In large part this is due to the very energy intense process of training neural networks[23]. This value is only anticipated to grow as neural networks expand in their size and scope to tackle more complex challenges.

The large energy consumption of neural networks is a byproduct of the massive amount of time and data needed to train accurate neural network models with current computer hardware[24]. In simple terms a neural network is a vast array of nodes that are interconnected via connections that have dynamic weights[25]. Inspired by biological neuron arrays in the human brain (hence the name "neural network") the nodes in a neural network represent neurons and the weighted connections between nodes represent synapsis[26]. Neural networks are able to process information inputs from a layer of input nodes called the input layer by propagating the input signal through intermediate nodes in the network

(called hidden layers) across the weighted connections. Eventually the signals reach a final output layer, and the node in the output layer that receives the highest signal is determined as the output field[27]. The key to a successful neural network is finding appropriate weights between all the nodes, such that the network is able to accurately observe trends in the input signals and predict an appropriate output[27]. This is referred to as "training" the network and is accomplished by providing the network with vast amounts of data sets that include sets of input data and their corresponding appropriate output[28]. The act of providing the neural network with training sets and updating the weights as each training case is processed is extremely time and energy costly[29]. In large part this is due to the architecture of modern computers where data storage and data processing occur in different hardware components of the computer[29]. This means that for each training instance of a neural network the entire array of values that represent the weights of the connections in the network must be shuttled back and forth between data storage and processing to be updated. This segregation in data storage and processing in modern computers is referred to as the "Von Neumann Bottleneck", or "Memory Wall"[30].

One promising solution to the growing energy demands of advanced computing is the field of neuromorphic computing[5]. Neuromorphic ("brain inspired") computing provides frameworks for novel computer architecture that integrates data storage and logic processing into a single component able to simultaneously store data, as well as perform logic operations[31]. By doing so neuromorphic computer hardware eliminates the largest energy consuming bottleneck in conventional computers, the Von Neumann bottleneck[32]. Neuromorphic hardware has been shown to dramatically reduce the energy consumption of neural networks in many applications, in some cases by over 99%[33].

Neuromorphic hardware accomplishes integrated data storage and processing by employing arrays of circuit elements that are able to exhibit a range of resistance states, which can be used to represent the values of elements in a matrix[34]. The elements in the matrix can then directly be read as data storage or used in simple math calculations[35]. In this way neuromorphic hardware is able to directly represent the weighted connections of a neural network and eliminate the need for data shuttling during the training process[35].

One of the most promising circuit elements used as fundamental elements in neuromorphic hardware is known as memristors[36]. Memristors are a fundamental passive circuit element, alongside resistors, capacitors, and inductors[37]. First theorized in 1971 by L. Chua[37] and fabricated for the first time

in 2008 at HP labs by Strukov et al[38], the memristor relates charge and flux. The key signature of a memristor is their pinched hysteresis loop response to periodic voltage and current signals[38]. This enables memristors to retain a resistance state determined by the most recent charge flow they experienced[37]. Memristors have been demonstrated to be able to process Boolean logic through simple logic circuits[39], as well as be able to be employed in large arrays for neuromorphic hardware[33]. Currently most of the methods for producing memristor based logic circuits are costly, low throughput, and impose severe size constraints [24]. This highlights the growing need for economic and scalable technologies capable of producing memristor based logic architecture.

1.2 Research Objectives and Thesis Organization

1.2.1 Research Objective

In broad terms the objective of this research is to develop the novel technology of direct laser writing as a viable method of producing inexpensive electronic components able to suit the growing needs of the fields of flexible electronics, and next generation computer hardware. This is accomplished through characterizing the properties of various metal and metal oxide materials deposited using direct laser writing in order to develop a more robust understanding of the process. As well, direct laser writing was used to produce several prototype flexible electronic components in order to demonstrate viable strategies that take advantage of the direct laser writing process to produce components suitable for computer hardware.

1.2.2 Thesis Organization

This Thesis is organized into six chapters.

Chapter 1: Introduction

The introduction provides a background on the motivation for the research, an overview of the thesis objectives and structure, as well as a literature review on topics relevant to the research. The Literature review covers the topics of (1) the current state of manufacturing processes for electronics, (2) an understanding of the functioning of memristors, and (3) various logic structures that use memristors to great effect in computing applications.

Chapter 2: Background review on Electronics Fabrication techniques and novel computer hardware applications

Chapter 2 provides a literature review on the current state of the art on several key topics. Firstly the current strategies used to fabricate flexible electronics are described. Subsequently Direct Laser Writing is introduced and explored as a novel method of producing inexpensive flexible electronics. Thirdly memristors are explored as a novel device that provide several unique strategies for novel computer hardware.

Chapter 3: Direct Laser Writing Process

Chapter 3 describes the key research findings of studies done using direct laser writing to deposit a variety of metal and metal oxide patterns. Materials and methods used in the direct laser writing process are outlined. Patterns deposited from copper, silver, nickel and iron are characterized using their electrical properties as well as chemical characterization techniques of XRD, XPS, RAMAN, and SEM.

Chapter 4: Fabrication of Copper Oxide based Memristors using Direct Laser Writing

Chapter 4 presents several strategies that employ direct laser writing to produce memristor components. The effects of changing laser settings on the non-linear current voltage response of the memristor components is studied using electrical characterization of fabricated components.

Chapter 5: Fabrication of Memristor Based Logic Structures using Direct Laser Writing

Chapter 5 presents several prototype devices capable of employing memristors into viable logic processing hardware. Flexible memristor based Boolean logic patterns are fabricated and characterized. Neuromorphic hardware produced from cross bar arrays of memristors is fabricated and characterized.

Chapter 6: Conclusions and Future Works

Chapter 6 summarizes the key findings from this thesis and outlines several avenues of future research directions in the field of direct laser writing fabrication.

Chapter 2
Literature Review

2.1 Manufacturing Processes of Flexible Electronics

2.1.1 Conventional Manufacturing Processes of Flexible Electronics

In principle any device or material can exhibit some degree of flexibility if it is thin enough, as the bending strain experienced is proportional to the dimensions of the device under bending[40]. This concept has been used to moderate success in adapting conventional silicon based manufacturing processes for making pseudo flexible electronic components [41]. In fact many devices that purport to exhibit macroscopic flexibility are in actually ultra-thin components with only minimal to moderate amounts of flexibility[7]. Many of the first-generation flexible electronics used this principle of thin film pseudo flexibility to great effect, [10]. However as these devices were not inherently flexible the accumulated bending strains would lead to detrimental device outcomes [11], and as such further methods of producing flexible electronics were desired.

In general terms there are three main approaches to fabricating flexible electronic devices [7]. The first approach relies on distributing conventional, non-flexible, components onto flexible substrates, and then connecting the components using electrically conductive and mechanically flexible connectors [42]. The second approach uses the development of electrically conductive organic materials that are inherently flexible as functional materials in electronic devices[9], [13], [43]. The third approach uses ultra thin films that are not necessarily flexible, but can be deposited onto flexible substrates to exhibit macroscopic flexibility[44]. Figure 2.1, adapted from Rogers et al.,[42] shows graphical representation of each of the approaches.

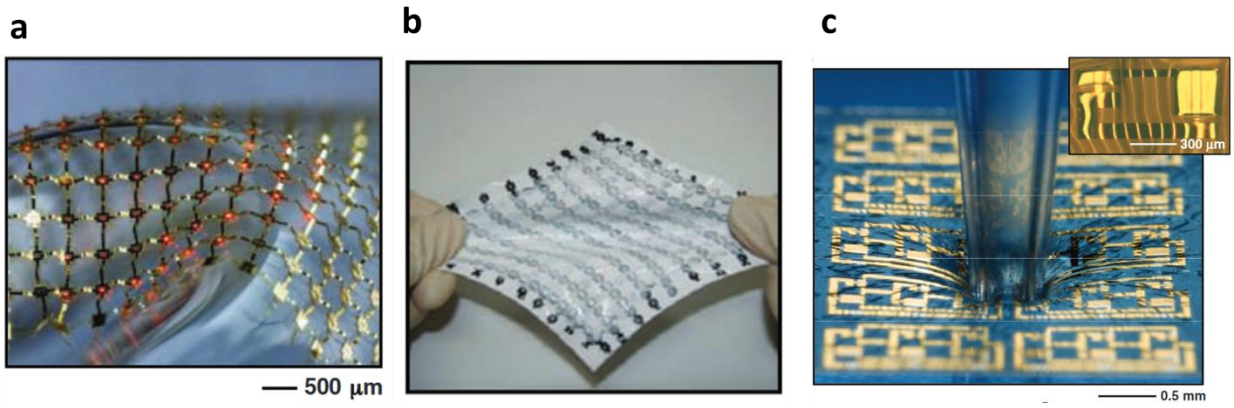

Figure 2-1 A) An array of LED devices linked by flexible connectors on a stretchable substrate. B) Flexible and stretchable electric circuit pattern. C) Thin silicon circuit printed onto flexible substrate, flexed in the center by a glass pipette tip. Adapted from Rogers et al [38].

The approach of linking conventional non-flexible components with flexible connectors has shown promise as outlined in the work done by Bao et al[45]. It was shown that through using this approach the high performance properties of the conventional components could be retained, thus leading to flexible devices with the potential to rival non-flexible devices in performance[46]. However, the applicability of this approach is limited by its high fabrication cost and low throughput. As well the need to space out the components and link them necessarily leads to devices that will be significantly larger than their non flexible counterparts [45], as there is an ever increasing pressure to reduce the size of electronics this is a major inhibiting feature of this approach.

The approach of using electrically conductive and intrinsically flexible organic materials has been successfully demonstrated by many groups[47]–[49]. Many of the conductive organic materials have been demonstrated to bear strains in excess of 100% , allowing for devices that are not only flexible but stretchable as well [48], [49]. One major limitation to this approach is that in most cases the flexible organic materials have poorer electrical properties when compared to conventional materials [13]. This can lead to devices with poorer performance in terms of device stability or high power consumption[13].

The approach of ultra-thin films deposited onto flexible substrates has been shown as possibly the most versatile of above mentioned strategies of producing flexible electronics[7]. Particularly the advent of thin film transistors has enabled the development of many different flexible electronic devices, such as displays [50], communication chips [51], and smart textiles [52]. In many cases the ultra thin film transistors are based on amorphous oxide semiconductors such as amorphous silicon[53], amorphous Zinc Tin Oxide [54], and several others [55]. However due to the limitations of amorphous materials the semiconductors tend to exhibit much lower charge carrier mobilities when compared to crystalline semiconductors, such as silicon [7]. This leads to these flexible devices typically showing poorer performance than conventional counterparts, such as device stability, or lower device ON/OFF ratios [7]. Alternative materials to amorphous metal oxide semiconductors for thin film transistors do exist, such as Single Wall Carbon Nanotubes (SWCNTS). However, these materials tend to suffer from costly and prohibitive manufacturing processes, which can result in poor device uniformity [56].

2.1.2 Laser Writing of Flexible Electronics

Direct Laser Writing is a general term for a group of techniques that has been used to refer to a wide variety of processes [57]–[60]. For this thesis the term direct laser writing will be used to describe a set of processes wherein a beam of focused laser irradiation is used to ablate, modify, or deposit material onto a working surface, without the use of a mask or lithography process. The interaction of the focused laser beam with the working substrate will determine whether the laser direct writing process is depositing, modifying or removing material from the working substrate[61]. Since laser processes where a laser is used to selectively remove material is typically referred to laser micromachining and is an established research field in its own right it is outside the scope of this work. The key benefit to direct laser writing processes is the aforementioned lack of necessary masking or lithography. This allows direct laser writing techniques to provide low cost and more rapid fabrication processes for flexible electronics.

Direct Laser writing as a process has been attracting increasing amounts of interest for the fabrication of electronic components recently . While much progress has been made in order to explore and develop direct laser writing , there are still many challenges that need to be addressed for direct laser writing to see widespread adoption. This represents a significant opportunity for research to advance the field of laser direct writing. Figure 2.2 shows the number of research publications per year that include the keywords direct laser writing (or some variation thereof such as laser direct writing) and electronics.

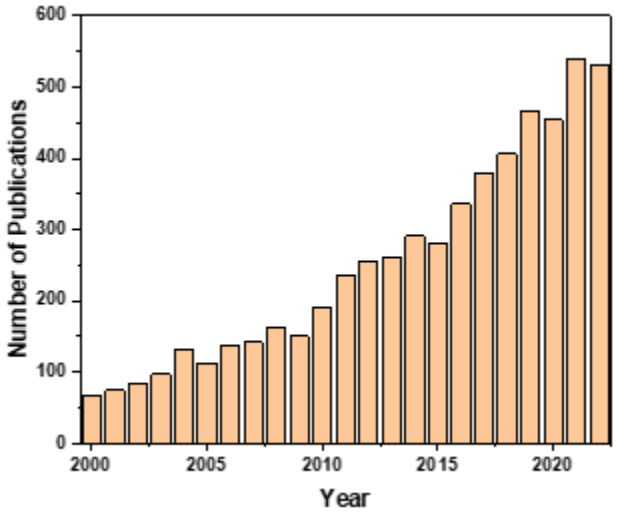

Figure 2-2 Research publications published per year that include the keywords "Direct Laser Writing" and "electronics" on Web of Science

A common strategy for using direct laser writing to deposit flexible conducting patterns is laser irradiation of precursors containing metal nanoparticles [15]. The laser irradiation is able to join the nanoparticles, through sintering, into continuous conductive networks. The main benefit to this technique is that the laser irradiation is able to achieve sintering action at temperatures low enough to still be suitable for use with flexible substrates [57].

The low temperature sintering is achieved through the use of plasmon resonance[62]. Plasmon resonance refers to the interaction of an electromagnetic wave with the electron conduction band of a metal nanoparticles. Electromagnetic waves, such as the irradiation from focused laser beams, is capable of stimulating oscillations in the electrons of metal nanoparticles, that create small temporary regions of delocalized electron fields near the surface of the nano particles called surface plasmons[63]. When a region with a high concentration of nanoparticles is irradiated the surface plasmon fields of neighbouring nanoparticles can overlap. In these overlapping regions high heat is generated due to the interfering plasmon fields[64]. These localized heating regions between nanoparticles provide the heating effect necessary to melt small regions of the nanoparticles and provide the sintering action necessary to form the nanoparticles into a continous network. Figure 2.3 adapted from Liao et al[62]. demonstrates the surface plasmon effect and how nearby particles can have overlapping fields. Since

the regions of plasmon interaction are very small the macroscopic temperature of the process remains fairly low, which is what allows the process to be used in high temperature sensitive applications. One main issue with this approach is that many techniques rely on pre-synthesized nano particles [15]. This leads to these techniques suffering from needing high cost raw materials and showing poor scalability due to the difficulty of acquiring large amounts of nanoparticles[58].

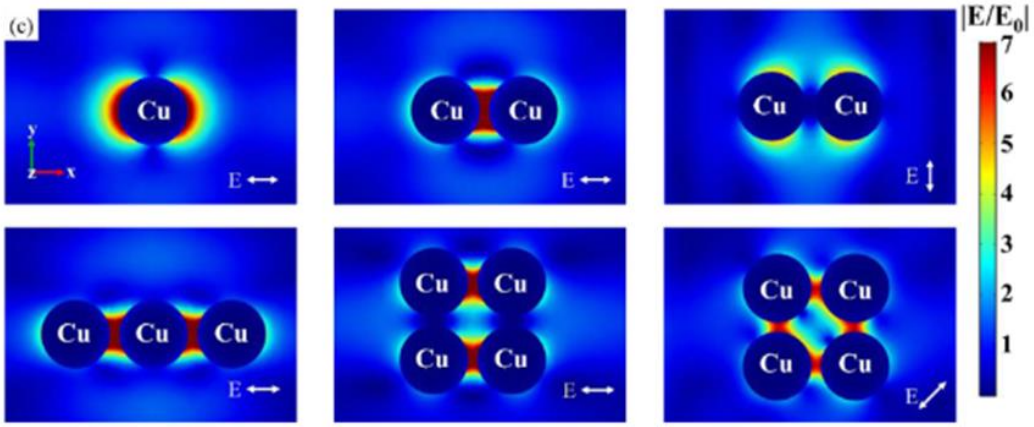

Figure 2-3 Overlapping electron fields from nearby nanoparticles receiving electromagnetic stimulation. Adapted from Liao et al [62]

In order to avoid the use of expensive precursors another technique of direct laser writing of precursors containing metal salts and reduction agents has been shown to be viable, most notably copper salts[65]. In this approach metal salts provide metal ions that can be reduced by the interaction of the laser irradiation with the organic agents within the precursor. Typically polyvinylpyrrolidone (PVP) is selected as the primary organic reduction agent [66]. PVP is used as it's degradation process is well understood [67]. The lactam side chain on PVP can be disrupted through laser irradiation, resulting in the formation of formic acid which can then interact with and reduce metal ions in solution[65]. Often, other organic molecules may be included to help facilitate the reduction of metal ions through the degradation of PVP [68]. Polyethylene glycol (PEG) is a common choice to include along side PVP, as it has been shown that the OH end groups of the PEG molecules are able to reduce the energy needed to disrupt the lactam ring of PVP [69], thus reducing incumbent energy needed to degrade the PVP. Figure 2.4 shows the PEG assisted photodegradation of PVP, along with the reduction mechanism of metal ions through formic acid. Oher chemicals such as polymethacrylic acid sodium salt (PMAA-NA)

[62], or sodium citrate ($Na_3C_6H_5O_7$) [70] have also been shown to be beneficial to the PVP degradation reaction.

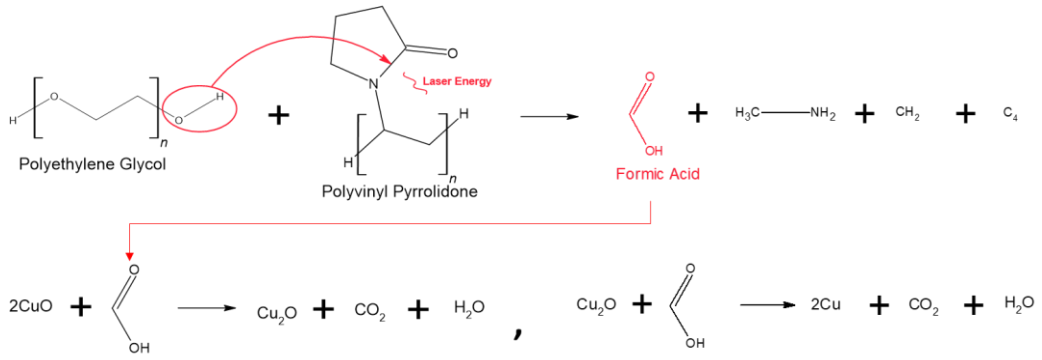

Figure 2-4 PEG Assisted Photo degradation of PVP leading to generation of formic acid. Subsequent reduction of copper ions through interacting with formic acid.

Once the metal ions in solution have been reduced they form nanoparticles, which can be subsequently sintered using the surface plasmon effect [71]. This allows metal salt solutions to produce metal nanoparticle networks with comparable properties to solutions that rely on nanoparticle precursors [72]. In addition the use of metal salts has been shown to exhibit a high degree of chemical control over the deposited materials in copper patterns [73]. This is done by controlling the amount of formic acid available to reduce the metal ions in solution during laser irradiation. Reducing formic acid content means that less of metal ions in solution are able to be reduced to the metallic copper state, and as such will be incompletely reduced and deposited as metal oxide nanoparticles [65]. The metal oxide nanoparticles can also be sintered to form continuous networks through conventional photothermal heating effects of laser irradiation. However, since oxides do not exhibit a surface plasmon effect due to the fact that they do not have a continuous conduction band like metals. This tends to lead to nanoparticle networks that have more sharp flat features, compared to round interconnected metal nanoparticle networks. Figure 2.5 adapted from Liao et al[62], demonstrates the difference in morphologies of metal nanoparticle networks, and metal oxide nanoparticle networks.

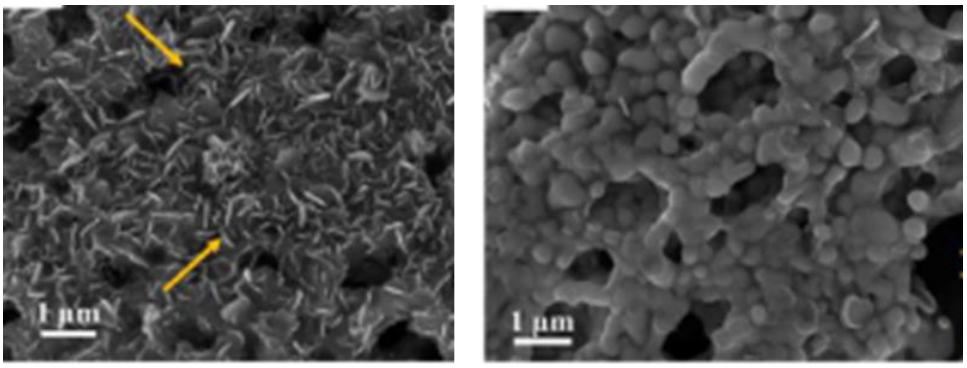

Figure 2-5 A) Copper oxide nanoparticle network formed from DLW B) Copper nanoparticle network formed from DLW Adapted from Liao et al [62]

There are two main strategies for controlling the chemical properties of copper patterns through PVP degradation. The first is by varying the amount of PVP included in the precursors solution [66]. This strategy is fairly straightforward, by applying an abundance of PVP in the precursors there is a guarantee that enough formic acid will be generated to fully reduce all the metal ions present, leading to highly metallic patterns [65]. And vice versa, by providing only a small portion of PVP not enough formic acid could be generated to reduce all the metal ions present, leading to oxide patterns [73]. The second strategy relies on varying the laser settings in order to selectively degrade the PVP present in the precursor. Since the degradation of the PVP is laser initiated, providing a high amount of laser incumbent energy encourages complete degradation of all the PVP present in the precursor, and thus an abundance of formic acid. By reducing the amount of laser energy applied to the sample decreasing amounts of PVP get degraded, thereby limited the generation of formic acid [72].

Direct Laser writing of copper and copper oxide patterns from metal salt precursors has been shown in previous works to be a viable method of rapidly producing flexible electronic components such as electrodes [70], capacitors[62], a range of sensing elements [72], [73], memory devices[74] and many more. Figure 2.6 adapted from various works, details the direct laser writing process that have been used to produce flexible sensors, capacitors, memory devices and electrodes. By utilizing the control over chemical properties functional devices can be made in simple, rapid, and inexpensive processes. As such there is growing interest in expanding the capabilities of direct laser writing. Several key areas have been identified as potential research avenues in the field of direct laser writing.

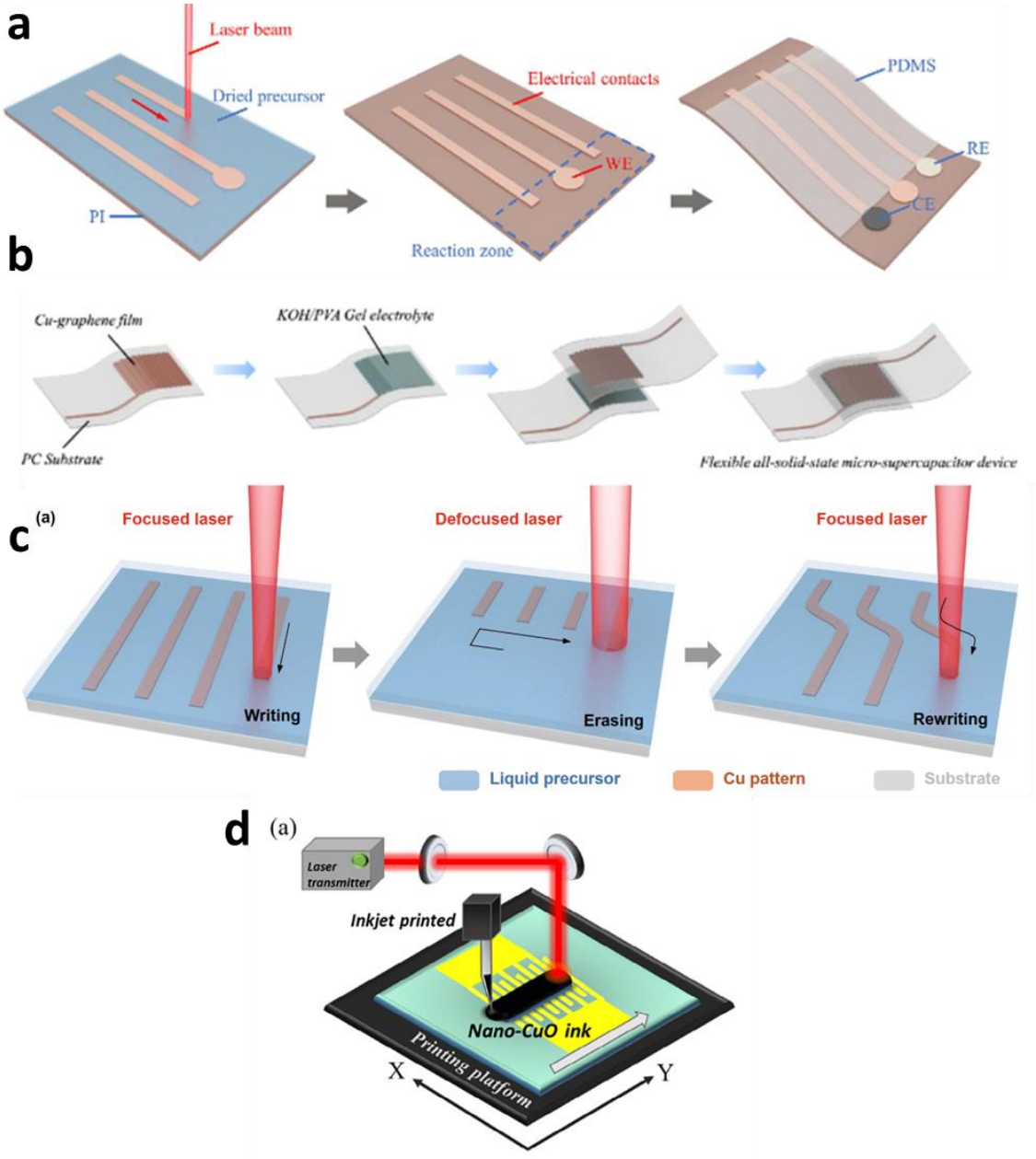

Figure 2-6 A) DLW process used to fabricate a flexible glucose sensor adapted from Zhou et al [73]. B) DLW process used to fabricate large area flexible capactiro Adapted from Liao et al[62], C) DLW process used to write and erase flexible electric circuits adapted from Zhou et al [69]. D) DLW process used to fabricate CuO based memory device adapted from Liu et al [74]

Firstly most of the works that have demonstrated successful use of direct laser writing of copper patterns utilized lasers in the ultra violet wavelength [75], [75], [76], demonstrating successful application of the direct laser writing process at near infrared wavelengths would improve the versatility and accessibility of the process.

Secondly, most of the work done using direct laser writing of metal salts focuses on copper and copper oxide patterns [65]. Being able to determine whether the key principles identified in direct laser writing can be applied to other metal systems would be very beneficial in expanding the scope of direct laser writing.

Thirdly direct laser writing has been shown to be adapt at producing planar components [61], [73], [77]. However, there is yet to be a strong demonstration of being able to produce 3D hierarchical components using direct laser writing. By developing techniques that can be used to implement 3D patterns with direct laser writing the versatility and scope of the process can be greatly expanded.

2.2 Memristors

2.2.1 Theoretical background of memristors

Memristors are the most recently discovered group of passive circuit components. The existence of the memristor was first proposed by Leon Chua in 1971. It was proposed that based on the relationships between the known passive circuit elements at the time (i.e. resistors, capacitors, and inductors) that a fourth element should exist, that relates electrical charge and flux[37]. This was shown to be necessary in order to have a complete description of the relationships between the four fundamental circuit variables of current, voltage, charge and flux[78]. Figure 2.7a adapted from Strukov et al, demonstrates the relations between the four fundamental circuit variables with the inclusion of the memristor. The memristor was postulated to have a non-linear resistance with a memory effect (hence the name memristor, as a portmanteau of memory resistor). The functional relation between charge and flux was represented as $d\phi = Mdq$ where M was the unit of memristance. It can be seen that if M was a constant then the relationship can be simplified to that of a resistor[37]. Therefor for the memristor to be of any significance the unit of M must also be a function of charge[37].

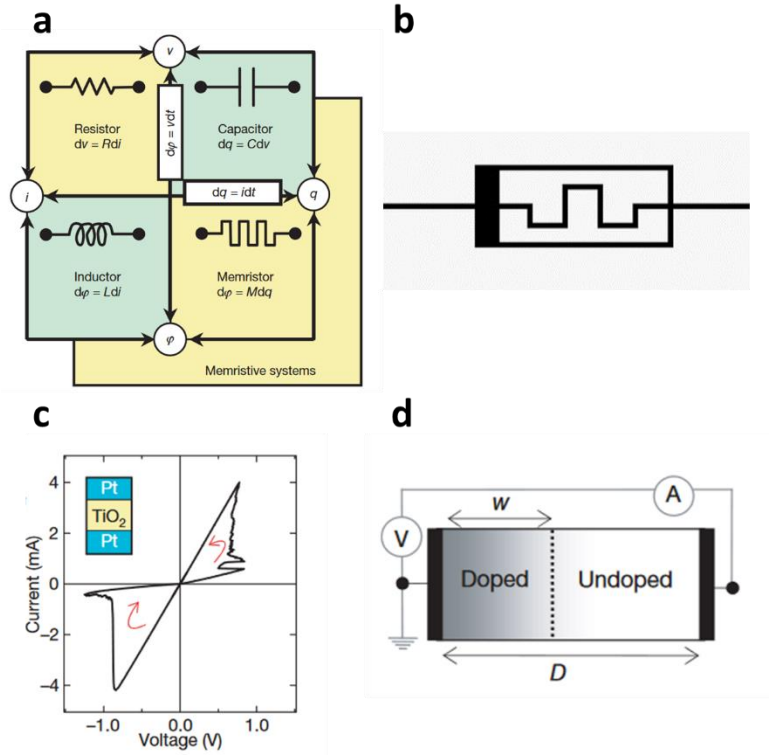

Figure 2-7 A) The four fundamental circuit values of voltage, charge, flux and current, along with the relationships between them B) The circuit element icon of a memristor C) the Pinched hysteresis loop in the I-V plane of the Pt/TiO/Pt device. D) The analytical representation of how the movement of oxygen vacancies within the TiO layer would affect the device resistance. Adapted from Strukov et al[38]

The first memristor device was fabricated by Strukov et al in 2008 who fabricated a cross point switch from a layer of titanium oxide sandwiched between 2 platinum electrodes[38]. In this the first physical model for how a memristor would physically link memristance and charge was presented. It was proposed that the resistance state of the memristor was controlled by an internal state variable that had a dependence on current. In the case of the Pt/TiO/Pt switch the state variable was a representation of the concentration of ionic dopants within the TiO layer. The regions within the TiO layer that contain dopants would have a significantly lower resistance than the undoped region. The application of an

electrical bias would cause the ionic dopants to drift and extend the highly conductive region thus lowering the overall device resistance, which could then be reversed by applying an electrical bias in the opposite polarity. This was also the first instance of the pinched hysteresis response in the current voltage plane which has since become a signature of memristor components[79]. In figure 2.7 the current voltage response of the device fabricated by Strukov et al is shown. It can be seen that at a positive bias of approximately 0.9 V the current jumps dramatically, this indicates that the resistance of the device has dropped. This is referred to the setting voltage of the device, as it indicates the applied electrical bias required to reduce the overall device resistance, and set it to a low resistance state (LRS). It relates the to electrical bias required to motivate the movement of the ionic dopants within the TiO layer. As well the device shows an increase in resistance at around -0.9 V, this is referred to as the resetting voltage as it indicates the voltage required to return the device to it's initial high resistance state (HRS).

Since then, memristor components have been fabricated from a variety of metal oxide systems, including silver oxide [80], copper oxide[76], [81], hafnium oxide [82], [83], and many others[84], [85]. Typically most systems follow the outline provided by Strukov et al in sandwiching an insulating metal oxide layer between two metal electrodes[5], this has come to be referred to metal/insulator/metal or M/I/M structured memristors [24]. As well other methods of producing non metal oxide materials that exhibit memristance have been demonstrated [86].

As the field of memristors has expanded components with different memristive responses have been developed. In broad terms memristors can be categorized into two groups, unipolar and bipolar memristors[87]. In bipolar memristors the electrical bias required to set and reset the device are opposite polarity, whereas in unipolar memristors the setting and resetting voltages are in the same polarity, and are only separated by the amount of the applied bias [88].

Several different memristor categories that exhibit resistive switching effects that are distinct from the metal oxide resistive switching have also been developed. Such as polymeric memristor systems that use ion based movement in organic materials to exhibit memristive behaviour[89] Or memristance in ferromagnetic systems[86]. In short there has been a rapid expansion in the development of memristor systems. The scope of this thesis will only primarily concern itself with resistive switching in metal oxides.

2.2.2 Resistive Switching in Metal Oxides

Due to the relatively new nature of memristor devices in many ways they are not as thoroughly understood as other key electrical components, as such design modelling and study of memristors is an ongoing field of research[84], [90]–[92]. The initial model proposed by Strukov to explain the physical phenomena behind the resistive switching effect observed in the TiO layer has been largely improved upon[93], [94]. The physical ion drift model is no longer broadly considered as the most accurate model of physical memristor phenomena, nevertheless it remains relevant as it is the foundation for many of the robust analytical models used to predict memristor behaviour[95].

Two primary models exist to describe the resistive switching in metal oxides[96]. The first model is that of the conductive filament (sometimes also referred to as conductive bridge) formation[97]. This model is considered the more applicable model [24] and has physical evidence for its existence in a wide range of metal oxide systems[98], [99]. The conductive filament formation occurs when localized ion drift forms a narrow region of highly concentration active ions under an external electrical bias[100]. The device starts in a high resistance state, and is switched to a low resistance state when the filament connects both electrodes. Upon applying an opposite electrical bias the filament ruptures and the device is returned to its initial high resistance state [101]. Depending on the nature of the active ions participating in the formation of the conductive filament conductive filament devices can be further sub divided into two categories. The first category is classified as when the active ions are cations, typically metal ions [80]. The second category uses the migration of anions, which in most cases is oxygen vacancies, or O^{-2} defects [102]. In anion based devices the conductive filament is typically a region of highly concentrated oxygen defects, whereas in cation devices the conductive filament is typically a metal filament[103]. Figure 2.8 adapted from Valov et al shows a schematic diagram of the formation of a conductive metal filament along with the corresponding changes in device resistance.

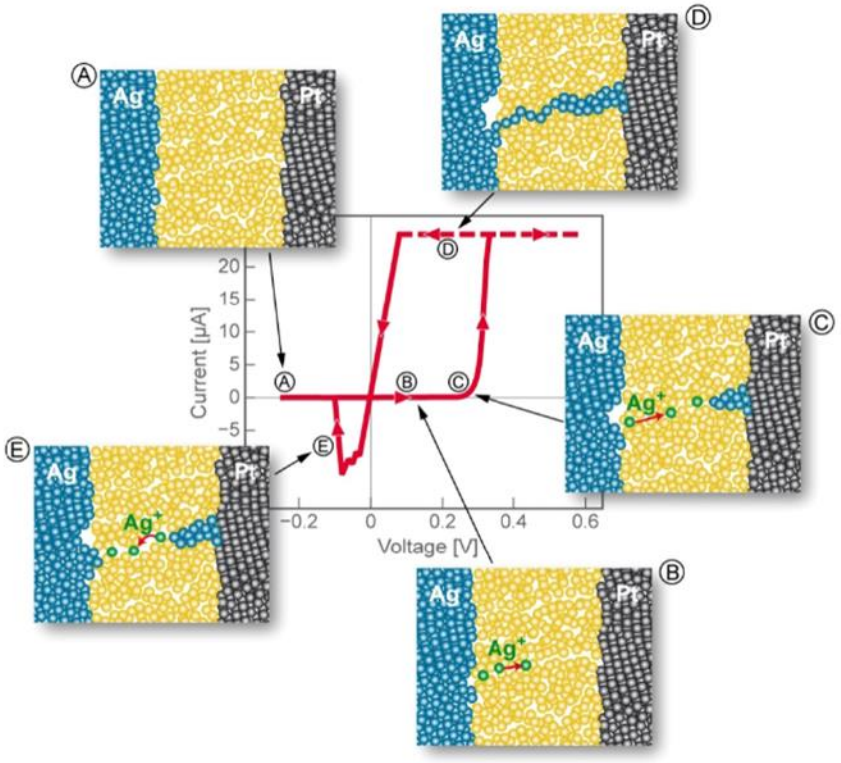

Figure 2-8 The various stages of conductive filament formation and rupture, along with their implications on overall device resistance adapted from Strukov et al [24]

In anion based devices electrically motivated ion drift is the primary process that occurs to form the conductive filament [24]. In cation based devices two processes occur, ion drift as well as redox of metal ion at the electrode [87]. This leads to the process being dependent on the redox reactions at both electrodes. In copper based systems this means the copper redox reactions of $Cu^{+} + e^{-} \leftrightarrow Cu$, or $Cu^{2+} +2e^{-} \leftrightarrow Cu$. These reactions are impacted by both the kinetics of charge transfer through the active layer, as well as the diffusion of the metal ions [104]. As such there is ongoing work studying the behaviour of ion migration in metal oxides, under thermal and electrical driven conditions[100].

Devices that use conductive filament formation as a means to achieve memristor behaviour typically require an initial electroforming step [105]. This refers to the initial application of an external electrical bias to promote the forming of the bulk of the conductive filament. Once the electroforming has been applied subsequent electrical biases work to affect the already predominantly established conducting filament[104]. This enables many of these devices to have ultra fast setting and resetting behaviour[92].

One major downside to conductive filament based devices is that the formation of the conductive filament is stochastic in nature[87]. As a result many devices become defective during the electroforming step. The most common type of defect is referred to as “hard setting” [83]. In hard setting the device is permanently set to the low resistance state through the formation of multiple conductive filaments[83].

The second model is described as the interface switching model. In this model the resistive switching phenomenon is attributed to the uniform migration of oxygen vacancies between two distinct metal oxide layers[81]. The work done by Zou et al., demonstrated fabrication of Cu/CuO/AgO/Cu cross point stacks that used the boundary transition between the CuO and AgO phases to exhibit bipolar resistive switching [106]. In the device migration of oxygen vacancies motivated by external electrical bias would change the relative fraction of the CuO and AgO phases. Due to the difference in resistivity between the AgO and CuO phases as the fraction of the CuO phase would decrease the overall device resistance would drop. Under an opposite electrical field oxygen the fraction of the CuO phase would increase and set the device to a high resistance state. Figure 2.9 is adapted from Zou et al and demonstrates the oxygen vacancy drift mechanism along with the pinched hysteresis response of the fabricated devices. The benefit to devices fabricated using the boundary transition mechanism is that they do not require an electroforming step. It has been shown that the electroforming step is one of the largest sources of defects in devices that operate using the conducting filament formation [107], which can lead to devices with poor consistency and device stability.

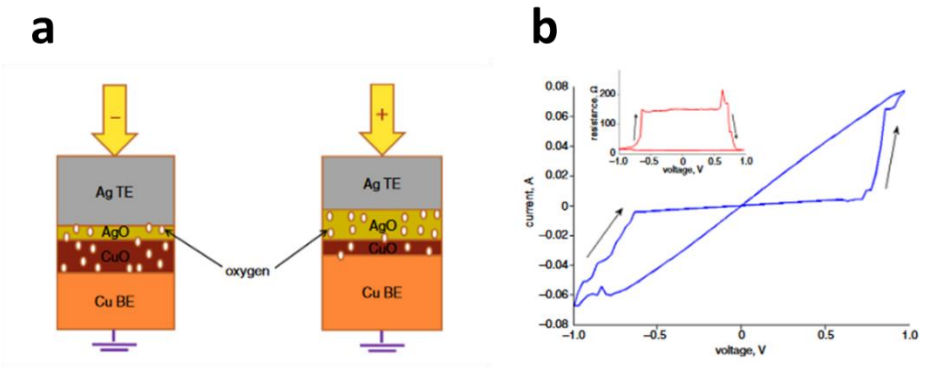

Figure 2-9 A) Schematic diagram of the interface boundary between the copper oxide and silver oxide layers, and how applied voltage bias can change the relative fraction of each layer B) The pinched Hysteresis loop of the fabricated Ag/AgO/CuO/Cu device. Adapted from Zou et al[106]

In both cases of the filament formation and interface switching the memristors are able to demonstrate intermediate resistance states between the high and low resistance states [34]. In the conductive filament formation based devices the intermediate states are defined as partial formation of the conductive filament [24]. In the interface switching based devices the intermediate states are defined as different proportions of the distinct oxides in the active layer[106].

In conductive filament based devices the conductive filament is thermodynamically unstable [92]. The high concentration of oxygen defects that form the conductive filament in anion based devices is energetically unfavorable [80], which leads to degradation of the conductive filament over time. As well in cation based devices the metal filament shows a higher chemical potential of the metal atoms within the filament than external leading to a thermodynamic drive to dissolve the filament [80]. This leads to many memristor devices showing some degree of instability in the low or intermediate resistance states [80].

2.3 Memristor Based Logic Structures

2.3.1 Boolean Logic Gates

Boolean logic is a branch of formal logic where all variables are considered only to be either true or false, which are often denoted by values of 1 and 0 respectively[108]. Boolean logic provides the foundation for modern computer operation as transistors are able to exhibit two separate resistance states, either high or low, which can be used to represent the Boolean values of 1 and 0[108]. Three simple Boolean operations make up the entirety of Boolean logic that enables modern computer logic, “Or”, “And”, and “Not” [108]. “And” and “Or” operations take in two values and return one value, and “Not” takes in one value and returns the opposite value[109]. The truth tables for the logic operations are outlined in Table 2.1.

Table 2-1 Truth Tables for Boolean "And" "Or" and "Not" functions

AND			OR			NOT	
Input 1	Input 2	Output	Input 1	Input 2	Output	Input 1	Output
0	0	0	0	0	0	0	1
0	1	0	0	1	1	1	0
1	0	0	1	0	1		
1	1	1	1	1	1		

Transistor based circuits have been designed that are able to effectively exhibit these Boolean logic operations[109]. Due to how fundamental these Boolean Logic operations are, they are typically referred to as "Logic Gates". All complex computer logic operation is a product of hundreds of thousands of interwoven logic gates processing Boolean Logic signals[110]. As such there is an ever-ongoing effort to reduce computing time and increase the logic density of computer chips through the improvement and simplification of Boolean Logic Gates[111]. The use of Memristors as Boolean Logic units has begun to attract attention as memristors are two-terminal devices, as compared to transistors which have three terminals (collector, emitter, and gate). Boolean "And" and "Or" gate circuits have been designed that utilize the resistive switching behaviour of memristors to simplify the circuitry used to process formal computer logic[112]. Schematic diagrams of Memristor based "And" and "Or" gates are outlined in Figure 2.10. It is key to note that there is no current method of producing a "Not" gate using memristors[39]. As a result any computer logic that does use memristor based logic circuits will also need to use conventional transistor technology. As such, methods of fabricating memristors suitable for use in logic gates should be compatible with conventional methods of fabricating computer hardware[112]. Practically this means that the fabrication method should be low temperature to avoid damaging silicon substrates used in conventional CMOS chips and avoid the use of chemicals that are corrosive or otherwise damaging to silicon substrates[112].

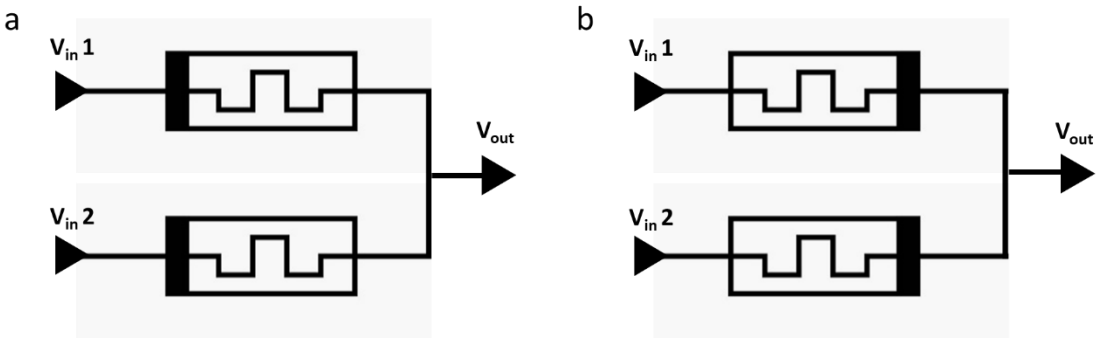

Figure 2-10 A) Memristor "And" Gate B) Memristor "Or" Gate

It can be seen that the memristor based "And" and "Or" gates are nearly identical in design, both using a pair of memristors that in essence act as a voltage divider circuit. The only difference between the two gates is that the memristors in the "And" gate are implemented in an opposite polarity to the memristors in the "Or" gate. In the circuit diagram icon of a memristor, the black bar on one end of the device is used to indicate polarity. Current passing from the black end to white end is the polarity that will set the device, and current passing from the white end to the black end will reset the device. Since memristors will exhibit a low resistance state if a current is passed in the same polarity as the setting voltage, and a high resistance state if a current is passed in the opposite polarity as the setting voltage, in limited cases a memristor can behave as a diode. In the role of Boolean Logic memristors are effectively treated as a switch that is set to either high or low resistance depending on the orientation of the current passing through it[39]. By treating the logic gates as voltage divider circuits simple relations can be used to find the output signal of the circuit given any set of inputs. For identical inputs (i.e. $V_{in}1 = 1$, $V_{in}2 = 1$, or $V_{in}1 = 0$, $V_{in}2 = 0$) there is no potential difference across the circuit and therefor the output will be the same as the inputs. In the case where there are alternating inputs (i.e. $V_{in}1 = 0$, $V_{in}2 = 1$, or $V_{in}1 = 1$, $V_{in}2 = 0$) the input signal will experience dynamic resistance within the circuit depending on the polarity of the memristors.

In the case of the "And" gate any input signal will experience the first memristor prior to the output node in the high resistance state, as it travelling in the polarity that will reset the device. It will then experience the second memristor just after the output node in the low resistance state, as it is travelling in the polarity that will set the device. As such the relation used to describe the output of the signal for this circuit is as outlined below[113].

$$V_{out} = V_{in} \frac{LRS}{LRS + HRS} \quad (1)$$

$$if\ HRS \gg LRS\ Then\ V_{out} \cong 0$$

In the case of the "Or" gate any input signal will experience the first memristor prior to the output node in the low resistance state, as it is travelling in the polarity that will set the device. It will then experience the second memristor just after the output node in the high resistance state, as it is travelling in the polarity that will reset the device. As such the relation used to describe the output signal for this circuit is outlined below[113].

$$V_{out} = V_{in} \frac{HRS}{LRS + HRS} \quad (2)$$

$$if\ HRS \gg LRS\ Then\ V_{out} \cong V_{in}$$

From the above relations it can be seen that the success of a memristor in Boolean logic relies on large differences in resistance between the low resistance state and high resistance state. There will inevitably be some signal degradation across memristor based logic gates due to the non-zero resistance of the low resistance state. This however can be alleviated by the integration of CMOS components such as inverters, which will be necessary in the overall function of the circuits to provide "Not" gate functions[39]. This means that while large differences between the resistance states of the device is important, there are diminishing returns to further increasing the gap between the states[39]. As well, for rapid signal processing a memristor that is able to switch between the high and low resistance state in very short periods of time is also desirable[112].

The real benefit to using memristor based logic gates comes when comparing the amount of individual components needed to form more complex logic circuits, such as adder circuits and multiplier circuits, with and without the use of memristor logic gates. Table 2.2 adapted from Mandel et al[39] outlines the differences in the number of components needed to complete a series of fundamental logic circuits when using conventional CMOS components, and when using memristor components. From this it can be seen that conventional computer chips that employ memristors will be able to achieve much higher logic density through the simplification of fundamental logic circuits. However, manufacture

techniques capable of producing memristor logic gates that are compatible with conventional CMOS chip materials still need to be developed in order to realize the full benefit of memristor based Boolean Logic[24].

Table 2-2 Comparing the number of components needed to make fundamental circuits using memristor based logic, and conventional CMOS based logic Adapted from Mandel et al [39]

Logic Circuit	Memristor based Logic Gates		MOSFET based Logic Gates	
	# of Memristors	# of CMOS Invertors	# of MOSFETS	# of CMOS Invertors
And	2	0	4	1
OR	2	0	4	1
Nand	2	1	8	2
Xor	6	2	10	2
Full Adder	18	4	22	3
8 Bit Carry Save Adder	288	64	352	48
8 Bit Wallace Tree Multiplier	208	40	280	28

2.3.2 Crossbar Logic Structure

Cross bar structure refers to a broad category of hardware architecture that describes an array of two terminal nodes that are formed at the intersection of sets of parallel top and bottom electrodes that are oriented perpendicular to each other [102]. Figure 2.11 adapted from Ielmini et al displays a typical cross bar structure. The sets of parallel electrodes are referred to as word lines and bit lines for the top and bottom respectively [5]. Memristors are formed at each node by applying a material that has shown resistive switching capability in between the top and bottom electrode. Thereby forming the critical metal/insulator/metal structure of a typical metal oxide based memristor[79]. The cross bar structure is the most widely employed structure of memristor based architecture [102]. In the array each memristor

is analogous to a memory bit, in that a value can stored into the memristor in the form of setting its resistance.

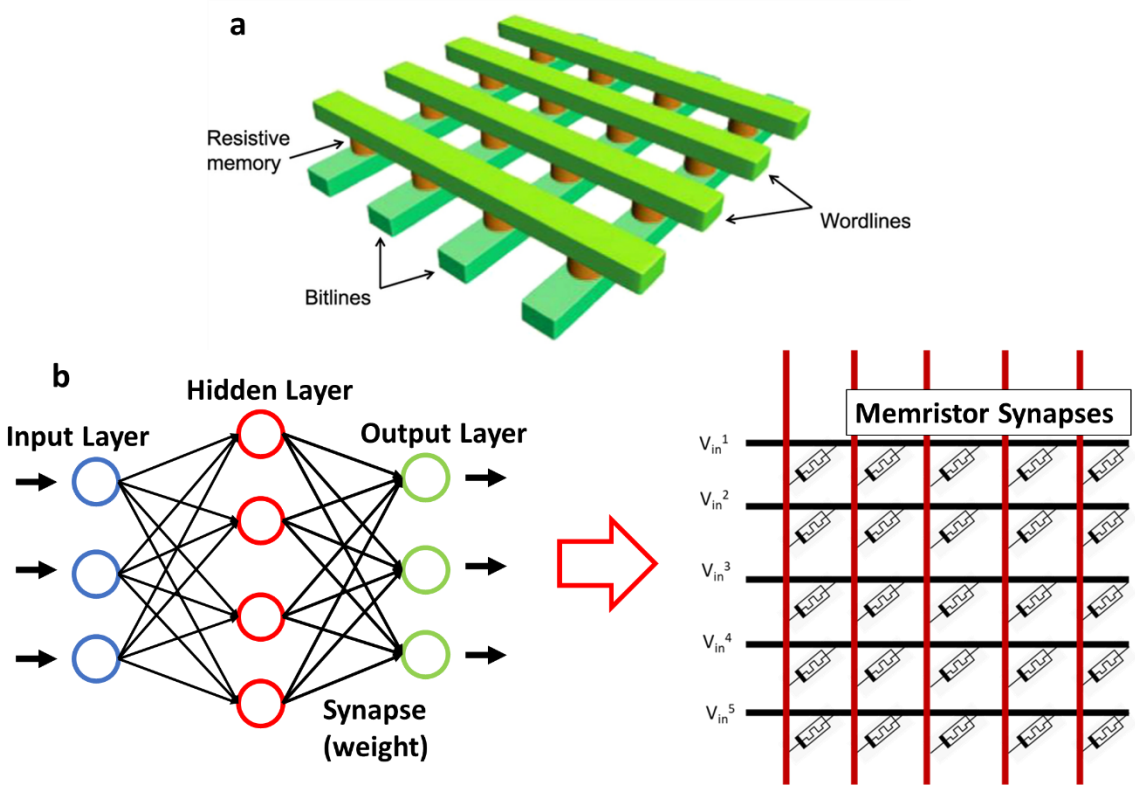

Figure 2-11 A) Memristor Cross bar Array diagram Adapted from Ielmini et al et al[102]. B) Graphical representation of a neural network being translated into memristor arrays

It can also be seen that through using the ability to set memristors to intermediate resistance states a range of values can be stored. Take for example a theoretical device that has a low resistance state of 10 Ω and a high resistance state of 100 Ω. Setting the device to the high resistance state would correspond to storing a memory value of zero, and setting the device to the low resistance state would correspond to storing a memory value of one. If it was desired to store a value of 0.5, then the device would be set to an intermediate state with a resistance halfway between the high and low resistance, in

this case about 55 Ω. The crossbar structure also allows for basic mathematical operations to take place within the array [99]. Using fundamental circuit laws values stored in the array can be directly accessed and changed without the need to shuttle information to any external piece of hardware[35]. This is driving the interest in crossbar architecture as it is what enables memristor based computer hardware to provide physical systems uniquely suited to representing neural networks, and the ability for in situ updating of the memristor weights bypasses the Von Neuman bottleneck[31].

Crossbar networks are of primary interest in providing specialized hardware for neural network based applications. The memristor nodes in the array behave as modifiable weights in the neural network. As well the ability to update weights in situ has shown to be able to dramatically improve the performance and reduce energy costs in a variety of neural network applications. The work done by Gao et al [114] demonstrated how a cross bar array of memristor elements could be used to develop neural networks designed for sound localization processes. By using the ability to update the weights of the memristors in the arrays with in-situ modifications to the array it was shown that they could reduce the power consumption of the neural network to less than 1% of using a conventional computer. Furthermore the size of the array was only 1024 total nodes. Which demonstrates that cross bar arrays don't need to be very large in order to be of use in real applications.

One of the main challenges that has been identified with cross bar array architecture is that of "sneak paths" within large arrays [115]. The sneak path refers to the potential for alternative low resistance paths to exist within a cross bar array that allow for a signal directed at a specific node to be diverted around the node and provide an erroneous response. Typically an individual node is read or updated by sending an electrical signal through its corresponding word and bit lines, i.e. to read or affect the node in the $(\boldsymbol{i}, \boldsymbol{j})$ position in the matrix a signal would be sent from the $\boldsymbol{ith}$ word line to the $\boldsymbol{jth}$ bit line, under the assumption that the electrical signal would pass directly from word line to bit line through the node at the specified location. However if there is an alternative path through the matrix that provides a lower resistance path for the electrical signal it will take the alternative route, as according to basic laws of circuits and electricity [115]. Figure 2.12 adapted from Li et al demonstrates how sneak paths may exist within a cross bar structure. This is most common when trying to read or affect a node set to the high resistance state [116]. The sneak path issue grows as the size of the cross bar array grows as more potential routes through the matrix exist [116]. As such the sneak path challenge is considered one of the primary challenges that needs to be addressed to enable the development of larger cross bar arrays

that are able to provide the hardware to support larger and more complex neural network applications[117].

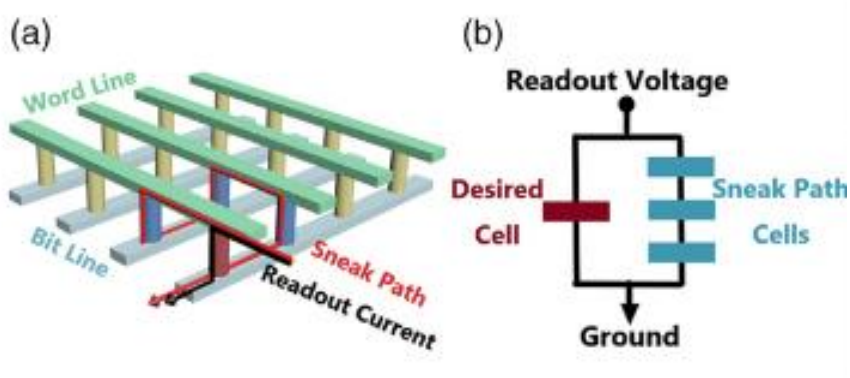

Figure 2-12 A) Graphical Representation of the sneak path problem in memristor cross bar arrays B) Erroneous reading due to sneak paths. Adapted from Li et al [115]

Another challenge facing the development of cross bar based hardware architecture is the limited options for fabrication techniques able to produce large arrays of memristor elements [24]. The most common methods of producing memristor cross bar arrays rely on fabrication techniques such as electron beam deposition[83] or nano imprint lithography [118], in addition to thin film deposition techniques. While these techniques offer very high spatial resolution they also limit the size of memristor arrays, as well they are low throughput and costly [83]. This highlights a growing need for new methods of producing memristor cross bar arrays that are rapid and inexpensive.

In summary this literature review presents a survey of the current fabrication methods available to create flexible and novel electronic devices. Many of the methods available to create flexible electronic devices suffer from high cost and low throughput. Direct Laser writing is introduced and explored as a new method of fabricating flexible electronic components. The key benefits of simple and rapid fabrication method, as well as the use of inexpensive raw materials are key driving factors in the growing interest in direct laser writing. Memristors are introduced as novel passive circuit elements with significant potential to create new computer hardware architecture that can greatly alleviate the energy costs associated with neural network based software applications. The fundamental properties of memristors are described and their implementation into several different computer hardware designs

is illustrated. The novel nature of memristor devices mean that currently there is not many proven fabrication methods that can create memristor devices suitable for computer hardware applications, that are also inexpensive and simple.

In this thesis we work to identify the research gap in developing low cost and simple fabrication techniques of memristor devices. By providing low cost memristor fabrication techniques the barriers to memristor based research can be reduced, and thereby memristor focused research can be accelerated. We work to leverage the low cost and simple process of direct laser writing techniques to develop a facile and inexpensive method of memristor fabrication. This is done by furthering the understanding of the fundamental laser material interactions that occur during direct laser writing and demonstrating successful strategies of fabricating memristors.

Chapter 3
Direct Laser Writing Process[1]

3.1 Introduction

In this chapter the process of direct laser writing using a near infrared laser will be explored in depth. First the techniques used to fabricate flexible metal patterns from metal salt precursor solution will be described. Then the electrical and chemical properties of deposited patterns will be characterized.

3.2 Materials and methods

3.2.1 Preparation of metal salt precursors

Metal salt precursor solutions were formulated from mixtures of metal nitrate salts and organic reduction agents in the form of Polyethylene glycol (PEG) and Polyvinylpyrrolidone (PVP). Metal nitrate salts were selected primarily due to their relatively low cost, ease of access and ease of handling. Additionally, many metal nitrates have high solubility in water and alcohols, allowing for the creation of precursor solutions with high concentrations of metal ions. PEG and PVP are selected as organic reduction agents due to their low cost, low toxicity, and high solubility in water and alcohols.

Aqueous precursors are formulated from 2 M metal nitrate solutions, 0.2 g/ml aqueous PVP, 0.1 g/ml aqueous PEG and deionized water in a volume ratio of 3:1:1:5 respectively. The precursor is then drop casted onto a polymer or glass substrate. The precursor solution is applied at a density of 0.21ul per mm^2, the coated substrate is then heated in a on oven for 50^{o}C for one hour to dehydrate the copper solution. Drying at higher temperatures risks the formation of bubbles in the drying precursor, these bubbles contribute to non-uniform precursor films that lead to poor consistency in the properties of deposited films. The coated precursor should not be left long between drying and laser treatment. Due to the hydrophilic nature of metal nitrates the dried precursor film will absorb moisture from the air if left over time. Excess water is detrimental to the laser writing process as energy from the laser is used to heat and boil the retained water which leads to deterioration in the quality of the deposited patterns.

[1] The contents of this chapter have been incorporated within a paper by Joshua Jones, Monika Snowdon, Shasvat Rathod and Peng Peng, titled “Direct Laser Writing of copper and copper oxide structures on plastic substrates for memristor devices” that has been published in the IOP Journal of Flexible and Printed Electronics available online at https://iopscience.iop.org/article/10.1088/2058-8585/acb0df/meta

The substrate is treated ahead of being coated with an oxygen plasma cleaner supplied by PIE Scientific in order to increase the hydrophilicity. The oxygen plasma improves hydrophilicity by bombarding the surface of the substrate with high energy oxygen ions that remove organic surface contaminants by disrupting organic chemical bonds. Oxygen plasma is selected as it is an environmentally friendly and economic method for cleaning and surface activation.

Alcohol based precursors are formulated by adding 0.006 M of the metal nitrate, 0.1g of PEG, and 0.2g of PVP per 1ml of Isopropyl alcohol. The solution is then sonicated for 30 minutes in order to ensure complete dissolution of the metal salt. The precursor is subsequently heated in a hot bath at 50^{o}C for 3 hours in order to obtain a thick spreadable paste. The paste is then spread onto polymer, or glass substrate manually using the draw bar technique. Shims are set on either side of the substrate during the paste application in order to control the thickness of the paste layer being deposited.

3.2.2 Laser Irradiation of metal salt precursors

The laser used for direct laser writing was a YLM-30 with a NIR1064 nm continuous wave ytterbium laser produced by IPG photonics. The laser is encased in a glovebox supplied by Miyachi with a protective glass sheet to prevent the escape of near infrared light. A three-axis gantry system is used to move the laser head relative to the sample stage. The laser, and gantry system are controlled simultaneously through an attached computer that runs DELTAMOTION^{TM} software. Laser treatment patterns are programmed into the software that enable control of the scanning pattern, laser power output, laser travel speed, and laser defocus. For this work unless otherwise specified the laser was focused to a spot size of 200um. Figure 3.1 shows a sample in the laser treatment chamber receiving focused laser irradiation to selectively deposit a copper pattern.

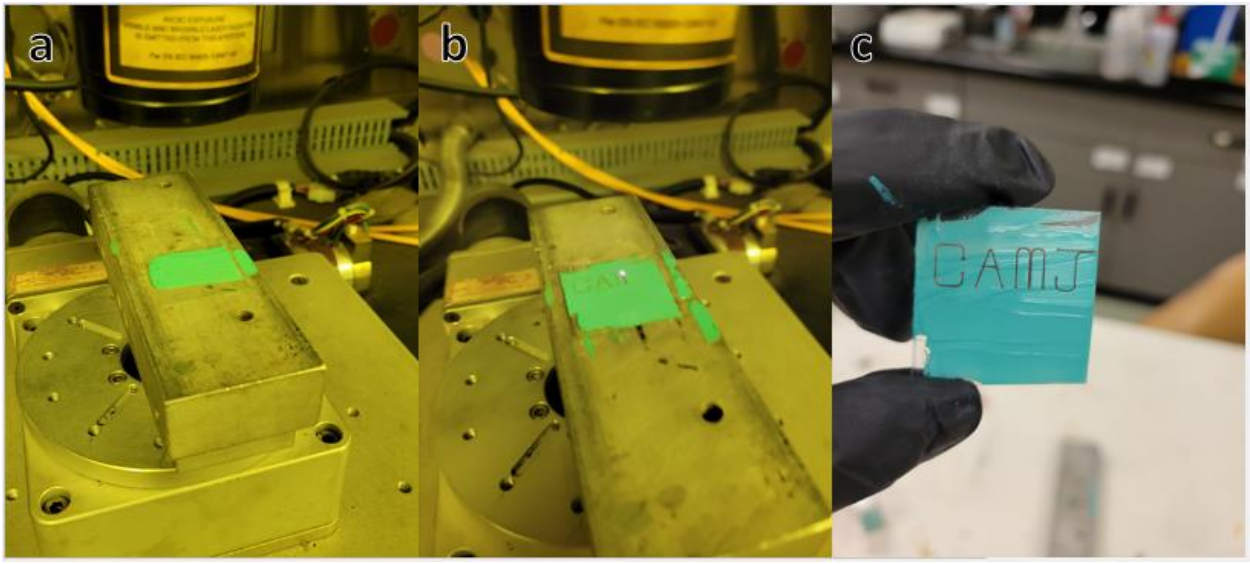

Figure 3-1 A) Flexible polymer substrate coated with copper precursor solution B). Sample in the process of receiving laser treatment C) Sample after treatment showing deposited copper pattern surrounded by unirradiated precursor

3.2.3 3.2.3 Characterization of deposited materials

Microstructure characterization was conducted using field emission scanning electron microscopy (LEO Zeiss FESEM), in situ Energy Dispersive X-Ray analysis (EDAX) was conducted during SEM imaging. X-Ray powder diffraction (XRD) analysis was conducted using a PANalytical Hr-XRD to identify the as-written materials. Copper was used as the anode material, with a two-theta scan range from 30º – 80º with a step size of 0.1º. X-ray photoelectron spectroscopy (XPS) was conducted using an Aluminum K alpha source gun with an energy step size of 0.1 eV to characterize the surface chemistry of printed samples. All the XPS spectra were corrected using the C 1 s peak at 284.8 eV as a reference. Raman spectrum was measured using a Renishaw micro-Raman spectrometer with an excited wavelength of 632 nm to analyze the composition of printed materials.

Electrical characterization was conducted using a Kiethley 4200 probe station. Current-voltage sweeps were conducted using source measure unit (SMU) probes, with a max time resolution of 1E-4 s, and a

max voltage resolution of 1E-13 V. Dynamic characterization tests were conducted using pulse measure unit (PMU) probes, with a max time resolution of 5E-9 s, and a max voltage resolution of 1E-11V.

3.3 Direct Laser Writing of Copper / Copper Oxide Patterns

Direct Laser Writing patterns of copper and copper oxides were deposited under a range of laser settings and changing precursor concentrations. The effects of laser settings and reduction agents on the direct laser writing process were observed through chemical characterization techniques, such as XPS, XRD and Raman analysis, as well as measuring the change in electrical properties. This was done in order to build a more robust understanding of the laser-chemical interactions that occur during the laser irradiation of the metal salt precursors. While other metal patterns, such as silver and nickel were also fabricated and characterized, the copper patterns received the most extensive analysis due to the high interest in copper and copper oxides as multifunctional materials[119].

3.3.1 Effect of Laser Writing Parameters

In order to observe the impact of laser settings on the properties of copper patterns produced by direct laser writing, 0.5mm polycarbonate films were coated with copper precursor and treated with laser irradiation at a range of different laser settings. The three laser settings of laser power, scan speed, and defocus were selected as the variables with the highest likelihood to have significant impacts on the properties of the deposited patterns. In all cases the laser was operated in a continuous wave mode. It is acknowledged that pulse mode operation of the laser would also likely enable further control of properties of the deposited patterns, however that avenue was not pursued due to the pulse mode operation of the laser used in this study being non-functional for the duration of the research.

Sheet resistance tests were conducted on copper patterns printed at a range of laser settings. Sheet resistance tests were conducted using the 4-point probe method typical for measuring sheet resistance in thin films. In order to prepare the samples a copper precursor solution was formulated from aqueous solutions of copper nitrate, polyethylene glycol, and polyvinyl pyrrolidone. The concentrations and mixing ratios of the ingredients used in the precursor solution are outlined in table 3.1. Sigma Aldrich chemicals supplied all chemicals used.

Table 3-1 Contents of aqueous copper precursor solution

	Concentration	Volume ratio
Copper Nitrate ($Cu(NO_3)_2$)	2 M	3
PEG, MW 5000	0.1g/ml	1
PVP, MW 2400	0.2g/ml	1
De-Ionized water	-	5

The copper precursor was drop-cast onto the substrates. In particular, 700 µl of copper ion precursor solution was applied to 33 mm^2 of a substrate. The coated substrate was then heated in an oven at 50^oC for one hour to dehydrate the copper solution. The laser used for direct laser writing was a YLM-30 with a NIR1064 nm continuous wave ytterbium laser produced by IPG photonics. The laser was focused on a spot size of 200 µm. After selective laser irradiation of the coated substrate was completed, the samples were rinsed with deionized water to remove the unirradiated regions. The direct laser writing process is carried out in an air environment at room temperature and humidity.

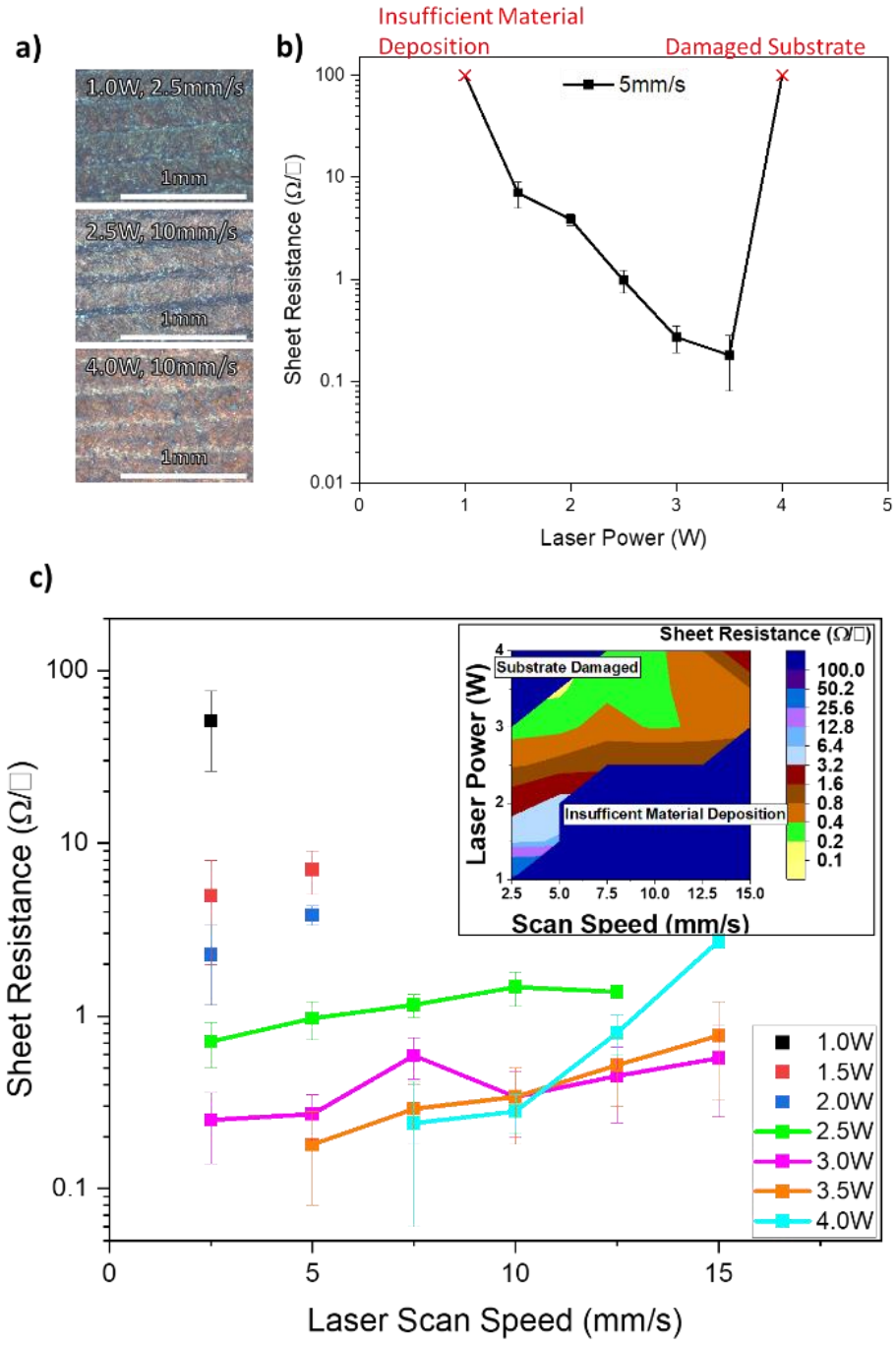

Figure 3-2 (a) Optical images of patterns deposited by DLW at changing laser settings; Sheet resistance as a function of (b) laser power and (c) speed. Inset: heatmap of sheet

resistance as a function of laser power and speed with regions highlighting unsuitable parameters due to substrate burning, and insufficient material deposition.

Figure 3.2b-c show the results of sheet resistance of as-written samples produced at a range of laser power, and scan speed. The electrical property of the deposited materials is highly dependent on the laser writing parameters. Generally, the trend presented shows a dramatic decrease in sheet resistance when increasing laser power from 1.0 to 3.0 W, see Figure 3.2b. A processing window for low resistance patterns seems to exist between 3.0 – 4.0 W of laser power when scan speed is 5 mm/s, before resistance increases again by order of 10^3 above 4.0 W due to burning and damaging of the flexible substrate, as the red cross indicated. In the low-power regime, the high resistance can be attributed to the high copper oxide content. At low laser power insufficient material was deposited to be able to form fully continuous copper sheets, as indicated by a red cross. Figure 3.2c-inset depicts laser settings that lead to either substrate burning or insufficient material deposition. The limit of laser treatment settings where substrate damage begins is influenced by the substrate material. A similar trend in the processing window for direct laser writing was observed when an 808 nm wavelength laser is used; below 1.0 W laser irradiated areas have insufficient reduction of copper ions and remain non-conductive, and above 4.5 W heating effects from laser irradiating cause damage to the substrate[65]. Here, fiber laser with 1064 nm wavelength shows a slightly lower damage threshold due to its larger heating effect compared to 808 nm [120]. Asides from laser power, laser scan speed can also alter the properties of as written structures. Figure 3.2c shows the relation between laser scan speed and sheet resistance from 2.5 to 15 mm/s. At higher laser power, low resistance can be achieved. This work's lowest sheet resistance values were accomplished at a laser power and travel speed of 3.0 – 3.5 W at 5 mm/s. The sheet resistance was 0.25 – 0.29 $\Omega/\square$, which is comparable to that of sintered copper nanoparticles, such as 0.3 $\Omega/\square$ done using intense pulsed light sintering[14], or the 0.17 $\Omega/\square$ obtained using 808nm wavelength laser[65], or 0.11 $\Omega/\square$ achieved through acid assisted thermal sintering [121]. By increasing the laser scan speed from 5 to 7.5 or 10 mm/s, the high power 4.0 W laser can also be used to fabricate highly conductive patterns. The results of this work are compared with other similar works in the literature in Figure 3.3a. It is found that fiber laser deposition power in this work that achieved the lowest sheet resistance is higher than most other works. This higher deposition power is a result of the low optical absorbance of copper ions at 1064nm compared to peak absorption near 800nm as indicated in Figure 3.3b. Therefore, the direct laser writing process also has the potential of offering different control freedom through altering the absorbance of precursor materials for practical applications. Additionally, the benefits of

direct laser writing are realized as it is a simple process that works without the need for expensive raw materials such as pre-fabricated copper nanomaterials.

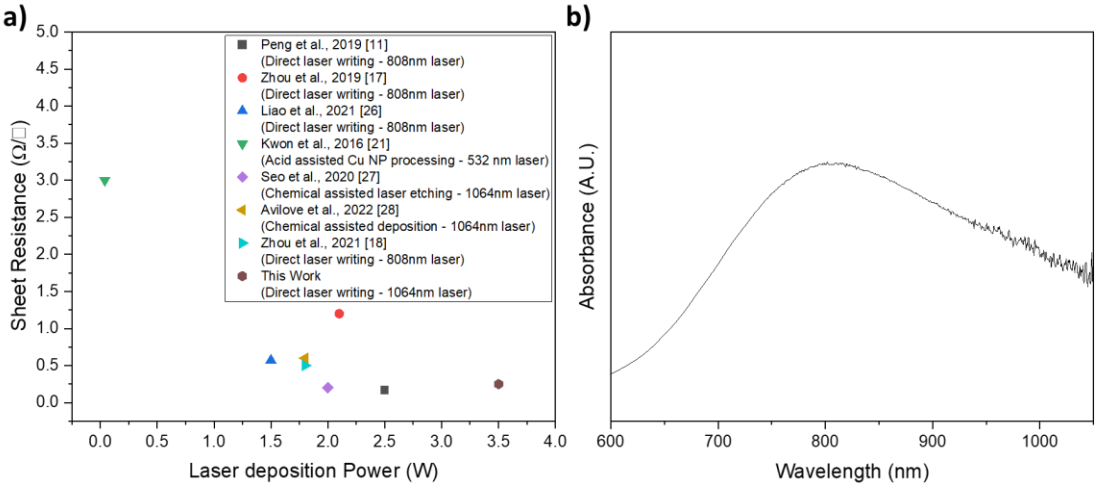

Figure 3-3 A) Summary of the lowest sheet resistances of laser deposited copper patterns via a variety of methods. B) Optical absorbance of 2.0 M Cu^{2+} aqueous solution

The impact of laser defocus on written patterns is also explored in **Figure 3.4**. Figure 3.4a shows the relation between defocus distance and sheet resistance for laser writing at 3.5 W scanning at 10 mm/s. It is observed that the lowest sheet resistance values are achieved at no defocus, with resistance increasing as defocus increased either into the sample surface (negative defocus) or away from the sample surface (positive defocus). By defocusing the laser, the spot size increases, resulting in the laser's energy being spread over a larger surface area. Figures 3.4b-g show optical micrographs of samples printed at varying defocus distances. The samples with positive defocus values show a dramatic change in pattern colour, with a change from red-brown to gray, indicating a transition from high copper content to high copper oxide content at increasing defocus. A corresponding increase in sheet resistance corroborates this. The negative defocus samples show a similar increase in sheet resistance, however there is not as much of a noticeable change in pattern colour. Instead, what becomes apparent is notable gaps between the lines of the laser path. When the gaps become severe, such as in

the sample fabricated with a defocus of -2mm in Figure 3.4d, the sheet resistance dramatically increases due to the lack of connectivity between each laser path. This reduction in laser path width is likely a product of the gaussian energy distribution profile of the laser used in this work. The laser energy profile is such that the highest energy values are achieved at the center of the beam. When the spot size is increased, only the area near the center of the spot retains enough laser energy to reduce copper ions. As such, no material is deposited near the edges of the laser spot, which results in the gaps between the laser paths. This effect could be minimized by tuning the overlapping of laser footprint when a larger printed area is investigated in future work.

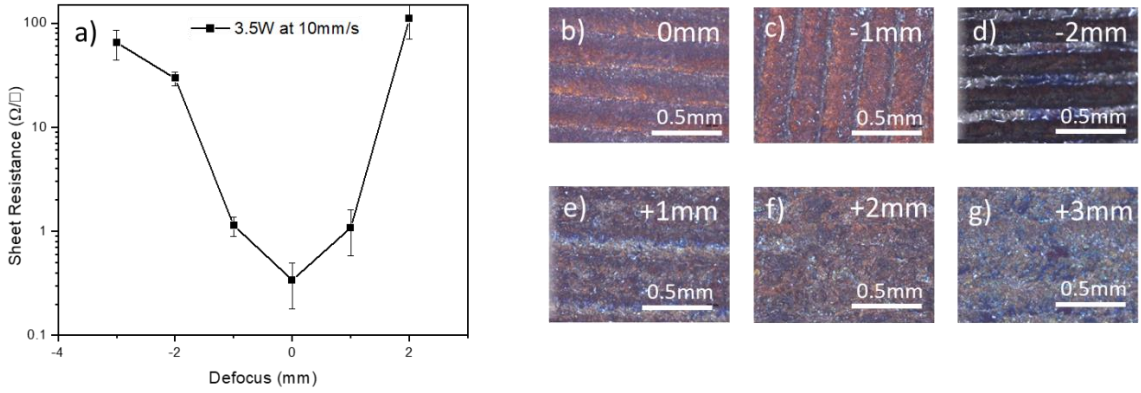

Figure 3-4 a) Sheet resistance of samples printed at 3.5 W at 10 mm/s with changing laser defocus. (b - g) Optical micrographs of patterns printed at different defocus distances.

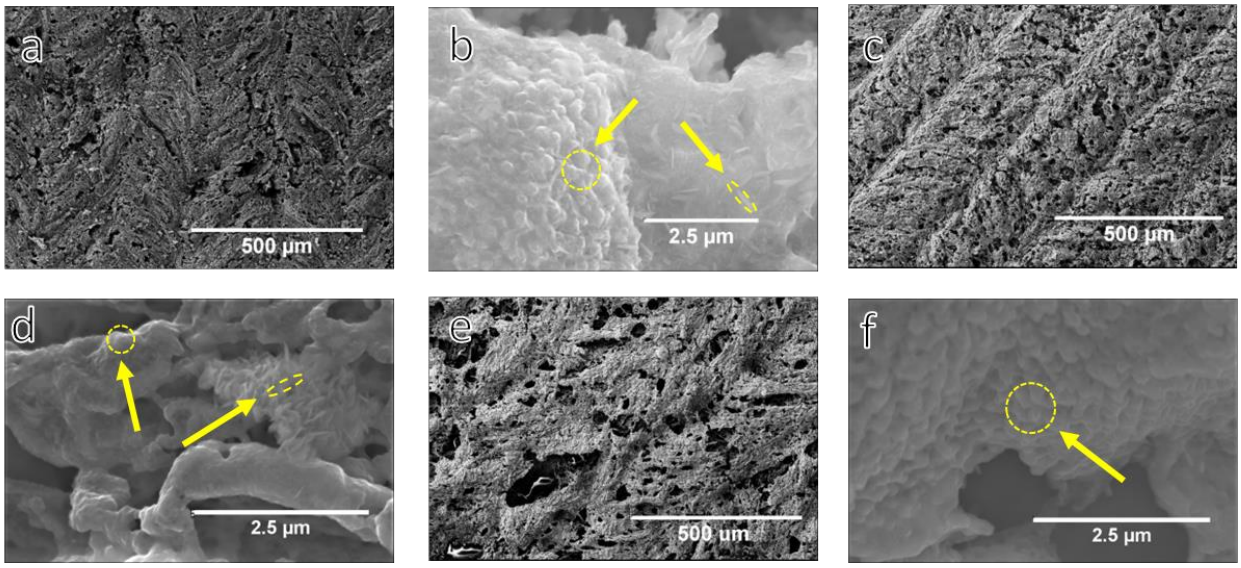

Figure 3-5 SEM images of patterns printed at (a,b) 1.0 W at 2.5mm/s, (c, d) 2.0 W at 10mm/s, and (e, f) 4.0 W at 10mm/s

Scanning electron microscopy was used to analyze the microstructure of deposited patterns at a range of laser power to help understand the change in conductivity with different laser writing parameters. Three samples correspond to a low, medium, and high laser power pattern. The low-power sample was printed at 1.0 W at 2.5 mm/s, the medium was at 2.5 W at 10 mm/s, and the high-energy one was printed at 4.0 W at 10 mm/s. Figure 3.5 shows the SEM images of these samples. In all samples, regardless of laser energy, the deposited pattern has a porous structure as shown in Figure 3.5a, d, e.

The porosity could be attributed to the evaporation of the precursor film during laser-induced heating[73]. Figure 3.5b shows the low power pattern at high magnification; there is a mixture of round interconnected nanoparticles, and sharp flat platelets, as marked by arrows. The round particles correspond to copper nanoparticles, whereas the platelets indicate copper oxide particles, similar to previous results [62], [65]. The medium power pattern shows a majority of the microstructure being dominated by round copper nanoparticles, with some dispersion of flat copper oxide platelets, see Figure 3.5d. In contrast, the high-power pattern illustrates a typical sintered structure without the presence of copper oxide, as shown in Figure 3.5f. The large smooth features indicate a high degree of sintering. It is worth noting that in all cases, the size of the copper particles remains consistent regardless of the laser power, suggesting the fast reduction and in-situ sintering process during writing minimizes the particle growth. The average copper nanoparticle size, as determined by image analysis, is 250 nm,

which is much larger than the reported laser-reduced copper nanoparticles with shorter wavelength [65] but comparable to that from chemical reduction processes [122]. It may suggest that the near infrared wavelength laser could decompose more reducing agents in a precursor to create an intensive reduction for particle growth with more heat effect when compared with short wavelength laser irradiation.

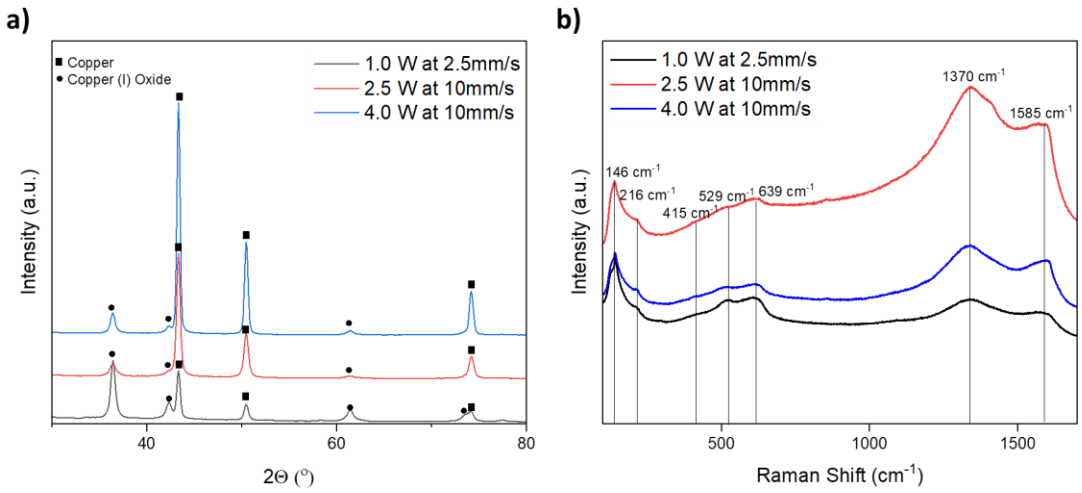

Figure 3-6 (a) XRD plots of DLW samples comparing the content of Copper and Copper (I) Oxide; (b) Raman plots of DLW samples showing the Carbon D and G band peaks.

The chemical composition of samples produced at varying laser parameters has been investigated to help understand the role of laser energy in determining the material properties of deposited patterns. The state of the carbon present in the sample as a product of the PEG and PVP included in the precursor copper ion solution has also been analyzed. XRD patterns in Figure 3.6a indicate that at increasing laser power, the content of the Cu_2O phase diminishes, and the metallic copper phase increases. The largest change in Cu_2O occurs between the 1.0 W and the 2.5 W, where a small increase is noted between the 2.5 W and the 4.0 W. It can be seen that by comparing the sheet resistance of the samples used in XRD analysis (31.7 $\Omega/\square$for 1.0 W at 2.5 mm/s, 1.5 $\Omega/\square$ for 2.5 W at 10 mm/s, and 0.3 $\Omega/\square$ for 4.0 W at 10 mm/s) to the Cu_2O content of each sample, the sheet resistance shows a strong dependence of the

presence of the Cu_2O phase. The decrease in Cu_2O indicates high laser power increases the reduction of the Cu^{2+} ions. It's also of note that in all cases no trace of a CuO phase was detected; this indicates that all the copper ions present in the precursor film were at least partially reduced. These results may help in understanding the reduction mechanism of the copper ions during direct laser writing, suggesting that during the reduction of the copper ions there is a preference to ensuring that all ions have been reduced from the Cu^{2+} state before any ions are fully reduced to the metallic state. This observation may be due to the slightly lower activation energy of reducing Cu^{2+} to Cu^{1+} than reducing Cu^{1+} to metallic Cu^0 (0.16 eV to 0.18 eV, respectively) [123]. These results indicate that varying laser writing parameters is a reliable way to select chemical compositions to alter the electrical properties of as-written structures.

Figure 3.6b shows the Raman spectra of these three samples showing the Carbon D and G peaks at 1370 cm^{-1} and 1585 $cm^{-1,}$ respectively [124]. The ratio of the height of the D peak to G peak is a good indicator of how structured the carbon in the sample is, as the D band corresponds to defects in a planar carbon lattice. In contrast, the G band corresponds to the presence of graphite-structured carbon sheeting. A high D/ G intensity ratio indicates a high concentration of defects obstructing the planar carbon structure[125]. In all of the samples analyzed, the D band showed a higher intensity than the G band, indicating that the sample's carbon is very amorphous. A series of peaks from 100 cm^{-1} to 650 cm^{-1} are also apparent in the Raman spectra for all samples. These peaks can be attributed to the presence of the Cu_2O phase, which shows five distinctive peaks (three strong peaks at 146 cm^{-1}, 216 cm^{-1}, and 639 cm^{-1}, and two weak peaks at 415 cm^{-1}, and 529 cm^{-1})[126]. Notably, no peaks associated with the CuO phase (296 cm^{-1}, and 343 cm^{-1}) are present in the Raman spectra for any sample. These data corroborate with the above discussion on the preference for partial reduction of copper ions.

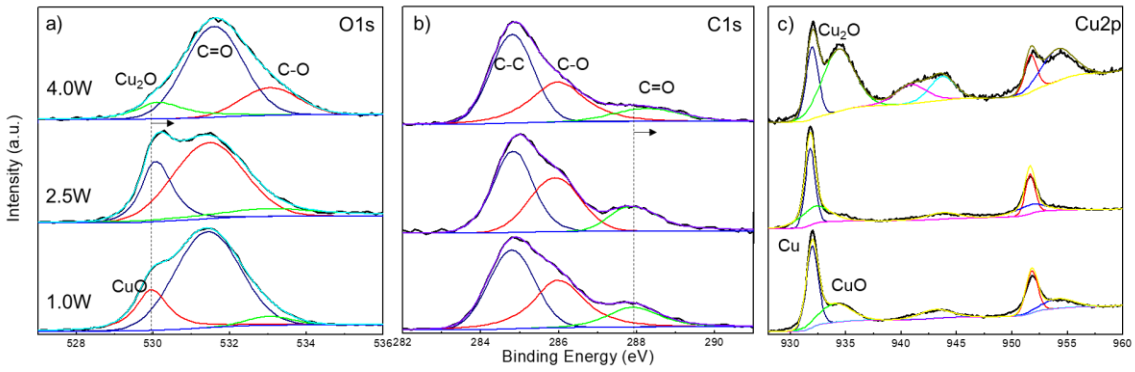

Figure 3-7 XPS patterns of Cu samples fabricated with different laser power: (a) O 1s band, (b) C 1s band, (c) Cu 2p band.

XPS has been used to analyze the chemical composition of the surface of patterns fabricated at differing laser parameters, as shown in Figure 3.7. In the O1s spectra in Figure 3.7a of the 1.0 W sample a peak at 529.9 eV is associated with the CuO bond[127]. It slightly shifts to 530.1 eV as the power increases to 4.0 W, suggesting the partial transformation of CuO to Cu_2O [127]. The peaks at 531.5 eV and 533 eV are ascribed to the C=O and C-O bonds, which are attributed to the residual PVP and PEG[67]. The former is from the hydroxyl end groups of the PEG chains, while the latter is the lactam side chain ring of the decomposed PVP[128] . Notably, the content of Cu_2O/CuO decreases from ~21.3 at.% to ~12.9 at.% as the power increases, indicating less of the copper ions are left in the partially reduced state at higher laser power.

These decomposition products are also visible in the C 1s spectrum in Figure 3.7b, in which the identified C-O bond at 285.9 eV confirms the presence of non-decomposed PEG. The C=O bond is located at 287.9 eV in the 1.0 W and 2.5 W samples. It has lower binding energy than that reported previously may be due to the coexistence of the C-N bond (~287 eV) from undecomposed PVP[67] . The C=O bond then shifts to 288.2 eV as the power increases to 4.0 W, indicating a sufficient decomposition of PVP at higher power. Formic acid from decomposed PVP is critical for copper reduction, thereby, a lower content of Cu_2O/CuO is identified in this case as we discussed in Figure 3.6a.

The spectrum of Cu2p in Figure 3.7c agrees well with the above discussion. The peak at 931.9 eV is associated with Cu/Cu_2O, while the peak at around 932.2-934.4 eV can be assigned to the Cu^{2+} species [69]. Furthermore, the content of Cu^{2+} species in the 4.0 W sample is significantly higher than that in the 1.0 W and 2.5 W samples, which may be due to the presence of more adsorbed insoluble for example hydroxides on the sample surface.

3.3.2 Effects of precursor solvent

Copper nitrate precursors were prepared using isopropyl alcohol (IPA) as a solvent, and irradiated in order to produce copper and copper nitrate based patterns. This was done in order to determine if the trends observed when using aqueous based precursors are applicable to precursors that use different solvents, in hopes of providing a more generally applicable model of direct laser writing processes. IPA was selected as it is safe to handle, inexpensive, easy to procure, and has a low vaporization temperature[129], meaning the process is likely to be suitable at low processing temperatures.

The IPA based precursor was also designed with the intention of addressing several shortcomings of aqueous based precursors. Namely the IPA based precursor is fabricated as a thick paste than can be spread directly onto a substrate and immediately irradiated to produce copper patterns. This eliminates the need for the intermediate drying step in the aqueous precursors, and thereby expediates the process. As well the thick paste enables deposition of multiple layers of copper patterns as the paste can be applied on top of existing copper patterns and irradiated to deposit successive layers. This is not possible with the aqueous precursor, as applying a successive layer of precursor solution onto an existing copper pattern results in degradation of the underlying layer. The degradation occurs during the drying step of the aqueous precursor due to the corrosive nature of the metal salt solution, and the elevated temperature.

Sheet resistance tests were conducted on copper patterns fabricated using laser writing of alcohol based precursors in order to determine if the relationship between laser power and material properties that was established for the aqueous precursors are still applicable to the alcohol based precursor. For the tests a 75 μm layer of paste was applied to the substrate. The IPA based precursor is applied to the substrate surface using the doctor blade technique. Heights dams on either side of the substrate are used to set the thickness of the applied precursor layer. Figure 3.8 shows the sheet resistance results of copper patterns printed from alcohol-based precursors. The patterns show a very similar trend to the aqueous precursors, with sheet resistance decreasing as laser power increases. The main difference between the

aqueous and paste precursor was that patterns were able to be deposited and achieve low sheet resistances at lower laser power values than when compared to the aqueous precursor. This can likely be attributed to the thicker paste layer absorbing more laser energy compared to the aqueous precursors. Overall the lowest sheet resistance achieved using the paste precursor is similar to that of the aqueous precursor 0.25 Ω/□ printed at 3.5 W at 5mm/s for the aqueous precursor, compared to 0.21 Ω/□ printed at 2.0 W at 5mm/s for the alcohol precursor. Also the increase in resistivity at the high energy range in the paste precursor is not attributed to substrate burning, instead at high laser powers the laser begins to ablate material from the center of the path, and only deposit material near the edge, leading to patterns with significant gaps. This is likely due to the gaussian energy profile of the laser beam, where high energy at the center of the beam leads to material ablation, whereas decreasing laser energy near the edges are suitable for material deposition. Overall this demonstrates that the precursor has only marginal effect on the direct laser writing process.

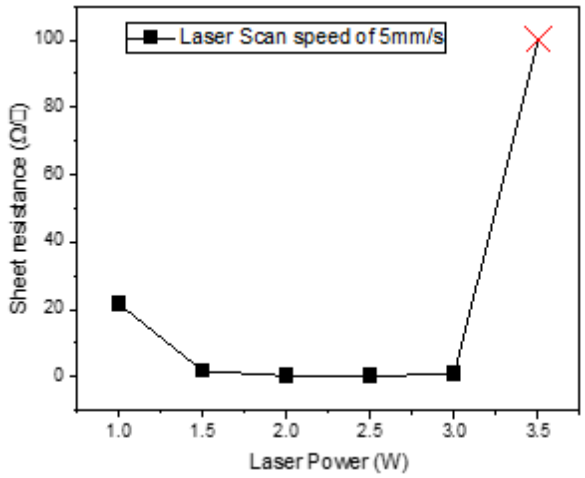

Figure 3-8 Sheet resistance values for copper patterns printed from IPA paste based precursors. Printed at Laser scan speed of 5mm/s with changing laser power

It was shown that patterns of two or more layers could be deposited by applying successive layers of paste precursor onto existing copper patterns and applying laser treatment. Several multi layer patterns are shown in figure 3.9. The thickness of a single layer is limited by the maximum penetration depth of the laser into the precursor paste. It was found that paste layers greater than 100 µm would retain a thin layer of paste precursor underneath the deposited materials, indicating that the maximum penetration

depth was roughly 100 µm. Applying successive layers of 75 µm ensured there was strong adhesion between successively deposited layers. Features such as overhangs and bridges were able to be fabricated. Figure 3.9 b shows a pattern where a square pattern is suspended above the substrate on four pillars.

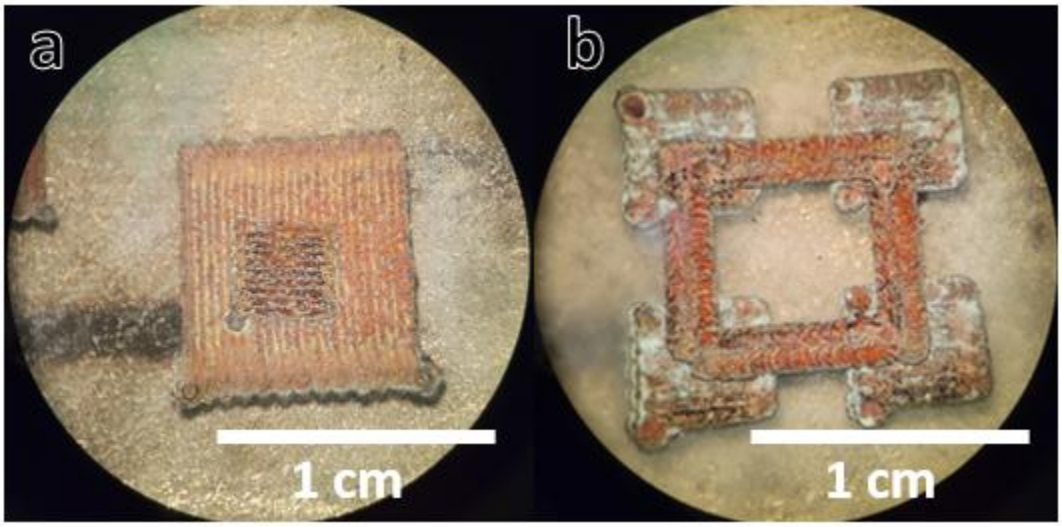

Figure 3-9 Multilayer patterns deposited using sequential layers of IPA based paste precursor. A) A smaller grid placed on top a larger base layer. B). A square bridge suspended on four pillars

The paste precursor was shown to have a moderately corrosive affect on the underlying patterns. Copper layers that remained submerged under the paste for extended periods would show notable discoloration. This can be attributed to the mildly oxidative nature of the metal salt solution [130]. Overall the resistance of the pattern would be unchanged unless left submerged for periods greater than an hour. This likely indicates that the degradation only affects near to the surface of the pattern.

3.4 Direct Laser Writing of Different Metallic Patterns

Aqueous precursor solutions of several metals were prepared and treated at a range of laser settings to determine whether the degree of control over material properties could be extended to other metals with a range of reduction potentials. Silver, Nickel and Iron were selected as other metals in order to provide

a broad range of reduction potentials. The Reduction potentials of Copper, Silver, Nickel and Iron are provided in table 3.2.

Table 3-2 Reduction potential of various metals

Metal	Standard Reduction Potential (V vs SHE)
$Ag^{+} + e^{-} \rightarrow Ag$	+ 0.8
$Cu^{2+} + 2e^{-} \rightarrow Cu$	+ 0.34
$Ni^{2} + 2e^{-} \rightarrow Ni$	-0.28
$Fe^{2+} + 2e^{-} \rightarrow Fe$	-0.45

All metal samples were prepared similar to the aqueous copper samples. 700 µL of precursor solution was drop casted onto 33mm^2 polymer substrates cleaned via oxygen plasma and dried in an oven to remove excess moisture. Patterns of each material were deposited at a range of laser power settings. Sheet resistance tests of patterns produced at ranging laser power settings are presented in Figure 3.10.

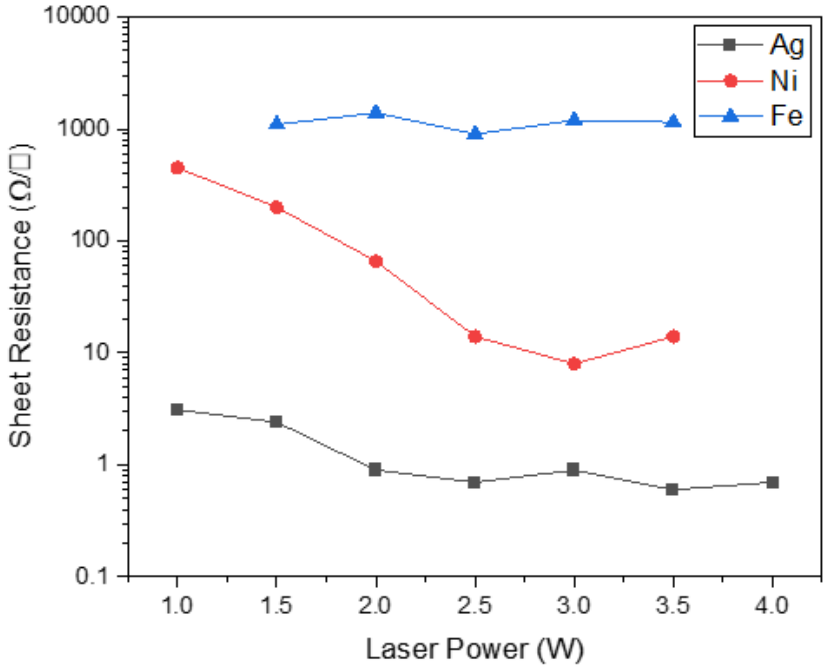

Figure 3-10 Sheet resistance values of Silver, Iron, and Nickel patterns deposited using direct laser writing

The conductivity of all the metals is similar, therefor the large differences in sheet resistance values can be attributed to varying degrees of oxide content in each pattern. The resistivity of silver patterns

fabricated using DLW of silver ion precursor films show much lower dependence on laser energy density than that of copper patterns. Very low resistances were achieved at a much lower applied laser energy density than copper patterns. As well there was no set of laser settings that deposited high resistance patterns, indicating that in no case were patterns containing a high content of silver oxide were deposited. This is likely due in large part to the much more cathodic nature of silver making it more thermodynamically inclined to form metallic silver over silver oxide when compared to copper which has several stable oxides[76]. Iron patterns also show a low sensitivity to changing laser power, with no clear trend between laser power and sheet resistance. In all cases the patterns showed very high resistivity. This is likely due to the highly anodic reduction potential of iron. PVP is only a moderate reduction agent [67], and may not be able to fully reduce iron ions regardless of the amount of incumbent laser energy. Nickel showed the highest sensitivity to laser power, showing a similar trend to copper samples. As laser energy increased sheet resistance of the copper patterns decreased. Notably the nickel patterns were unable to achieve sheet resistance values comparable to the silver or copper patterns. Overall it can be seen that the reduction potential of a metal ion is the largest predictor in its suitability for direct laser writing. Low reduction potential metals such as silver can readily achieve conductive metallic patterns. Metals with moderate reduction potentials show a high sensitivity towards laser energy density and can selectively deposit either metallic or metal oxide patterns. Metals with high reduction potentials will struggle to deposit metallic patterns. Changing the content of reduction agents may be able to address these challenges, i.e. reducing the amount of reduction agents in low reduction potential metals may assist in being able to generate metal oxide patterns.

3.5 Direct Laser Writing of Copper-Nickel Alloys

Copper-Nickel aqueous precursor solutions were prepared and treated using laser irradiation at a range of laser settings in order to determine whether or not direct laser writing is capable of producing metal alloys. Copper and Nickel were selected as they were both previously in previous chapters to have success in depositing metal patterns with direct laser writing. As well copper and nickel are known to have complete solubility with each other[131], and as such could act as a strong test to determine if direct laser writing is capable of producing homogenous alloys.

Sheet resistance tests were conducted on samples printed from Cu:Ni precursors containing 50:50 and 60:40 volume ratios of Nickel Nitrate and Copper Nitrate, respectively. Table 3.3 details the constituents of the copper nickel precursor solutions.

Table 3-3 Contents of the Ni-Cu alloy precursor solutions

	Concentration	Volume Ratio	
		Cu:Ni 50:50	Cu:Ni 40:60
Copper Nitrate ($Cu(NO_3)_2$)	2 M	1.5	1.2
Nickel Nitrate ($Ni(NO_3)_2$)	2M	1.5	1.8
PEG, MW 5000	0.1g/ml	1	1
PVP, MW 2400	0.2g/ml	1	1
De-Ionized water	-	5	5

Similar to previous samples copper nickel precursor solutions were drop cast onto oxygen plasma cleaned polymer sheets. 700 µl of metal ion precursor was applied per 33mm^2 of surface area. All sheet resistance test samples were printed at a scan rate of 5mm/s and the laser power was varied in order to observe the effect of changing laser energy. Figure 3.11 shows the results of the sheet resistance tests conducted on the Ni-Cu samples. It can be seen that there is strong similarities to the sheet resistance tests of the pure copper and nickel samples shown in previous chapters. This provides strong evidence that the reduction of metal ions through the photoreduction of PVP is uninhibited by the presence of multiple metal ions. At low laser energy the high resistance can be attributed to the formation of metal oxides, and as the laser energy increases the resistance drops as more metal phase is deposited. The lowest sheet resistances for both the 50:50 and 40:60 Cu:Ni samples were achieved at 3.5 W, and were 1.8 Ω/□ and 2.1 Ω/□ respectively.

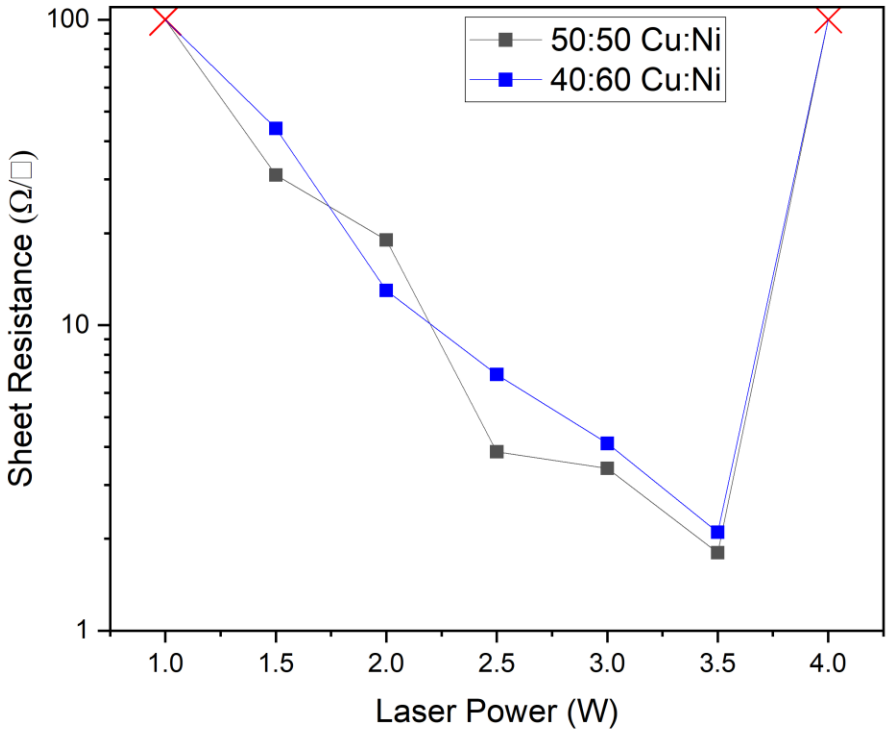

Figure 3-11 Sheet resistance values of the Ni-Cu patterns printed at 5mm/s laser scan speed and changing laser power

XRD analysis was conducted on the deposited samples in order to determine whether or not the metallic copper and nickel phases were deposited as a homogenous alloy. Figure 3.12 shows the XRD spectra of the copper nickel samples at varying laser powers. The strong presence of a copper-nickel peak in the 60:40 samples at a 2θ value of 44° indicates that most of the metallic phase is deposited as a copper nickel alloy[132]. This indicates that direct laser writing is capable of producing homogenous alloy phases from precursors with multiple metal ions. It can also be seen that the copper nickel peak shifts slightly from 44° in the 60:40 samples, to 43.7° in the 50:50 samples, as shown in Figure 3.12b. This is a result of the changing lattice parameter in the copper-nickel phase as more of the alloy is made up copper, which has a slightly larger atomic radius than nickel (128 pm and 123pm respectively). This indicates that the proportion of metals in the alloy phase is directly impacted by the ratio of metals in the precursor solution. It can also be seen that in both the 60:40 and 50:50 samples the nickel oxide

content increases as the laser energy decreases. The concentration of each phase present in the samples as determined through XRD analysis is detailed in table 3.4. This agrees well with the sheet resistance tests which predicted a higher oxide content at lower laser energies. It is also worth noting that there is no presence of a copper oxide phase, even in samples with the lowest laser energies. In fact, as laser energy decreases the content of the metallic copper phase increases. This is likely a product of the difference in reduction potentials between the Cu^{2+} and Ni^{2+} ions. Copper has a lower reduction potential when compared to nickel (-0.34 V and 0.28 V respectively). As laser energy decreases and incomplete photodegradation of the PVP leads to an insufficient supply of electrons to fully reduce all the of the metal ions present the copper ions are preferentially reduced before the nickel ions, meaning that it is only the nickel ions that are left without sufficient amounts of electrons and are then deposited as oxides. The alloying composition of the Nickel copper phase present in each sample is unaffected by the laser energy, as can be seen that the position Cu-Ni peak at 44^{o} and 43.7^{o} in the 40:60 and 50:50 samples respectively, is unaffected by laser energy, as can be seen in figure 3.12b. This is of note due to the fact that in the low laser energy cases a significant portion of the metallic copper phase is present. Since copper and nickel have unlimited solubility the fact that the metallic copper phase is retained separate from the alloy phase is worth noting. This may be able to be attributed to the very rapid synthesis process of direct laser writing. In regions where the nickel is only partially reduced the nearby fully reduced copper does not have enough time to diffuse towards regions with fully reduced nickel to join the alloying phase, and are instead deposited as metallic copper along side nickel oxide.

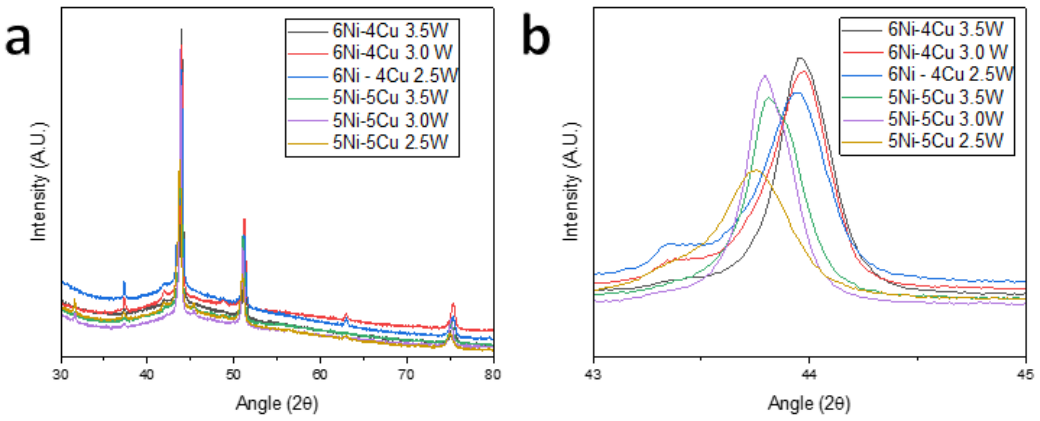

Figure 3-12 A) XRD Spectra of Ni-Cu patterns printed at changing laser settings B) Close up of the Ni-Cu peak near to 44º

Table 3-4 Weight percent of various metal and metal oxide phases in the Ni-Cu samples printed at changing laser settings

Phase	60:40			50:50		
	2.5 W	3.0 W	3.5 W	2.5 W	3.0 W	3.5 W
Cu-Ni	68	76	92	64	79	95
Cu	11	8	1	9	5	1
Ni	-	1	1	1	2	1
NiO	21	15	6	26	14	3
Cu_2O	-	-	-	-	-	-

Figure 3.13 shows SEM images of the microstructure of the 60:40 Ni:Cu sample printed at 2.5 W and 5mm/s laser settings. It can be seen that the microstructure is very similar to that of the pure copper metal. The microstructure is a highly porous network of interconnected nanoparticles. The nanoparticles are predominantly round and spherical, with a small dispersion of rough flakey particles. The round nanoparticles correspond to the metallic phases whereas the flakey particles are the NiO phase[132]. This agrees well with the XRD analysis indicating a small but notable oxide content.

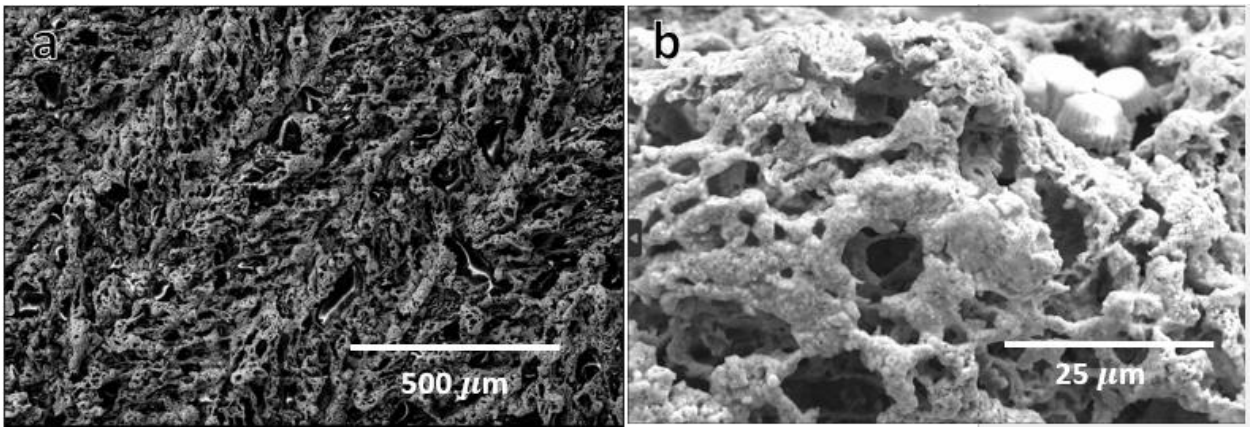

Figure 3-13 SEM images of Ni-Cu pattern at A) Low magnification B) High Magnification

EDAX mapping was done concurrently with SEM imaging to obtain a better representation of the dispersion of the elements within the sample. EDAX measurements were taken at an excitation voltage of 20 kV, and the energy resolution of the scans was 130 eV. A large area scan of the sample indicated that the sample had an atomic concentration ratio of 61% Nickel, and 39% copper. This agrees well with the ratio in the precursor solution of 60% Nickel and 40% copper. Figure 3.14 shows the EDAX concentration maps of Oxygen, Copper, and Nickel alongside the SEM secondary electron image of the region. It can be seen in figure 3.14b,c that the copper and nickel are predominantly uniform through the sample. However, there are some regions where a slightly higher concentration of nickel corresponds to a lower concentration of copper. This indicates that there is likely some fluctuation in elemental concentration within the deposited patterns. EDAX point analysis were conducted at regions identified as having non uniform metal concentrations, as shown in figure 3.15. It can be seen that the area that corresponds to higher nickel concentration also shows the rough flakey texture, and a higher than normal oxygen concentration. The changing atomic concentrations are outlined in table 3.5 This indicates that the regions of high nickel concentration are likely regions where nickel oxide is present. As well it can be seen that the area of higher copper concentration also corresponds to lower oxygen content. This indicates that the regions of higher copper content are likely regions where the pure metallic copper phase is present. These results agree well with the XRD analysis that indicates that the alloy phase is very homogenous, with its concentration largely predetermined by the concentration of the metal ions in the precursor, and variations in elemental dispersion likely being due to the inclusion of nickel oxide and metallic copper.

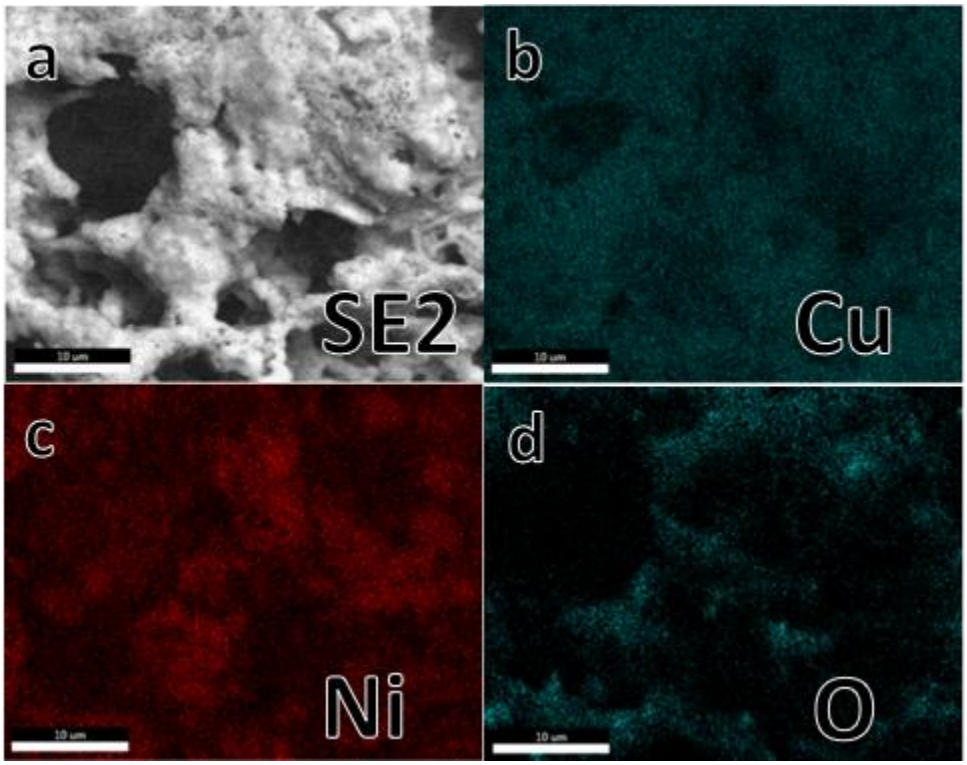

Figure 3-14 In-Situ EDAX measurements of atomic concentrations. A) SEM secondary electron image B). Copper atomic content C). Ni atomic Content. D) Oxygen content

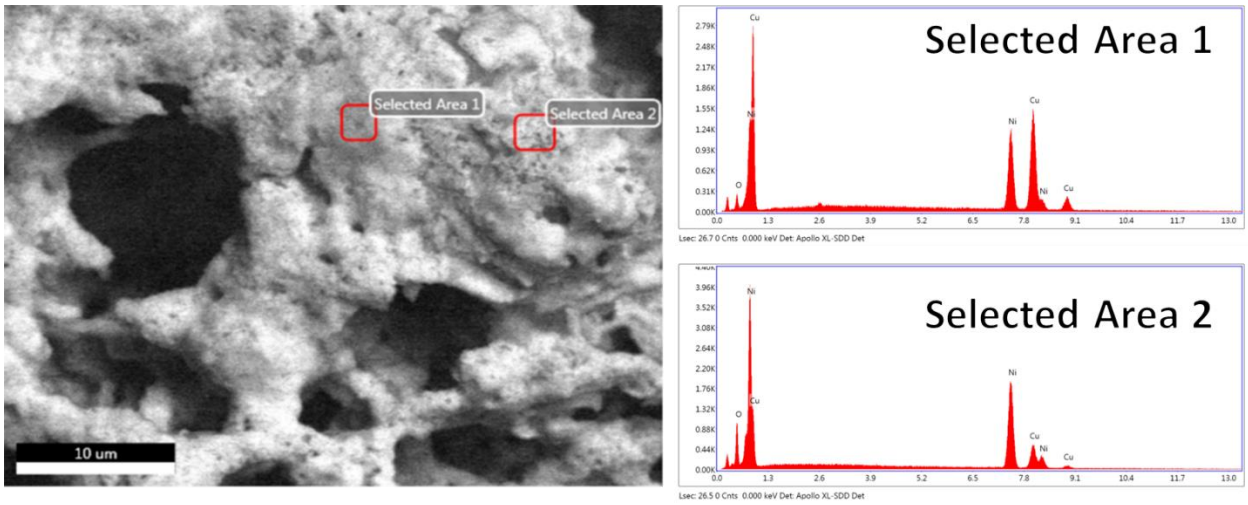

Figure 3-15 EDAX Point measurements of select areas on the Ni-Cu sheet

Table 3-5 Changing atomic concentrations in Ni-Cu alloys at different regions by use of EDAX elemental mapping

Region	Atomic %		
	Cu	Ni	O
Bulk	36	55	7
Select Area 1	56	36	2
Select Area 2	22	66	11

3.6 Summary

In summary direct laser writing was demonstrated successfully using a near infrared laser. Furthermore the characterization of copper patterns deposited using direct laser writing demonstrate a strong correlation between laser energy and chemical properties. It was shown that the photodegradation of the PVP in the precursor is largely responsible for chemical state of the deposited materials. It was shown that the aqueous precursor solvent could be substituted with IPA with minimal impact on the photodegradation of PVP. By using an alternative, alcohol-based precursor that was formed as a thick paste multi-layer patterns could be successfully deposited.

Direct laser writing of other metals was also demonstrated. It was shown that the reduction potential of a metal ion is a key factor in its suitability for direct laser writing. Metals with highly anodic reduction potential were not sensitive to changing laser conditions, and mostly deposited as oxides. Metals with intermediate reduction potentials showed a high sensitivity to changing laser settings. They could be selectively deposited as either metals or metal oxide by choosing appropriate laser settings. Metals with highly cathodic reduction potentials were tolerant to changing laser settings, and mostly deposited as metals.

Direct Laser writing of alloys was also demonstrated through the writing of Cu-Ni patterns. It was shown that alloy composition was largely homogenous and dependent on the composition of the precursor solution. The alloy patterns were shown to be highly sensitive to changing laser settings. At low laser settings atomic segregation became notable as the amount of the alloy phase decreased and separate metal and metal oxide phases increased. The composition of the alloy phase remained constant under changing laser settings.

Chapter 4
Direct Laser Writing of Memristors

4.1 Introduction

In this chapter several memristor devices fabricated through direct laser writing are presented and the resistive switching response of the devices are characterized. The impact of laser settings and device geometry on resistive switching is studied.

4.2 Planar Memristor

4.2.1 Properties of Planar Structure

Planar memristor patterns were printed onto polycarbonate sheets coated with aqueous copper precursor where a copper oxide rich region was printed between copper electrodes. For an initial prototype interdigital electrode pattern demonstrated in Figure 4.1a, was designed in order to maximize surface area between the Cu and Cu_2O regions. In this device both electrodes are metallic copper and the active layer is Cu_2O. Cu_2O has been previously shown to exhibit resistive switching effects through conductive filament formation [87].

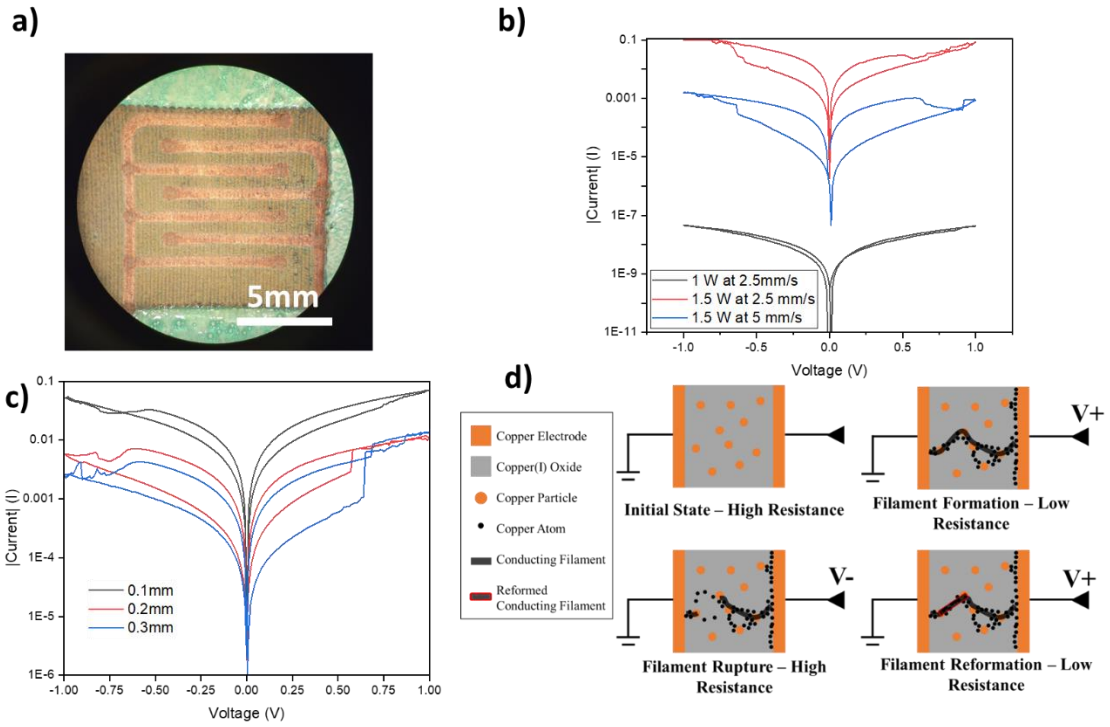

Figure 4-1 (a) An image of interdigital electrode pattern. (b) Current – Voltage loops of the devices with varying laser parameter settings for the Cu2O rich regions, and (c) varying widths of the Cu2O region. (d) A schematic of the filament formation in the Cu2O rich region.

All interdigital electrode patterns were printed in a single step to form integrated flexible planar Cu/Cu_2O/Cu structures, with separate laser settings used to print the copper rich conducting electrodes, and the Cu_2O rich inter-electrode regions. In all cases the laser settings used to print the conducting electrodes were constant, 3.5 W at 5 mm/s. The laser parameters used to print the inter-electrode regions were varied to observe the effect of changing Cu/Cu_2O content on the memristive characteristics. Three different laser settings (1.5 W at 2.5mm/s, 1.5 W at 5mm/s, and 1.0 W at 2.5mm/s) for the interelectrode regions were used to control the composition. After the writing of the interdigital patterns and subsequent removal of untreated precursor, an initial forming current is passed through the pattern. This forming step is necessary to determine the polarity of the device as the electrodes on either side of the oxide region are the same material, which means that the device has no inherent polarity. During the initial forming, the bulk of the conductive filament is formed in the orientation of the applied electrical

bias[62]. Once the conducting filament has been formed, applying subsequent electrical biases in the same orientation as the initial forming bias will support the migration of oxygen vacancies and copper defects to conducting filament. Applying an electrical bias in the opposite orientation will cause the migration away from the filament, eventually causing the filament to rupture [93]. Devices formed using either a positive or negative bias showed no notable differences in switching behavior.

After writing and forming the devices, all tests were run as a voltage sweep from 0 → +1V→-1V→0, the current compliance in the test was 100 μA. Figure 4.1b show the current - voltage (I-V) curves for the interdigital electrode patterns with varying laser settings for the Cu_2O rich region. The I-V curve changes dramatically in response to changing laser settings. When a direct voltage sweep was applied from 0 → 1 V to 0 V an increase in the current occurs at ~ 0.75 V for 1.5 W at 2.5mm/s and 1.5W at 5mm/s samples. The drop in resistance at this point marks the transition from the high resistance state (HRS) to the low resistance state (LRS) and is indicative of the successful formation of a conductive filament through the copper oxide region. When the voltage is swept from 0 V to -1 V and back to 0 V, a decrease in current is observed at ~ - 0.7 V. This indicates the device had been reset to its initial high resistance state, which corresponds to the rupturing of the conductive filament. In the sample fabricated at laser parameters of 1.0 W at 2.5mm/s the current ratio between the LRS and the HRS is less than 2, with no clearly defined distinction between the high resistance and low resistance states. At the 1.5 W at 2.5mm/s laser parameters the LRS/HRS current ratio is of 10^1. At the 1.5 W at 5mm/s laser parameters, the LRS/HRS current ratio was increased to 10^2.

4.2.2 Switching Mechanisms

When the devices switch between the HRS and LRS not only does the overall resistance of the device change, but the type of conduction in the device also changes. Figure 4.2 shows the change in the nature of the conduction between the LRS and HRS of a device printed at 1.5 W at 5mm/s. In the HRS as the voltage increases from 0.1 V to 0.5 V the current increases non-linearly, whereas in the LRS across the same voltage range the current increases linearly. The nonlinear conduction is indicative that in the HRS the device is conduction limited by a Schottky Barrier [133]. The Schottky barrier is present as in the absence of a conductive filament the current trough the device must cross from a conductor (the copper electrode) to a semiconductor (the copper oxide region). The linear conduction in the LRS is indicative that the device is experiencing Ohmic conduction, which confirms the that the conductive filament has formed from metallic copper.

The setting and resetting voltage of the device being 0.7V is a large benefit to the potential of the device in computing applications. There is a balance to be struck in ideal setting/resetting voltages. Setting voltages that are too high (e.g. in excess of 10V) will require high amounts of applied energy to switch the state of the device, this is not ideal for computing applications where reduction in energy consumption is the objective [5]. Setting voltages that are too low indicate instability of the LRS state, as the setting voltage is directly linked to the energy required to overcome the barrier to migration of the ions within the electrolyte[107]. A minimum energy barrier is required to prevent the ions from dissolving back into the bulk oxide immediately after being formed [80].

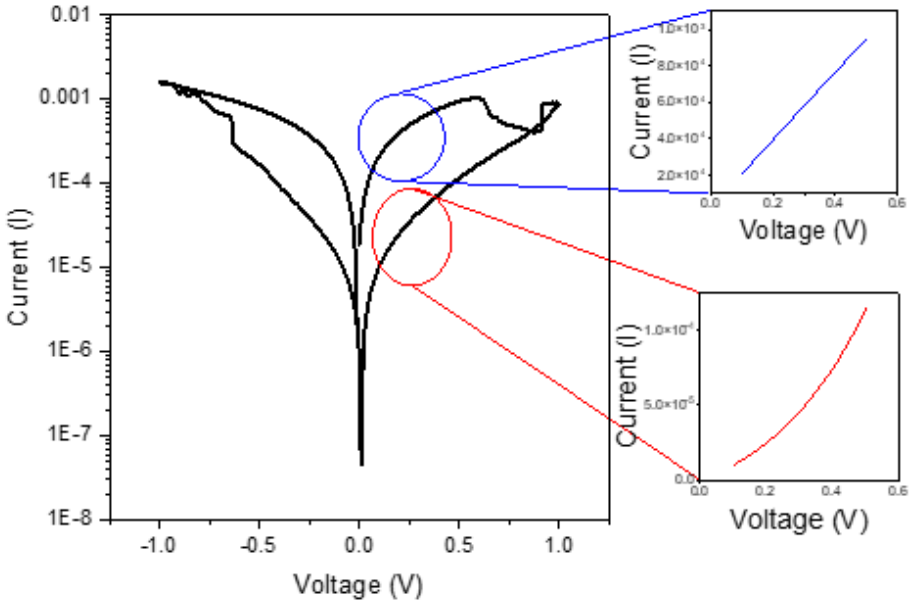

Figure 4-2 I-V curve of planar Cu/Cu_2O/Cu memristor pattern fabricated from direct laser writing. Inserts show the change in conductivity between the HRS and LRS.

In most cases of resistive switching in transition metals the active layer between the electrodes is on the order of nanometers as observed in literatures [98], [101], [119]. In the fabricated devices of this study the active layer is on the order of millimeters. It is likely that the presence of metallic copper in the Cu_2O region allows for easier filament growth by acting as intermediate electrodes for the filament to grow in a stepwise fashion linking the interspersed copper particles as indicated in Figure 4.1. To observe the effect of macroscopic electrode distance on the resistive switching effects interdigital electrodes were fabricated with Cu_2O interdigital regions ranging in distance from 0.1 – 0.3mm. For all

samples the Cu_2O region were deposited at the same laser settings of 1.5 W at 2.5mm s^{-1}. The I-V loop characteristics are presented in Figure 4.1c. Regardless of electrode gap spacing all samples showed the transition between the LRS and HRS at ~ 0.7V.

4.2.3 Stability of As-Written Planar Memristor

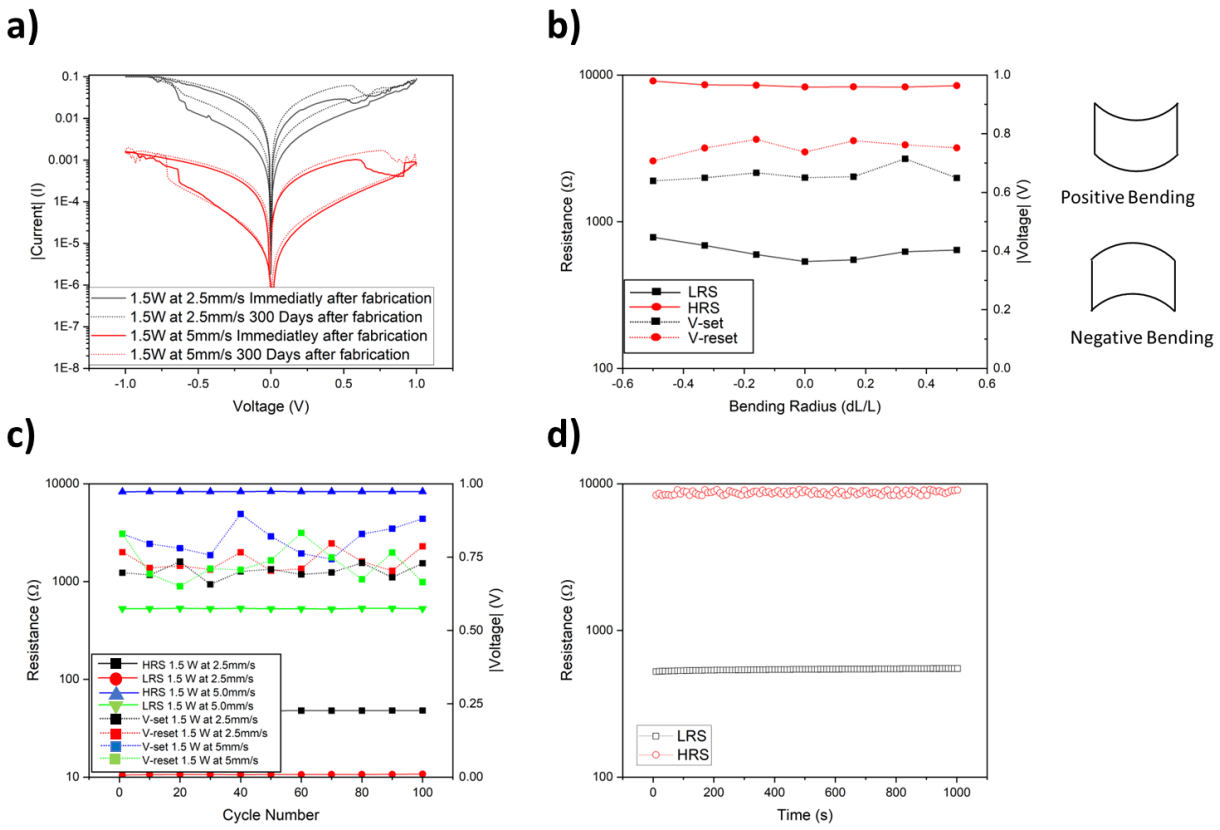

Figure 4-3 (a) Current-Voltage response of devices immediately after fabrication and after 300 days in storage. (b) Switching behaviour of a devices fabricated with a 1.5 W at 5mm/s laser setting under bending. (c) Endurance of devices across subsequent Current-Voltage sweeps. (d) Non-volatile memory retention of the LRS and HRS over time.

This as-written device shows a high degree of stability over time. Figure 4.3a compares the I-V response of devices tested immediately after fabrication, to the same devices tested after 300 days of storage in air. Devices were stored in a non-climate-controlled setting and were allowed to experience changes in ambient temperature and humidity. It can be seen that the resistive switching effect is preserved, with no obvious differences in the I-V response of the devices after 300 days. Effect of bending on memristive properties has also been investigated. A device fabricated using 1.5 W and 5 mm/s laser settings was tested under a series of bending conditions. Bending of the device was induced by compressing the flexible substrate laterally and allowing the device to flex either upwards or downwards. Bending intensity was measured as the change in sample width. At the most severe bending case the bending radius of the device was measured at 5mm. Figure 4.3b shows the effect of bending radius on the memristive response of devices. All bend tests were conducted at 22 ^{o}C and a relative humidity of 30%. The memristive response is stable across a wide range of applied bending from upwards or downwards. Downward bending tended to induce slightly higher increases in the resistivity of the device's LRS and HRS. This may be due to the tensile stresses incurred during downward bending being more prone to create cracks in the brittle copper oxide rich region, than the compressive stresses incurred during upward bending. Endurance tests with similar method reported in[80] were conducted on several devices, where the devices were subjected to 100 successive 0 → +1V→-1V→0 cycles. Figure 4.3c indicates that the resistance of the LRS and HRS remained constant in all devices across all the cycles. The setting and resetting voltages showed a high degree of variance during the test, typically ranging from |0.6| V to |0.8|V. However, no clear trend in setting or resetting voltages indicated that setting and resetting behaviour was also consistent across the test. The ability to retain different non-volatile resistance states of devices over time has been demonstrated in Figure 4.3d. A device fabricated at 1.5 W at 5mm/s laser settings was set to either the HRS or LRS and then subsequently 0.1 V pulses were applied once every ten seconds to measure the resistance of the device. Both the LRS and HRS of the device showed stability in resistivity over time, indicating that the devices can retain the different resistance states without the need for a constant external energy supply.

The temperature sensitivity of the device was also investigated. The current-voltage response of a device fabricated using 1.5 W at 5mm/s laser settings was measured at a range of temperatures from room temperature up to 100^{o}C. The I-V response of the device at elevated temperatures is demonstrated in figure 4.4. The as fabricated device was shown to have significant sensitivity to temperature with the I-V response of the device changing noticeably at temperatures as low as 40^{o}C. The conductivity of the

LRS drops at increasing temperatures, which can likely be attribute to the metallic nature of the conductive filament, as most metals show an increase in resistance at increasing temperature. Device behaviour becomes unstable above 80ºC, and at 100ºC practically no resistive switching effect is retained. The detrimental effects of temperature on the device were shown to be non-permanent, as after the device was allowed to return to room temperature the resistive switching behaviour of the device returned. However, it is worth noting that after heating the device required a reapplication of the electroforming step. This indicates that elevated thermal energy likely interferes with the conductive filament formation process, which has been noted in other works[80]. As well, it indicates that elevated temperature treatment may be a viable way to return devices to an initial un formed state, which may provide a strategy for fixing devices that show hard setting defects during electroforming.

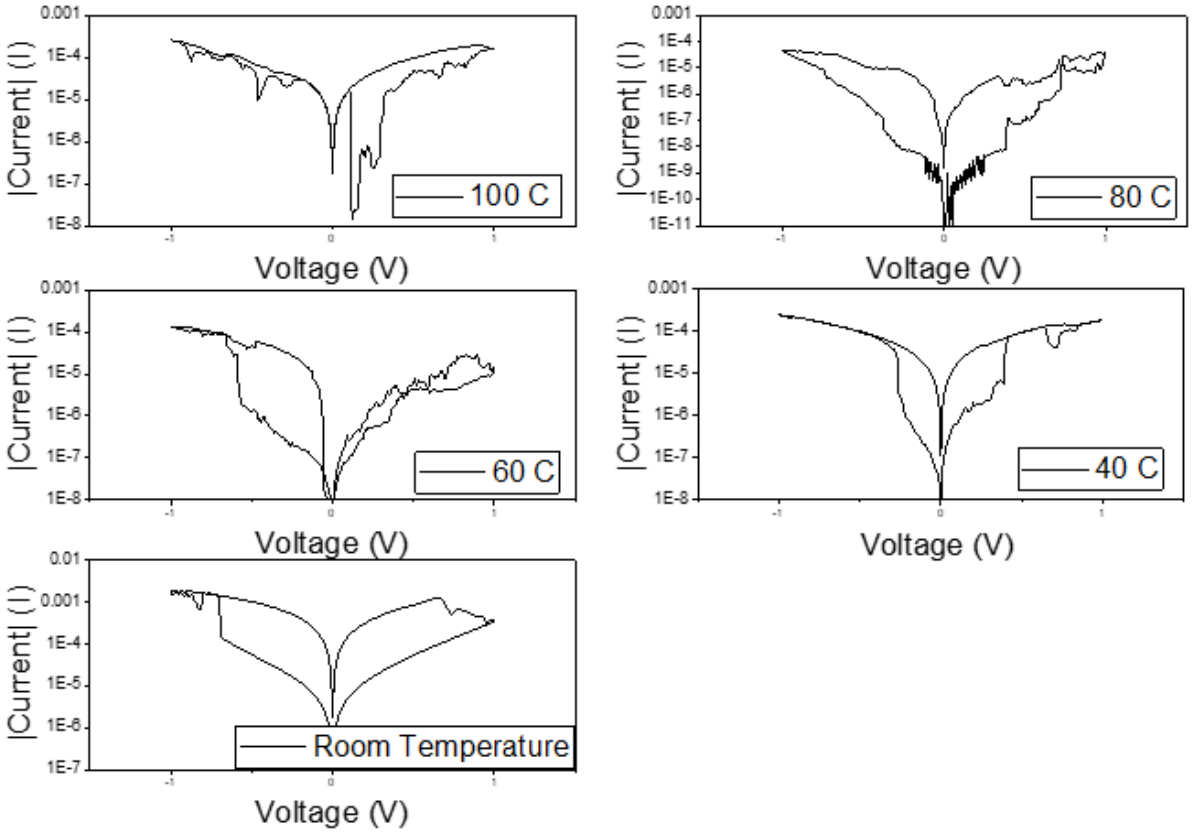

Figure 4-4 Changing I-V curves of a planar Cu/Cu_2O/Cu device fabricated at laser settings of 1.5W at 5mm/s when tested at elevated temperatures.

4.2.4 Rational Design of Planar Memristor

After the successful demonstration of using direct laser writing to fabricate flexible memristor devices in a rapid manner with inexpensive raw materials additional efforts where made to refine the design of the planar memristor devices. Several iterative designs of planar memristor patterns are outlined below. All designs retained the basic structure of a $Cu/Cu_2O/Cu$ planar pattern, but focused on reducing the size of the components. The resistive switching effect is retained in devices that are much smaller than the initial interdigital design. Several different patterns showed the ability to demonstrate resistive switching. The first pattern, called colinear uses a single laser path that varies the laser power across its length in order to deposit a copper oxide region between two metallic copper ends. The second pattern, called parallel, uses multiple laser passes to deposit a layer of copper oxide between two metallic copper layers. Figure 4.5 shows examples of the colinear and parallel memristor patterns along with I-V responses of several devices printed using each pattern.

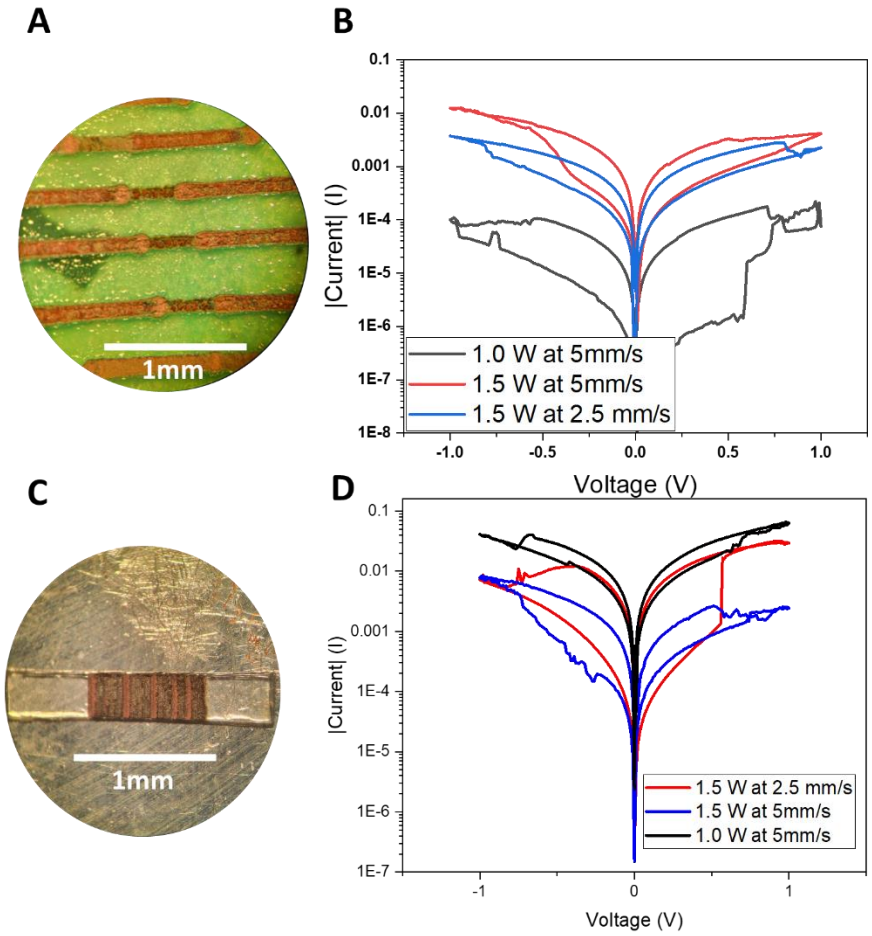

Figure 4-5 A) optical micrograph of colinear planar memristor pattern. B) I-V hysteresis response of colinear memristor patterns printed at changing laser settings. C) Optical micrograph of parallel planar memristor pattern. D) I-V hysteresis response of parallel memristor patterns with a fixed electrode distance of 0.1 mm and printed at changing laser settings

In all the colinear samples the laser power used to print the outside terminals of the patterns was 3.5 W at 10mm/s for all samples. The width of the copper oxide region was maintained at 0.2 mm in all samples. Samples printed using 1.0 W at 5mm/s , 1.5 w at 5mm/s, and 1.5 W at 2.5 mm/s laser settings for the copper oxide region were fabricated. Similar to the interdigital pattern the devices required a forming step in order to determine device polarity. The impact of laser settings on I-V hysteresis was very similar to the interdigital pattern. All devices displayed setting and resetting behaviour near to +/-

0.5 V, indicating that the applied bias needed to form a conductive filament in the colinear patterns was similar to that in the interdigital patterns. In the sample printed at 1.0 W at 5mm/s the ratio of HRS/LRS was 50. In the 1.5 W at 5 mm/s sample the ratio of HRS/LRS was 10. In the 1.5 W at 2.5mm/s sample the ratio of HRS/LRS reduced to 5. This shows a trend in increasing ratio in HRS/LRS as the energy density used to print the copper oxide region decreases.

In the parallel memristor patterns the laser power used to print the metallic copper was 3.5 W at 10 mm/s for all samples. Several different copper oxide region spacings were printed, however the samples showed the most consistent behaviour at a copper oxide spacing of 0.1mm. The I-V plots shown in Figure 4.5d all have copper oxide region spacings of 0.1mm. Samples printed using 1.0 W at 5mm/s , 1.5 w at 5mm/s, and 1.5 W at 2.5 mm/s laser settings for the copper oxide region were fabricated. Similar to the interdigital and colinear patterns the devices required a forming step in order to determine device polarity. All devices showed setting and resetting behaviour near to +/-0.5 V. In the sample printed at 1.5 W at 2.5 mm/s the ratio of HRS/LRS is 20. In the 1.0 W at 5mm/s and 1.5 W at 5mm/s samples the HRS/LRS ratios were determined to be close to 5.

Overall this indicates that the laser settings used to print the copper oxide region had a much larger effect on overall device resistance than the device geometry, indicating that direct laser writing has the potential to be a versatile method of producing a variety of planar memristor designs.

4.3 Fabrication of 3D Memristors

3D memristor patterns were deposited using direct laser writing of successive layers of alcohol based copper precursor pastes. Cu/Cu_2O/Cu memristor devices were fabricated from two layer patterns. The applied paste for both layers was set to 75 μm with the use of height setting shims. Both layers were printed at a laser setting of 3 W at 10mm/s. After the base layer was deposited the second layer of paste was allowed to sit on top the deposited pattern for 20minutes prior to laser treatment. This was done in order to have the acidic nature of the paste passively form a thin layer of copper oxide on the base layer through chemical corrosion.

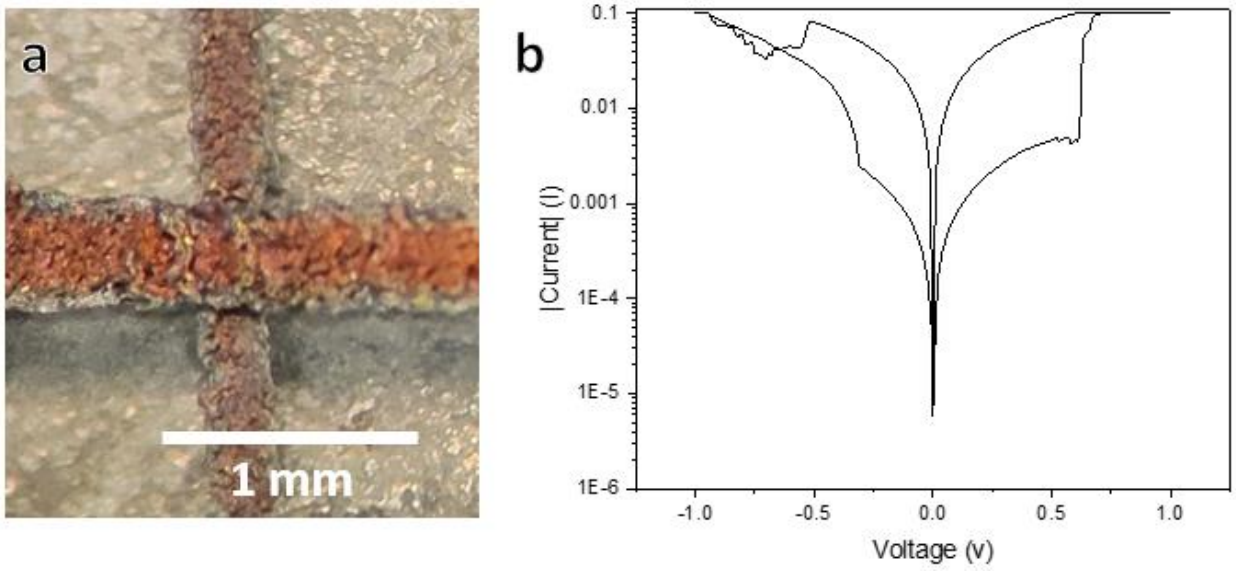

Figure 4-6 A). Optical Micrograph of 3D memristor device. B) I-V hysteresis response of 3D memristor device

The device showed bipolar memristor behaviour when tested under +/- 1V voltage sweeps. Figure 4.6 shows the I-V response of the device. The memristor response of the device is very similar to that of the planar patterns. Setting and resetting occurred near to +/-0.7 V, as well the conduction in the HRS is shown to be non-linear, and the conduction in the LRS is linear. This indicates that the filament formation mechanism in the 3D patterns is very similar to that in the planar patterns.

Subsequent 3D memristors were fabricated using 3 layer patterns. The applied paste for all three layers was set to 75 µm. The top and bottom layers were printed at laser settings of 3 W at 10mm/s, and the middle layer was printed at laser settings of 1 W at 10mm/s. This was done in order to create a thick Cu_2O layer between the top and bottom electrode. Figure 4.7 shows the 3 layer device and corresponding I-V response. The I-V response of the device differs dramatically from the previously fabricated devices. The device exhibited unipolar switching, being able to be set regardless of the polarity of the applied voltage bias The device shows a dramatically increased HRS/LRS. The HRS of the device is 500 MΩ and the LRS of the device is 5 KΩ. The LRS of the device was also very unstable, as soon as the applied current dropped below 0.25 V the device would reset to the HRS. While the mechanism contributing to this dramatic change in I-V response is not yet fully understood it provides

an illustrative example of the diverse memristor devices that could be fabricated using direct laser writing. This demonstrates that the I-V response of memristor devices fabricated using direct laser writing can be altered by using multi layer memristor patterns.

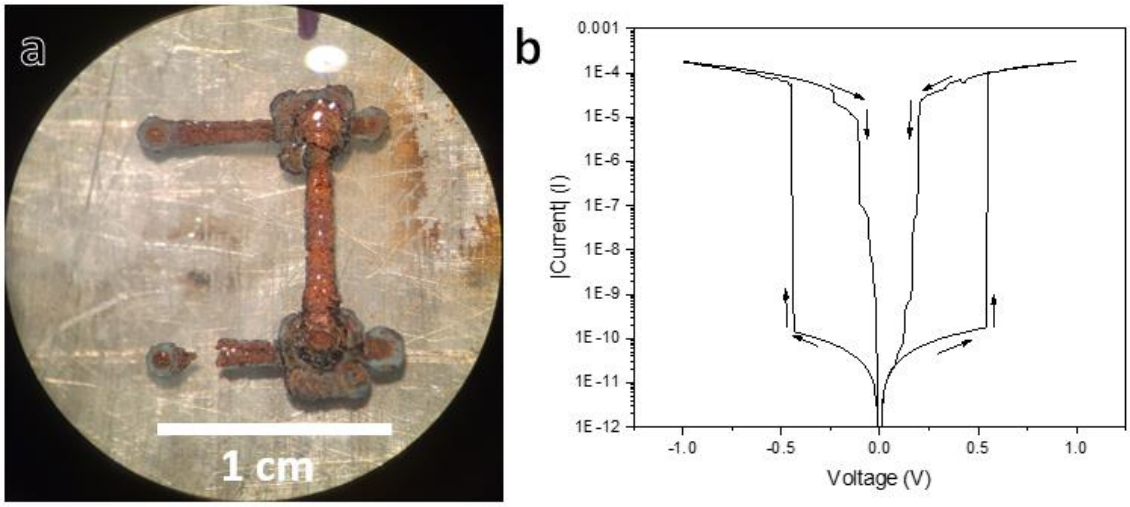

Figure 4-7 A) Optical micrograph of three layer 3D memristor pattern. B) I-V hysteresis response of the three layer 3D memristor device

It was also shown that memristor devices could be fabricated using laser brazing of copper wires with the copper precursor paste as the joining material. A small volume of alcohol based precursor paste would be applied between wires and laser irradiation is used to treat the paste to form a solid joint. Figure 4.8 shows 2 copper wires joined using copper precursor paste. The mechanical properties of the joint where very poor as low laser energy was used in order to encourage a joint with high copper oxide content. The I-V response of a copper wire joint formed at a laser setting of 1.5 W at 10mm/s is shown in figure 4.8. The memristive response of the joint shows high similarity to the memristor devices formed from planar and 3D direct laser written patterns, indicating that the filament formation that occurs in the sample with direct laser written electrodes is maintained when using the wires as electrodes. This may be a facile and low cost method of producing memristors using direct laser writing.

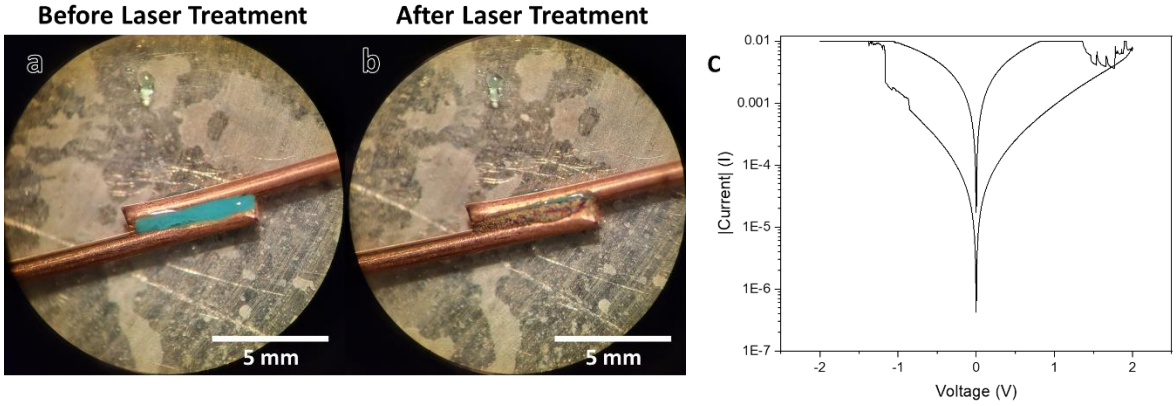

Figure 4-8 A,B) Optical micrographs of brazed copper wire memristor devices before and after laser irradiation. C) I-V Hysteresis response of wire-wire brazed memristor devices.

4.4 Summary

Direct laser writing was shown to be a facile and versatile method of fabricating memristor devices. Planar Cu/Cu_2O/Cu patterns were fabricated that demonstrated bipolar resistive switching at +/- 0.7 V. The transition from non-linear conduction in the HRS to ohmic conduction in the LRS indicates that conductive filament formation was responsible for the resistive switching effect. The resistivity of the devices in the HRS and LRS showed a high sensitivity to changing laser setting used to print the copper oxide regions of the device. Several different planar patterns were printed, it was shown that device geometry and size has minimal impact on the device performance. Patterns were shown to be stable over long periods of time and a range of bending states. 3D memristor patterns were also fabricated. It was shown that the switching effect demonstrated in the planar patterns was retained in the 3d patterns.

Chapter 5
Direct Laser Writing of Logic Structures with Memristors

5.1 Introduction

In this chapter several prototype logic structures are fabricated using direct laser writing. Planar Boolean logic gates are fabricated, and their signal processing characteristics are analyzed. Memristor cross bar arrays are fabricated and characterized. The effect of electrode material on memristor array performance and consistency is discussed.

5.2 Boolean Logic Gates

5.2.1 Fabrication of Logic Gates

Memristor based “And” and “Or” gates were fabricated from planar patterns of direct laser deposited copper and copper oxide from aqueous precursors. Parallel lines of copper and copper oxide were deposited at laser settings of 3.5 W at 10mm/s and 1.5 W at 5mm/s respectively. A UV laser was then used to selectively ablate copper material and leave patterns of two parallel memristor devices connected at one end through a copper region. The Fabrication procedure is outlined in Figure 5.1a, the fabricated memristor logic gates are displayed in Figure 5.1b. The fabrication of “And” and “Or” gates are nearly identical. The only difference is during the electroforming step where the polarity of the devices was set such the memristor devices were oriented towards or away from each other, in order to achieve either an “And” or “Or” gate.

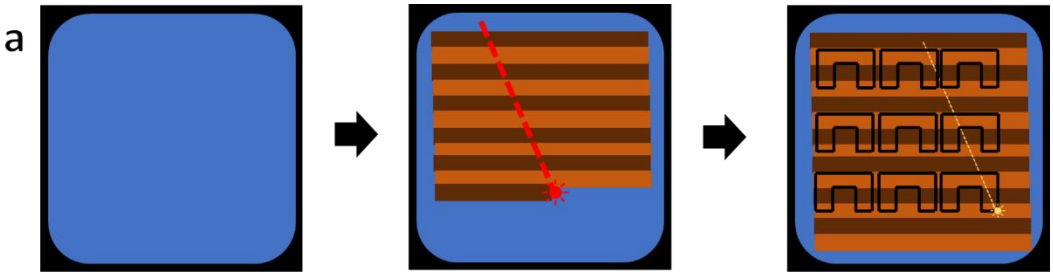
a

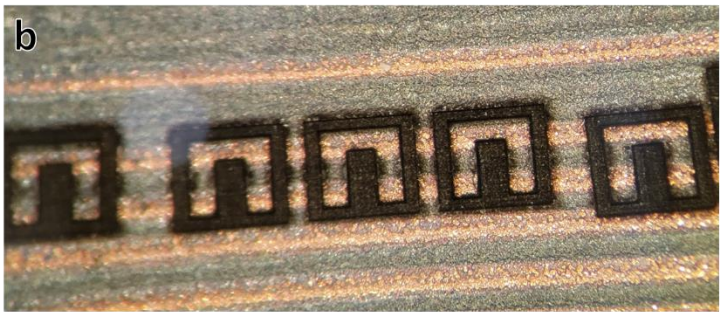
b

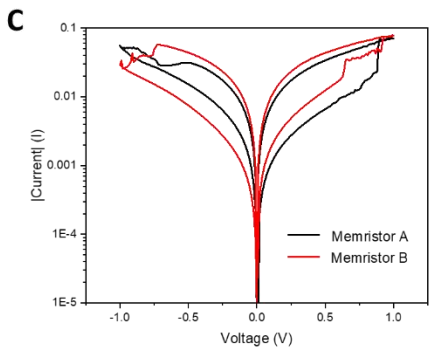
c
|Current| (I)
0.1
0.01
0.001
1E-4
1E-5
-1.0
-0.5
0.0
0.5
1.0
Voltage (V)
Memristor A
Memristor B

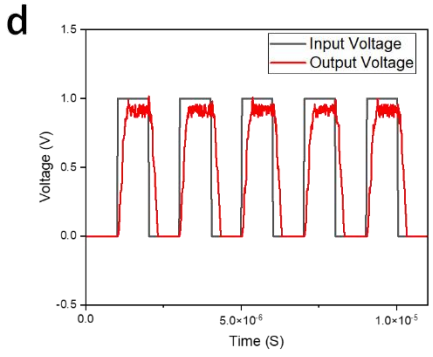
d
Input Voltage
Output Voltage
Voltage (V)
1.5
1.0
0.5
0.0
-0.5
0.0
5.0×10⁻⁶
1.0×10⁻⁵
Time (S)

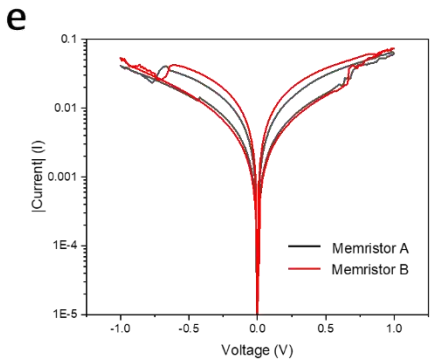
e
|Current| (I)
0.1
0.01
0.001
1E-4
1E-5
-1.0
-0.5
0.0
0.5
1.0
Voltage (V)
Memristor A
Memristor B

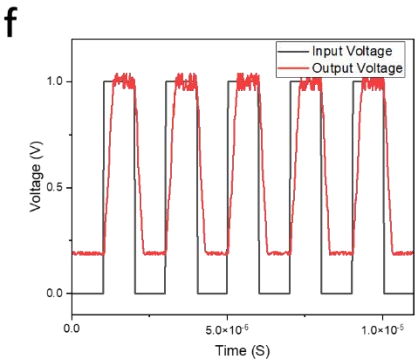
f
Input Voltage
Output Voltage
Voltage (V)
1.0
0.5
0.0
0.0
5.0×10⁻⁶
1.0×10⁻⁵
Time (S)

Figure 5-1 A) Schematic of memristor logic gate fabrication. B) Optical Micrograph of fabricated memristor logic gates. C) I-V hysteresis response of the memristor pair in the logic "Or" gate. D) Signal Processing delay of the logic "Or" gate. E) I-V hysteresis response of the memristor pair in the logic "And" gate. F) Signal Processing delay of the logic "And" gate

5.2.2 Logic "Or" Gate

The I-V response of the two memristors that comprised an "Or" gate device were characterized. Figure 5.1c shows the I-V hysteresis of both memristors in the device, it can be seen that the response of both devices is very similar. In device A the low and high resistance states are measured at 14 Ω and 130 Ω respectively. In device B the low and high resistance states are measured at 11 Ω and 100 Ω respectively. In both cases the ratio of HRS/LRS is about 10. The dynamic response of the or gate was measured. The voltage input at the B terminal was maintained at zero, and a square wave input signal was applied at the A terminal. The voltage potential at the copper region linking memristors A and B was read as the output voltage. The input signal had an amplitude of 1V and a period of 1E-6 seconds. This is done to simulate switching between the case where both inputs are zero, and the case where one input is zero and the other is one (where the device should output a value close to 1)

The time resolution of the test was 15 nanoseconds. Figure 5.1d shows the dynamic response of the or gate to the periodic input signal. The gate would take on average 350 ns to produce a stable output signal. The output signal of the gate was on average 0.91 V. This correlates to a signal degradation of 9% across the gate. Signal degradation is calculated as the difference between the input signal and output signal, divided by the input signal.

$$Signal\ Deg = \frac{\Delta V}{V_{in}} x\ 100$$

5.2.3 Logic "And" Gate

An "And" gate device was fabricated and the I-V response of the two memristors were characterized. Figure 5.1e shows the shows the I-V hysteresis response of both memristors in the device. In both devices the ratio of HRS/LRS is roughly 5. The dynamic response of the "And" gate as measured. The voltage input at the B terminal was maintained at 1V and a square wave input signal was applied at the A terminal. The input signal had an amplitude of 1V and a period of 1E-6 seconds. This is done to

simulate a switching between the case where both inputs are one (where the device should output a signal of one) and the case where one input is positive and the other is zero (where the device should output a signal of zero). The case where both inputs is zero is trivial, with no applied input there cannot be any output.

The gate would take on average 300 ns to produce a stable output signal, as shown in Figure 5.1f. The gate also showed a leak signal of about 0.2 V, this can be attributed to the low difference between the high and low resistance states. As discussed earlier the ability to produce a useable signal from a memristor based logic gate relies on a large difference between the high and low resistance state [112].

5.2.4 Logic "Control" Gate

A third control gate was fabricated similar to the "And" and "Or" gates. In this design the memristors in the device were set so that they had opposite polarities to each other. In this case any input signal will experience the first memristor prior to the output node in the low resistance state, as it travelling in the polarity that will set the device. It will then experience the second memristor just after the output node also in the low resistance state, as it is travelling in the polarity that will set the device. In essence in this device the memristors should show no difference in resistivity, the result being that the voltage drop across each memristor is identical, and therefor the output voltage should be half the input voltage. The memristor devices used in the control gate both showed similar I-V responses, with an HRS/LRS ratio of 10. In the control scenario the ratio between HRS and LRS will not affect the output as both devices will be set to the LRS The dynamic response of the control gate was measured. The voltage input at the B terminal was maintained at 0V and a square wave input signal was applied at the A terminal. As expected the device had an output near to 0.5 V when an input signal was applied. This confirms that the signal processing that fabricated devices are exhibiting is a product of the memristive switching within the two terminals of the device.

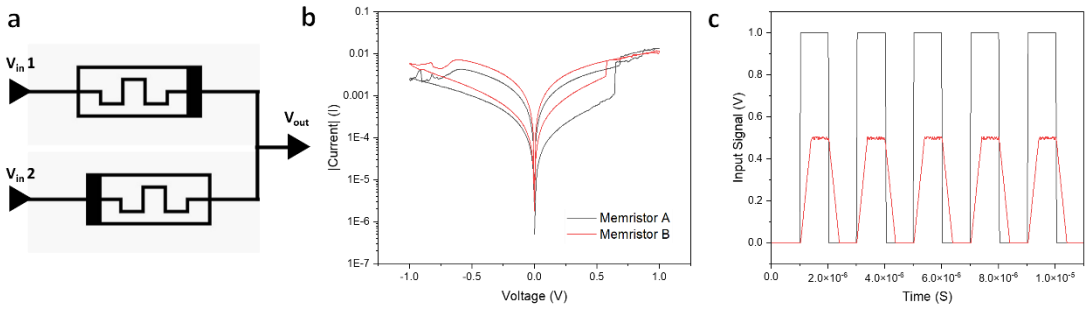

Figure 5-2 A) circuit diagram of the logic "Control" Gate B) I-V hysteresis response of the memristor pair in the logic control gate. C) Signal Processing of logic Control Gate

5.3 Crossbar Logic Structure

5.3.1 Cu/Cu_2O/Cu Crossbar Arrays

Several cross bar arrays were fabricated using direct laser writing of metal salt solutions using a range of precursors and laser settings. The effect of electrode material and laser settings on I-V response, device retention, and device consistency were observed.

A 10 x 10 cross bar array of Cu/Cu_2O/Cu memristors was fabricated using alcohol-based copper precursors. The patterns were printed in a two layer configuration, the applied paste for both layers was set to 75 µm with the use of height setting shims. Both layers were printed at a laser setting of 3.5W at 10mm/s. After the base layer was deposited the second layer of paste was allowed to sit on top the deposited pattern for 20minutes prior to laser treatment. Of the 100 fabricated nodes one third were sampled at random to establish device consistency. Of the 33 sampled nodes 12 displayed a consistent resistive switching response. The samples that did show resistive switching had consistent setting and resetting behaviour. All samples displayed bipolar switching behaviour with set and reset voltages occurring between 0.4 – 0.6 V. A high degree of variance in the high and low resistance states of the nodes can be observed. In most cases the ratio of HRS/LRS is roughly 10, with the LRS exhibiting a resistance between 40 – 100 Ω and the HRS exhibiting a resistance between 500 – 1000 Ω. However, several nodes demonstrated much higher HRS and LRS values, on the order of 100 times that of the rest of the functional nodes. This indicates that further work is needed to improve the reliability and consistency of fabricating cross bar arrays using Cu/Cu_2O/Cu patterns.

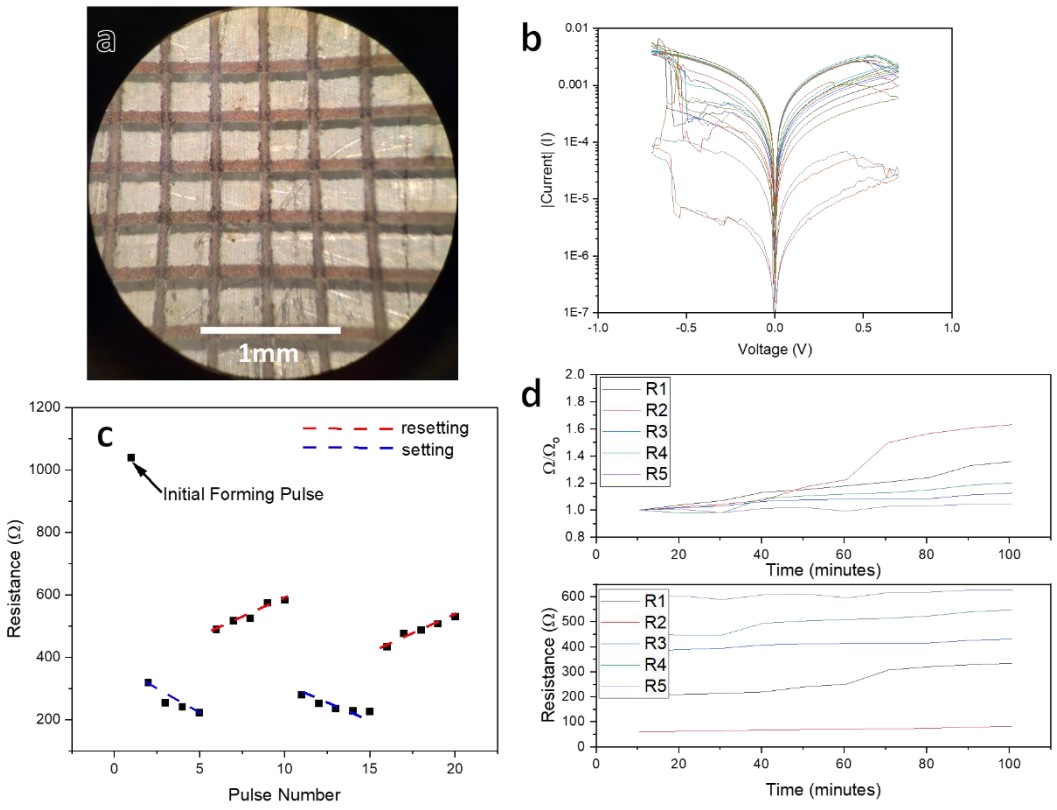

Figure 5-3 A) Optical Micrograph of Cu/Cu2O/Cu memristor array. B) I-V hysteresis responses of the successful nodes in the array. C). Read Write test results of Cu/Cu2O/Cu memristor showing multiple programmable resistance states. D) Non-volatile retention of the multiple resistance states of a Cu/Cu2O/Cu device

The devices fabricated in the array successfully showed the ability to be programmed to multiple intermediate resistance states between the HRS and LRS through the use of "read-write" tests. A "read-write" tests refers to a method of measuring the dynamic response of a memristor device. It is comprised of a sequence of short pulses intended to incrementally change the resistance of the device. A schematic of a typical "read-write" test is shown in Figure 5.4 Writing pulses refer to voltage pulses with amplitudes equal to or greater than the setting/resetting voltage of the device, these are intended to affect a change in overall device resistance. They are analogous to changing or writing new data into a

memory unit, hence the term writing pulse. Reading pulses refer to voltage pulses with amplitudes significantly less than the setting/resetting voltage of the device. They are intended to measure the resistance of the device without affecting a change in the resistance state. They are analogous to reading the information stored in a memory unit, hence the term reading pulse.

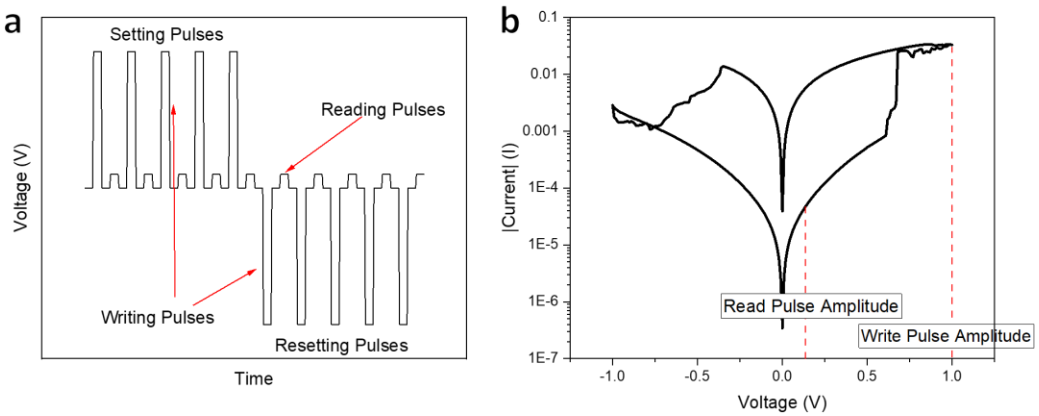

Figure 5-4 A) Schematic diagram of read-write pulse test schedule B). Typical I-V hysteresis of a bipolar memristor, with suitable voltage amplitudes for read write test pulses highlighted

Writing pulses of +/1 V for 100ns were used to incrementally set and reset the resistances of the device. Sequences of 5 setting pulses followed by 5 resetting pulses were used to observe the ability to select for multiple resistance states. The incremental setting and resetting behaviour of the device was very consistent. The first setting or resetting pulse in the sequence would affect the greatest change in overall device resistance, and subsequent pulses of the same orientation would affect incremental changes. Typically, the first pulse in a sequence would affect a change in resistance of about 300 - 400 Ω, and subsequent pulses would affect changes of about 25 Ω. This indicates that the bulk of the conductive filament formation / disruption is occurring in the first pulse. This rapid programming time can likely be attributed to the low energy barrier to cation migration seen in copper oxides [96], allowing for rapid movement of coper ions to form the conductive filament. The sintered nanoparticle microstructure may also contribute to the rapid response time of the device. The nanostructured microstructure provides an

abundance of grain boundaries, which are areas of low atomic packing density [134]. These provide pathways where the energy barrier to ion migration is further reduced, allowing high ion mobility.

The retention of the multiple resistance states was measured in order to observe the volatility of the multiple resistance states. The device would be set to a resistance state through incremental pulses and then a read pulse would be applied once every ten minutes to monitor the change in resistance over time. Five resistance states, ranging from 100 Ω to 600 Ω were set and tested. The results of the memory retention tests are shown in figure 5.3, it can be seen that overall the device showed a high degree of retention of the different memory states. Overall as the resistance state increased the more stable the device performed. This can be attributed to the conductive filament, which contributes to the lower resistance state, being unstable and degrading over time. Overall this demonstrates that memristor devices fabricated from direct laser writing having the potential to act as non-volatile memory.

5.3.2 Ag/Cu_2O/Cu Crossbar Arrays

The effect of electrode material on the consistency of the nodes in the cross bar array was analyzed by fabricating a subsequent array with a silver base layer. The filament formation in coper oxide is shown to be cation controlled, as evidenced by the ohmic conduction of the LRS. As a result the electrode material is known to have significant impacts on filament formation through affecting the oxidation and reduction processes that occur at the electrode surface during filament formation [90]. The electrodes can directly participate in filament formation by acting as a charge carrier path in the metal ion redox reaction [90]. If there is a low charge carrier migration rate then a depletion of charge near the anode can inhibit formation of the conductive filament [90]. The vacancy formation energy (i.e. the energy required to extract oxygen atoms from the electrode) is also a key component of electrode performance, as it is necessary to generate oxygen atoms at the electrode-oxide interface to support the redox reactions of metal ions in the conductive filament [90]. Silver is a popular choice as electrode material in memristor devices due to its low vacancy formation energy [76]. As such a subsequent cross bar array was fabricated using a silver base layer in order to improve the consistency and performance of the cross bar arrays.

A 20 x 5 cross bar array of Ag/Cu_2O/Cu memristors was fabricated using direct laser writing of aqueous silver precursor as a base layer, and an alcohol based copper precursor for the second layer, as shown in Figure 5.5a. The silver layer was printed at a laser setting of 3.5 W at 5mm/s. The thickness of the copper layer was set to 100 µm, and the copper was deposited at a laser setting of 2 W at 10mm/s. Of the 100 nodes 25 were randomly selected for testing and 18 demonstrated a consistent resistive switching response. Of the nodes that did fail they typically showed one of two main types of defects, shown in figure 5.5c. Most of the nodes that failed exhibited hard setting behaviour, i.e. the device would be permanently set to the low resistance state during the electroforming step and fail to reset to the high resistance state. Several nodes also exhibited successful resistive switching for several cycles before being permanently set to the high resistance state. This may be attributed to premature disruption of the conductive filament due to joule heating of the filament [101]. Once the conductive filament is formed the vast majority of the current flowing through the device flows through the conductive filament, as electricity will naturally take the path of least resistance. Since the width of the filament is typically 10 of nanometers in scale, even low currents can lead to high current densities within the filament and high joule heating, which can lead to premature burn out of the filament [101]. To address this issue a current compliance limit of 10 µA was set for most of the I-V characterization tests of the devices in the array. Once the compliance limit was instituted the instances of premature filament disruption stopped. This indicates that the stability of the devices fabricated in this array have a high sensitivity to current density.

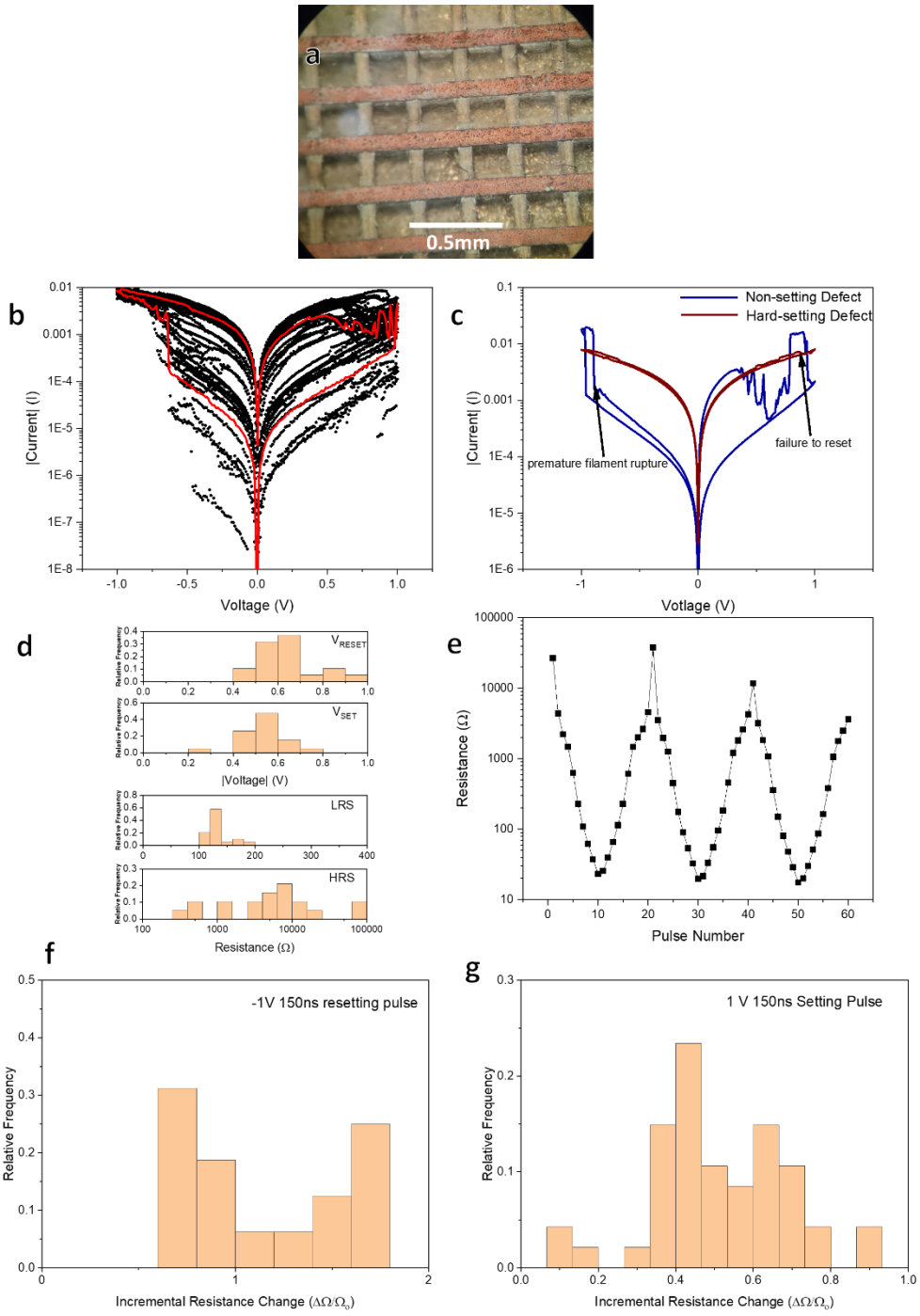

Figure 5-5 A) Optical Micrograph of Ag/Cu_2O/Cu array. B) Point cloud of I-V response of memristor devices within the Ag/Cu_2O/Cu array with a representative I-V response outlined in red. C) I-V Reponses of non-setting defect and Hard setting defect. D)

Histogram distributions of Vset, Vreset, HRS and LRS of memristors within the Ag/Cu_2/Cu array. E) Read Write test results of Ag/Cu_2O/Cu memristor device showing multiple programmable resistance states. F) Histogram distribution of the resistance change in response to resetting pulses. G) Histogram distribution of the resistance change in response to setting pulses

All of the nodes tested displayed consistent bipolar switching behaviour. There was highly consistent switching behaviour across all tested nodes, shown in figure 5.5b. Typical setting and resetting voltage occurring at +/- 0.6 V. The resistivity of the low resistance state was also highly consistent across all the nodes, with the average resistivity being 125 Ω. The resistance of the high resistance state varied more significantly. Most devices demonstrated a resistance of approximately 8000 Ω – 20000 Ω, with some devices showing resistance as low as 500 Ω or as high as 100000 Ω. This may be able to be attributed to semi-hard setting of the devices during electroforming. Semi hard setting is a defect very similar to hard setting, varying only in that some degree of resistive switching is maintained in the device. Typically this takes the form of an unaffected low resistance state, and a reduction of resistance in the high resistance state [83]. As discussed previously the device showed high sensitivity to hard setting defects, the consistency of the low resistance state, and high variation in the high resistance state all support the theory that semi hard setting may be responsible for the high variation in device performance. Figure 5.6 shows a Ag/Cu_2O/Cu device that exhibited semi hard setting. In the device the initial HRS of the device is 100 kΩ, after the forming the HRS of the device resets to 1 kΩ, which is maintained upon subsequent passes. The LRS of the device is unaffected by the semi hard setting.

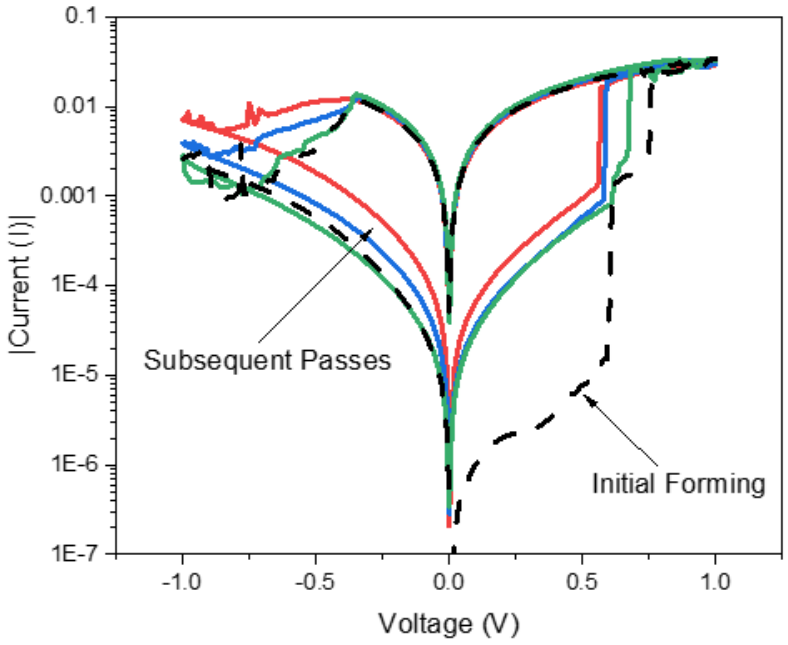

Figure 5-6 Semi Hard setting defect in Ag/Cu_2O/Cu memristor as seen through the change in the HRS of the device across multiple voltage sweeps

The devices in the Ag/Cu_2O/Cu array showed the ability to be successfully programmed to multiple intermediate resistance states through read writing tests, as shown in figure 5.5e. Writing pulses of +/- 1V for 150 ns were used to in incrementally change the resistance of the device. Sequences of 10 setting pulses followed by 10 resetting pulses were used to demonstrate the ability to select for intermediate resistance states. The device showed consistent incremental setting and resetting characteristics. The change in resistivity of a setting or resetting pulse shows strong dependence on the initial resistance of the device. During setting the average incremental change in resistance was shown to be a reduction in resistance of about 50 percent of the initial resistance. During resetting the average incremental change was shown to be an increase of about 100 percent of the initial resistance. The resetting showed more variability in incremental resistance change than setting. The device showed a low degree of non volatile memory retention. Typically the low resistance state was only sustained for several seconds before degrading, making it hard to accurately monitor.

The increased HRS/LRS ratio, and improved device consistency of the Ag/Cu_2O/Cu cross bar array over the Cu/Cu_2O/Cu array demonstrates that the performance of the device is heavily dependent on the choice in electrode materials.

5.4 Summary

Memristor based logic structures were successfully fabricated using direct laser writing. Boolean logic "And" and "Or" gates were fabricated from planar patterns. The Boolean gates demonstrated rapid response times of approximately 300 ns to input signals. Moderate signal degradation was observed in the logic gates due to the moderate differences between the HRS and LRS of the memristors in the devices.

Cross bar memristor arrays were successfully fabricated using hierarchical patterns. A Cu/Cu_2O/Cu crossbar array was fabricated. Moderately consistent resistive switching behavior was observed between memristor nodes in the array. Nodes within the array demonstrated multiple resistance states that could be programmed using ultra short voltage pulses. The ultra fast programming of the device was attributed to high ion mobility within the copper oxide region. The multi level resistance of the device was shown to be non-volatile and stable over a period of over an hour.

An Ag/Cu_2O/Cu crossbar array was fabricated in order to observe the effect of electrode material on device performance. It was demonstrated that the silver electrode improve device consistency and increased the average HRS/LRS ratio of the nodes within the array. This was attributed to Silver's highly beneficial properties for enabling the redox reactions that form the conductive filament. However, the device also showed an increased sensitivity to several types of defects over the Cu/Cu_2O/Cu array. Namely hard setting and semi-hard setting defects. The sensitivity to semi hard setting defects lead to a high degree of variability in the HRS of the memristors within the device. Nodes within the array also demonstrated multiple resistance states that were programmable through ultra short voltage pulses. The larger difference in resistivities between the HRS and LRS of the device enabled more intermediate resistance states to be observed. The device showed very consistent setting and resetting behaviour. However device volatility increased significantly, and the low and intermediate states of the device were only maintained for several seconds or less.

Chapter 6
Conclusion

6.1 Conclusion

The objective of this thesis was to explore the use of direct laser writing for fabrication of inexpensive electronics components. Successful fabrication of flexible memristor devices and prototype memristor logic hardware indicate that direct laser writing has potential as a viable method for flexible electronics fabrication. Furthermore, direct laser writing was demonstrated as a versatile process through the successful fabrication of a wide range of different memristor patterns, including planar, 3D, and wire-wire joining.

Direct Laser writing was proven as a viable process when using a laser in near infrared wavelengths. The relationship between the photodegradation of PVP and chemical state of the deposited metal patterns was studied through depositing copper patterns at a range of changing laser parameters. The process window is defined at the upper limit by high laser energy damaging the substrate material, and at the lower limit by insufficient laser energy leading to poor material deposition. Lower laser energy leads to copper oxide patterns through incomplete degradation of PVP limiting the amount of formic acid available to reduce the copper ions. High laser energy ensure complete degradation of PVP and an abundance of formic acid, leading to metallic patterns. This relationship is preserved when substituting aqueous precursor solvent with IPA solvent. A thick precursor paste could be formulated from a highly concentrated IPA based precursor that enabled the fabrication of multi layered patterns. Other metal salt precursors were treated in order to determine the suitability of direct laser writing for depositing a range of metal patterns. It was shown that the reduction potential of the metal ion is key in determining suitability for direct lase writing. Highly anodic metal ions were most likely to be deposited as metal oxides regardless of laser settings. Highly cathodic metal ions were most likely to be deposited as metals regardless of laser settings. Metals with intermediate reduction potentials showed a high sensitivity to laser settings and could be selectively deposited as either metals or metal oxides.

A series of $Cu/Cu_2O/Cu$ memristor were fabricated using direct laser writing. Planar patterns printed onto flexible substrates demonstrated consistent bipolar resistive switching at voltages near to +/- 0.7 V through the formation of a conductive filament. The resistive switching showed a high sensitivity to the laser settings used to print the copper oxide region. HRS/LRS ratios as high as 10^2 could be achieved

through tuning the laser settings. The devices were shown to be tolerant over a large range of bending strains and a long period of time. The resistive switching effect was shown to be highly tolerant to changes in device geometry and size. 3D patterns fabricated from multiple layered patterns demonstrated similar resistive switching effects to the planar patterns. The resistive switching effect was shown to be highly sensitive to the addition of interlayers in the 3D pattern.

Prototype memristor logic structures were fabricated with direct laser writing. Boolean "And" and "Or" gates were fabricated from planar patterns of memristor pairs. The devices showed rapid signal processing, being able to process input signals in approximately 300 ns. Moderate leak current and signal degradation was noted in the logic gates, which was attributed to the moderate differences between the HRS and LRS of the memristor pairs. Cross bar memristor arrays were fabricated and characterized. $Cu/Cu_2O/Cu$ memristor array showed a high failure rate of nodes within the matrix. The nodes that were stable demonstrated a moderate degree of variability. The ability to program different resistance states was demonstrated through the use of ultra short voltage pulses. Applied pulse times as short as 100ns were sufficient to affect significant change in the device resistance state. The device showed non-linear programming behavior, with initial voltage pulses affecting the greatest change in resistance and subsequent pulses affecting marginal changes in resistance. An $Ag/Cu_2O/Cu$ cross bar array was fabricated an characterized. The inclusion of a silver electrode decreased the failure rate of nodes in the array. The HRS/LRS of the device also increased through the use of a silver electrode. The $Ag/Cu_2/Cu$ array also showed the ability to program intermediate resistance states, with 150ns pulses being sufficient to affect a change in device resistance. The programming behaviour of the device was shown to be highly consistent. The $Ag/Cu_2O/Cu$ array also showed a higher sensitivity to hard setting and semi hard setting defects which led to a high degree of variability in the HRS of the memristors.

6.2 Future Work

There are several potential research directions in the field of direct laser written electronics. Further research into finding strategies that enable the deposition of a broader range of metals should focus on identifying suitable reduction agents with higher reduction potentials to enable the deposition of highly anodic metal ions. As the range of materials that can be deposited by direct laser writing expands so does the versatility and potential usefulness of the process.

Lasers with smaller spot sizes should be utilized in order to produce devices that are smaller and have finer features. This will help demonstrate the viability of direct laser writing as a process that has

relevance to modern electronics. Optimization of laser settings for copper oxide based memristor devices will provide logic gates with lower leak currents / signal degradation. As well direct laser writing may be a suitable process for depositing a range of metal oxide materials for metal oxide based resistive switching devices. Since the metal oxide is of primary interest for the switching layer, the ability to produce metallic patterns may be of secondary importance.

The devices fabricated in this work showed high sensitivity to material changes at the electrodes or in the switching layer. Further work should be done to identify ideal combinations of electrodes and metal oxides to further improve the performance of the fabricated memristors.

References

[1] S. Al-Fedaghi and A. Hassouneh, “Modeling the Engineering Process as a Thinging Machine: A Case Study of Chip Manufacturing,” in *Cybernetics and Automation Control Theory Methods in Intelligent Algorithms*, Cham, 2019, pp. 67–77. doi: 10.1007/978-3-030-19813-8_8.

[2] M. M. M. SARCAR, K. M. RAO, and K. L. NARAYAN, *Computer Aided Design and Manufacturing*. PHI Learning Pvt. Ltd., 2008.

[3] J. F. Ziegler *et al.*, “IBM experiments in soft fails in computer electronics (1978–1994),” *IBM J. Res. Dev.*, vol. 40, no. 1, pp. 3–18, Jan. 1996, doi: 10.1147/rd.401.0003.

[4] S. Logothetidis, *Handbook of flexible organic electronics: materials, manufacturing and applications*. Waltham, MA: Woodhead Pub, 2014.

[5] A. Thomas, “Memristor-based neural networks,” *J. Phys. Appl. Phys.*, vol. 46, no. 9, p. 093001, Feb. 2013, doi: 10.1088/0022-3727/46/9/093001.

[6] K. Lawrence, *“Chipageddon”: What the Global Chip Drought Means for Manufacturing and Supply Chains*. London, 2021. doi: 10.4135/9781529789683.

[7] M. Mirshojaeian Hosseini and R. Nawrocki, “A Review of the Progress of Thin-Film Transistors and Their Technologies for Flexible Electronics,” *Micromachines*, vol. 12, no. 6, p. 655, Jun. 2021, doi: 10.3390/mi12060655.

[8] J. Kim, T.-I. Lee, J. Shin, T.-S. Kim, and K. Paik, “Bending Properties of Anisotropic Conductive Films Assembled Chip-in-Flex Packages for Wearable Electronics Applications,” *IEEE Trans. Compon. Packag. Manuf. Technol.*, pp. 208–215, 2016, doi: 10.1109/TCPMT.2015.2513062.

[9] T. Someya, T. Sekitani, S. Iba, Y. Kato, H. Kawaguchi, and T. Sakurai, “A large-area, flexible pressure sensor matrix with organic field-effect transistors for artificial skin applications,” *Proc. Natl. Acad. Sci.*, vol. 101, no. 27, pp. 9966–9970, Jul. 2004, doi: 10.1073/pnas.0401918101.

[10] T. Loher, M. Seckel, B. Pahl, L. Bottcher, A. Ostmann, and H. Reichl, “Highly integrated flexible electronic Circuits and Modules,” in *2008 3rd International*

Microsystems, Packaging, Assembly Circuits Technology Conference, Oct. 2008, pp. 86–89. doi: 10.1109/IMPACT.2008.4783814.

[11] K. D. Harris, A. L. Elias, and H.-J. Chung, “Flexible electronics under strain: a review of mechanical characterization and durability enhancement strategies,” *J. Mater. Sci.*, vol. 51, no. 6, pp. 2771–2805, Mar. 2016, doi: 10.1007/s10853-015-9643-3.

[12] R. Saleh, M. Barth, W. Eberhardt, and A. Zimmermann, “Bending Setups for Reliability Investigation of Flexible Electronics,” *Micromachines*, vol. 12, no. 1, p. 78, Jan. 2021, doi: 10.3390/mi12010078.

[13] J. Y. Oh *et al.*, “Intrinsically stretchable and healable semiconducting polymer for organic transistors,” *Nature*, vol. 539, no. 7629, pp. 411–415, Nov. 2016, doi: 10.1038/nature20102.

[14] J. Ryu, H.-S. Kim, and H. T. Hahn, “Reactive Sintering of Copper Nanoparticles Using Intense Pulsed Light for Printed Electronics,” *J. Electron. Mater.*, vol. 40, no. 1, pp. 42–50, Jan. 2011, doi: 10.1007/s11664-010-1384-0.

[15] Z. Yin, C. Lee, S. Cho, J. Yoo, Y. Piao, and Y. S. Kim, “Facile Synthesis of Oxidation-Resistant Copper Nanowires toward Solution-Processable, Flexible, Foldable, and Free-Standing Electrodes,” *Small*, pp. 5047–5052, Aug. 2014, doi: 10.1002/smll.201401276.

[16] X. Song, S. Yang, Z. Huang, and T. Huang, “The Application of Artificial Intelligence in Electronic Commerce,” *J. Phys. Conf. Ser.*, vol. 1302, no. 3, p. 032030, Aug. 2019, doi: 10.1088/1742-6596/1302/3/032030.

[17] G. Zeba, M. Dabić, M. Čičak, T. Daim, and H. Yalcin, “Technology mining: Artificial intelligence in manufacturing,” *Technol. Forecast. Soc. Change*, vol. 171, p. 120971, Oct. 2021, doi: 10.1016/j.techfore.2021.120971.

[18] K.-H. Yu, A. L. Beam, and I. S. Kohane, “Artificial intelligence in healthcare,” *Nat. Biomed. Eng.*, vol. 2, no. 10, Art. no. 10, Oct. 2018, doi: 10.1038/s41551-018-0305-z.

[19] N. C. Eli-Chukwu, “Applications of Artificial Intelligence in Agriculture: A Review,” *Eng. Technol. Appl. Sci. Res.*, vol. 9, no. 4, pp. 4377–4383, Aug. 2019, doi: 10.48084/etasr.2756.

[20] X. Zhai *et al.*, “A Review of Artificial Intelligence (AI) in Education from 2010 to 2020,” *Complexity*, vol. 2021, p. e8812542, Apr. 2021, doi: 10.1155/2021/8812542.

[21] R. Abduljabbar, H. Dia, S. Liyanage, and S. A. Bagloee, “Applications of Artificial Intelligence in Transport: An Overview,” *Sustainability*, vol. 11, no. 1, Art. no. 1, Jan. 2019, doi: 10.3390/su11010189.

[22] M. Crenes and P. Criqui, “Between 10 and 20% of electricity consumption from the ICT* sector in 2030?”.

[23] T.-J. Yang, Y.-H. Chen, J. Emer, and V. Sze, “A method to estimate the energy consumption of deep neural networks,” in *2017 51st Asilomar Conference on Signals, Systems, and Computers*, Oct. 2017, pp. 1916–1920. doi: 10.1109/ACSSC.2017.8335698.

[24] I. Valov, R. Waser, J. R. Jameson, and M. N. Kozicki, “Electrochemical metallization memories—fundamentals, applications, prospects,” *Nanotechnology*, vol. 22, no. 25, p. 254003, May 2011, doi: 10.1088/0957-4484/22/25/254003.

[25] Y. Goldberg, “A Primer on Neural Network Models for Natural Language Processing,” *J. Artif. Intell. Res.*, vol. 57, pp. 345–420, Nov. 2016, doi: 10.1613/jair.4992.

[26] F. Zhao and Y. Zeng, “Dynamically Optimizing Network Structure Based on Synaptic Pruning in the Brain,” *Front. Syst. Neurosci.*, vol. 15, 2021, Accessed: Mar. 21, 2023. [Online]. Available: https://www.frontiersin.org/articles/10.3389/fnsys.2021.620558

[27] N. Kriegeskorte and T. Golan, “Neural network models and deep learning,” *Curr. Biol.*, vol. 29, no. 7, pp. R231–R236, Apr. 2019, doi: 10.1016/j.cub.2019.02.034.

[28] G. A. Carpenter, “Neural network models for pattern recognition and associative memory,” *Neural Netw.*, vol. 2, no. 4, pp. 243–257, Jan. 1989, doi: 10.1016/0893-6080(89)90035-X.

[29] R. Livni, S. Shalev-Shwartz, and O. Shamir, “On the Computational Efficiency of Training Neural Networks,” in *Advances in Neural Information Processing Systems*, 2014, vol. 27. Accessed: Mar. 21, 2023. [Online]. Available: https://proceedings.neurips.cc/paper/2014/hash/3a0772443a0739141292a5429b952fe6-Abstract.html

[30] X. Zou, S. Xu, X. Chen, L. Yan, and Y. Han, “Breaking the von Neumann bottleneck: architecture-level processing-in-memory technology,” *Sci. China Inf. Sci.*, vol. 64, no. 6, p. 160404, Apr. 2021, doi: 10.1007/s11432-020-3227-1.

[31] P. Yao *et al.*, “Fully hardware-implemented memristor convolutional neural network,” *Nature*, vol. 577, no. 7792, Art. no. 7792, Jan. 2020, doi: 10.1038/s41586-020-1942-4.

[32] H.-S. P. Wong and S. Salahuddin, “Memory leads the way to better computing,” *Nat. Nanotechnol.*, vol. 10, no. 3, Art. no. 3, Mar. 2015, doi: 10.1038/nnano.2015.29.

[33] D. Ielmini and H.-S. P. Wong, “In-memory computing with resistive switching devices,” *Nat. Electron.*, vol. 1, no. 6, Art. no. 6, Jun. 2018, doi: 10.1038/s41928-018-0092-2.

[34] H. Lin, C. Wang, Q. Hong, and Y. Sun, “A Multi-Stable Memristor and its Application in a Neural Network,” *IEEE Trans. Circuits Syst. II Express Briefs*, vol. 67, no. 12, pp. 3472–3476, Dec. 2020, doi: 10.1109/TCSII.2020.3000492.

[35] K.-U. Demasius, A. Kirschen, and S. Parkin, “Energy-efficient memcapacitor devices for neuromorphic computing,” *Nat. Electron.*, vol. 4, no. 10, Art. no. 10, Oct. 2021, doi: 10.1038/s41928-021-00649-y.

[36] S. P. Adhikari, C. Yang, H. Kim, and L. O. Chua, “Memristor Bridge Synapse-Based Neural Network and Its Learning,” *IEEE Trans. Neural Netw. Learn. Syst.*, vol. 23, no. 9, pp. 1426–1435, Sep. 2012, doi: 10.1109/TNNLS.2012.2204770.

[37] L. Chua, “Memristor-The missing circuit element,” *IEEE Trans. Circuit Theory*, vol. 18, no. 5, pp. 507–519, Sep. 1971, doi: 10.1109/TCT.1971.1083337.

[38] D. B. Strukov, G. S. Snider, D. R. Stewart, and R. S. Williams, “The missing memristor found,” *Nature*, vol. 453, no. 7191, pp. 80–83, May 2008, doi: 10.1038/nature06932.

[39] S. Mandal, J. Sinha, and A. Chakraborty, “Design of Memristor – CMOS based logic gates and logic circuits,” in *2019 2nd International Conference on Innovations in Electronics, Signal Processing and Communication (IESC)*, Mar. 2019, pp. 215–220. doi: 10.1109/IESPC.2019.8902355.

[40] “Mechanics of Materials: Bending – Normal Stress » Mechanics of Slender Structures | Boston University.” https://www.bu.edu/moss/mechanics-of-materials-bending-normal-stress/ (accessed Mar. 21, 2023).

[41] D. Baran, D. Corzo, and G. Blazquez, “Flexible Electronics: Status, Challenges and Opportunities,” *Front. Electron.*, vol. 1, 2020, Accessed: Mar. 15, 2023. [Online]. Available: https://www.frontiersin.org/articles/10.3389/felec.2020.594003

[42] J. A. Rogers, T. Someya, and Y. Huang, “Materials and Mechanics for Stretchable Electronics,” *Science*, vol. 327, no. 5973, pp. 1603–1607, Mar. 2010, doi: 10.1126/science.1182383.

[43] W. Lesslauer, J. Richter, and P. Läuger, “Some Electrical Properties of Bimolecular Phosphatidyl Inositol Membranes,” *Nature*, vol. 213, no. 5082, pp. 1224–1226, Mar. 1967, doi: 10.1038/2131224a0.

[44] F. C. Luo and W. A. Hester, “Design and fabrication of large-area thin-film transistor matrix circuits for flat-display panels,” *IEEE Trans. Electron Devices*, vol. 27, no. 1, pp. 223–230, Jan. 1980, doi: 10.1109/T-ED.1980.19844.

[45] R. Bao *et al.*, “Flexible and Controllable Piezo-Phototronic Pressure Mapping Sensor Matrix by ZnO NW/p-Polymer LED Array,” *Adv. Funct. Mater.*, vol. 25, no. 19, pp. 2884–2891, 2015, doi: 10.1002/adfm.201500801.

[46] C. Goßler *et al.*, “GaN-based micro-LED arrays on flexible substrates for optical cochlear implants,” *J. Phys. Appl. Phys.*, vol. 47, no. 20, p. 205401, Apr. 2014, doi: 10.1088/0022-3727/47/20/205401.

[47] D.-H. Kim, R. Ghaffari, N. Lu, and J. A. Rogers, “Flexible and Stretchable Electronics for Biointegrated Devices,” *Annu. Rev. Biomed. Eng.*, vol. 14, no. 1, pp. 113–128, 2012, doi: 10.1146/annurev-bioeng-071811-150018.

[48] N. Lu and D.-H. Kim, “Flexible and Stretchable Electronics Paving the Way for Soft Robotics,” *Soft Robot.*, vol. 1, no. 1, pp. 53–62, Mar. 2014, doi: 10.1089/soro.2013.0005.

[49] B. Sun *et al.*, “Recent advances in flexible and stretchable electronic devices via electrospinning,” *J. Mater. Chem. C*, vol. 2, no. 7, pp. 1209–1219, 2014, doi: 10.1039/C3TC31680G.

[50] K. Bock, “Polymer Electronics Systems - Polytronics,” *Proc. IEEE*, vol. 93, no. 8, pp. 1400–1406, Aug. 2005, doi: 10.1109/JPROC.2005.851513.

[51] N. Münzenrieder, L. Petti, C. Zysset, T. Kinkeldei, G. A. Salvatore, and G. Tröster, “Flexible Self-Aligned Amorphous InGaZnO Thin-Film Transistors With Submicrometer Channel Length and a Transit Frequency of 135 MHz,” *IEEE Trans. Electron Devices*, vol. 60, no. 9, pp. 2815–2820, Sep. 2013, doi: 10.1109/TED.2013.2274575.

[52] A. Nathan and B. R. Chalamala, “Special Issue on Flexible Electronics Technology, Part II: Materials and Devices,” *Proc. IEEE*, vol. 93, no. 8, pp. 1391–1393, Aug. 2005, doi: 10.1109/JPROC.2005.851509.

[53] C. B. Park, “Investigation of the electromechanical stability of low temperature polycrystalline silicon thin-film transistors governed by types of stress,” *Solid-State Electron.*, vol. 160, p. 107616, Oct. 2019, doi: 10.1016/j.sse.2019.05.012.

[54] K. Nomura, H. Ohta, K. Ueda, T. Kamiya, M. Hirano, and H. Hosono, “Thin-Film Transistor Fabricated in Single-Crystalline Transparent Oxide Semiconductor,” *Science*, vol. 300, no. 5623, pp. 1269–1272, May 2003, doi: 10.1126/science.1083212.

[55] K. Nomura, H. Ohta, A. Takagi, T. Kamiya, M. Hirano, and H. Hosono, “Room-temperature fabrication of transparent flexible thin-film transistors using amorphous oxide semiconductors,” *Nature*, vol. 432, no. 7016, Art. no. 7016, Nov. 2004, doi: 10.1038/nature03090.

[56] A. Nathan and B. R. Chalamala, “Special Issue on Flexible Electronics Technology, Part 1: Systems and Applications,” *Proc. IEEE*, vol. 93, no. 7, pp. 1235–1238, Jul. 2005, doi: 10.1109/JPROC.2005.851525.

[57] B. Li *et al.*, “Foldable Paper Electronics by Direct-Write Laser Patterning,” in *2017 19th International Conference on Solid-State Sensors, Actuators and Microsystems (transducers)*, New York, 2017, pp. 335–338. Accessed: Mar. 16, 2023. [Online]. Available: https://www.webofscience.com/wos/woscc/full-record/WOS:000426701400084

[58] M. F. El-Kady and R. B. Kaner, “Direct Laser Writing of Graphene Electronics,” *ACS Nano*, vol. 8, no. 9, pp. 8725–8729, Sep. 2014, doi: 10.1021/nn504946k.

[59] L. Hirt, A. Reiser, R. Spolenak, and T. Zambelli, “Additive Manufacturing of Metal Structures at the Micrometer Scale,” *Adv. Mater.*, vol. 29, no. 17, p. 1604211, May 2017, doi: 10.1002/adma.201604211.

[60] H. Naesstroem, F. Brueckner, J. Volpp, and A. Kaplan, “Laser metal deposition of copper on diverse metals using green laser sources,” *Int. J. Adv. Manuf. Technol.*, vol. 107, Mar. 2020, doi: 10.1007/s00170-020-05117-z.

[61] A. Piqué, N. A. Charipar, H. Kim, R. C. Y. Auyeung, and S. A. Mathews, “Applications of laser direct-write for embedding microelectronics,” in *Advanced Laser Technologies 2006*, Apr. 2007, vol. 6606, pp. 192–200. doi: 10.1117/12.729635.

[62] J. Liao, W. Guo, and P. Peng, “Direct laser writing of copper-graphene composites for flexible electronics,” *Opt. Lasers Eng.*, vol. 142, p. 106605, Jul. 2021, doi: 10.1016/j.optlaseng.2021.106605.

[63] R. B. M. Schasfoort, *Handbook of Surface Plasmon Resonance: 2nd Edition*. Royal Society of Chemistry, 2017.

[64] W. Hou and S. B. Cronin, “A Review of Surface Plasmon Resonance-Enhanced Photocatalysis,” *Adv. Funct. Mater.*, vol. 23, no. 13, pp. 1612–1619, 2013, doi: 10.1002/adfm.201202148.

[65] P. Peng *et al.*, “One-step selective laser patterning of copper/graphene flexible electrodes,” *Nanotechnology*, vol. 30, no. 18, p. 185301, May 2019, doi: 10.1088/1361-6528/aafe4c.

[66] H. Lee and M. Yang, “Effect of solvent and PVP on electrode conductivity in laser-induced reduction process,” *Appl. Phys. A*, vol. 119, no. 1, pp. 317–323, Apr. 2015, doi: 10.1007/s00339-014-8970-6.

[67] Y. Xiong, I. Washio, J. Chen, H. Cai, Z.-Y. Li, and Y. Xia, “Poly(vinyl pyrrolidone): A Dual Functional Reductant and Stabilizer for the Facile Synthesis of Noble Metal Nanoplates in Aqueous Solutions,” *Langmuir*, vol. 22, no. 20, pp. 8563–8570, Sep. 2006, doi: 10.1021/la061323x.

[68] A. Shishov, D. Gordeychuk, L. Logunov, and I. Tumkin, “High rate laser deposition of conductive copper microstructures from deep eutectic solvents,” *Chem. Commun.*, vol. 55, no. 65, pp. 9626–9628, Aug. 2019, doi: 10.1039/C9CC05184H.

[69] X. Zhou, W. Guo, and P. Peng, “Laser Erasing and Rewriting of Flexible Copper Circuits,” *Nano-Micro Lett.*, vol. 13, no. 1, p. 184, Dec. 2021, doi: 10.1007/s40820-021-00714-3.

[70] W. Zhou, Y. Yu, S. Bai, and A. Hu, “Laser direct writing of waterproof sensors inside flexible substrates for wearable electronics,” *Opt. Laser Technol.*, vol. 135, p. 106694, Mar. 2021, doi: 10.1016/j.optlastec.2020.106694.

[71] X. Zhou, W. Guo, Y. Zhu, and P. Peng, “The laser writing of highly conductive and anti-oxidative copper structures in liquid,” *Nanoscale*, vol. 12, no. 2, pp. 563–571, 2020, doi: 10.1039/C9NR07248A.

[72] X. Zhou, W. Guo, J. Fu, Y. Zhu, Y. Huang, and P. Peng, “Laser writing of Cu/Cu O integrated structure on flexible substrate for humidity sensing,” *Appl. Surf. Sci.*, vol. 494, pp. 684–690, Nov. 2019, doi: 10.1016/j.apsusc.2019.07.159.

[73] X. Zhou, W. Guo, Y. Yao, R. Peng, and P. Peng, “Flexible Nonenzymatic Glucose Sensing with One-Step Laser-Fabricated Cu2O/Cu Porous Structure,” *Adv. Eng. Mater.*, vol. 23, no. 6, p. 2100192, 2021, doi: 10.1002/adem.202100192.

[74] H. Liu, “Laser assisted ink-printing of copper oxide nanoplates for memory device,” *Mater. Lett.*, pp. 127097–127101, 2020.

[75] E. A. Avilova *et al.*, “Direct Laser Writing of Copper Micropatterns from Deep Eutectic Solvents Using Pulsed near-IR Radiation,” *Nanomaterials*, vol. 12, no. 7, Art. no. 7, Jan. 2022, doi: 10.3390/nano12071127.

[76] Y. Yao, W. Guo, Z. Hui, C. Jin, and P. Peng, “Laser Fabricated Cu2O-CuO/Ag Nanocomposite Films for SERS Application**,” *ChemistrySelect*, vol. 7, no. 6, p. e202104357, 2022, doi: 10.1002/slct.202104357.

[77] A. Piqué, S. A. Mathews, B. Pratap, R. C. Y. Auyeung, B. J. Karns, and S. Lakeou, “Embedding electronic circuits by laser direct-write,” *Microelectron. Eng.*, vol. 83, no. 11, pp. 2527–2533, Nov. 2006, doi: 10.1016/j.mee.2006.06.004.

[78] L. Chua, “If it’s pinched it’s a memristor,” *Semicond. Sci. Technol.*, vol. 29, no. 10, p. 104001, Oct. 2014, doi: 10.1088/0268-1242/29/10/104001.

[79] H. Kim, M. R. Mahmoodi, H. Nili, and D. B. Strukov, “4K-memristor analog-grade passive crossbar circuit,” *Nat. Commun.*, vol. 12, no. 1, p. 5198, Dec. 2021, doi: 10.1038/s41467-021-25455-0.

[80] E. Carlos, R. Branquinho, R. Martins, A. Kiazadeh, and E. Fortunato, “Recent Progress in Solution-Based Metal Oxide Resistive Switching Devices,” *Adv. Mater.*, vol. 33, no. 7, p. 2004328, 2021, doi: 10.1002/adma.202004328.

[81] K. Park and J.-S. Lee, “Flexible resistive switching memory with a Ni/CuO_x/Ni structure using an electrochemical deposition process,” *Nanotechnology*, vol. 27, no. 12, p. 125203, Mar. 2016, doi: 10.1088/0957-4484/27/12/125203.

[82] M. B. González *et al.*, “Chapter 19 - Synaptic devices based on HfO2 memristors,” in *Mem-elements for Neuromorphic Circuits with Artificial Intelligence Applications*, C. Volos and V.-T. Pham, Eds. Academic Press, 2021, pp. 383–426. doi: 10.1016/B978-0-12-821184-7.00028-1.

[83] F. Chen *et al.*, “Recent progress in artificial synaptic devices: materials, processing and applications,” *J. Mater. Chem. C*, vol. 9, no. 27, pp. 8372–8394, Jul. 2021, doi: 10.1039/D1TC01211H.

[84] H. Lv *et al.*, “Evolution of conductive filament and its impact on reliability issues in oxide-electrolyte based resistive random access memory,” *Sci. Rep.*, vol. 5, no. 1, Art. no. 1, Jan. 2015, doi: 10.1038/srep07764.

[85] G. Bersuker *et al.*, “Metal oxide resistive memory switching mechanism based on conductive filament properties,” *J. Appl. Phys.*, vol. 110, no. 12, p. 124518, Dec. 2011, doi: 10.1063/1.3671565.

[86] X. Wang and Y. Chen, “Spintronic memristor devices and application,” in *2010 Design, Automation & Test in Europe Conference & Exhibition (DATE 2010)*, Mar. 2010, pp. 667–672. doi: 10.1109/DATE.2010.5457118.

[87] L. L. Wei, D. S. Shang, J. R. Sun, S. B. Lee, Z. G. Sun, and B. G. Shen, “Gradual electroforming and memristive switching in Pt/CuO $_x$ /Si/Pt systems,” *Nanotechnology*, vol. 24, no. 32, p. 325202, Aug. 2013, doi: 10.1088/0957-4484/24/32/325202.

[88] L. Yin *et al.*, “Two-Dimensional Unipolar Memristors with Logic and Memory Functions,” *Nano Lett.*, vol. 20, no. 6, pp. 4144–4152, Jun. 2020, doi: 10.1021/acs.nanolett.0c00002.

[89] G. Zhou, Z. Ren, L. Wang, B. Sun, S. Duan, and Q. Song, “Artificial and wearable albumen protein memristor arrays with integrated memory logic gate functionality,” *Mater. Horiz.*, vol. 6, no. 9, pp. 1877–1882, 2019, doi: 10.1039/C9MH00468H.

[90] K. Zhang, Y. Ren, P. Ganesh, and Y. Cao, “Effect of electrode and oxide properties on the filament kinetics during electroforming in metal-oxide-based memories,” *Npj Comput. Mater.*, vol. 8, no. 1, Art. no. 1, Apr. 2022, doi: 10.1038/s41524-022-00770-2.

[91] C. Nail *et al.*, “Atomistic mechanisms of copper filament formation and composition in Al $_2$ O $_3$ -based conductive bridge random access memory,” *J. Appl. Phys.*, vol. 122, no. 2, p. 024503, Jul. 2017, doi: 10.1063/1.4990979.

[92] N. Xu *et al.*, “Bipolar switching behavior in TiN/ZnO/Pt resistive nonvolatile memory with fast switching and long retention,” *Semicond. Sci. Technol.*, vol. 23, no. 7, p. 075019, May 2008, doi: 10.1088/0268-1242/23/7/075019.

[93] F. Nardi, S. Larentis, S. Balatti, D. C. Gilmer, and D. Ielmini, “Resistive Switching by Voltage-Driven Ion Migration in Bipolar RRAM—Part I: Experimental Study,” *IEEE Trans. Electron Devices*, vol. 59, no. 9, pp. 2461–2467, Sep. 2012, doi: 10.1109/TED.2012.2202319.

[94] S. Larentis, F. Nardi, S. Balatti, D. C. Gilmer, and D. Ielmini, “Resistive Switching by Voltage-Driven Ion Migration in Bipolar RRAM—Part II: Modeling,” *IEEE Trans. Electron Devices*, vol. 59, no. 9, pp. 2468–2475, Sep. 2012, doi: 10.1109/TED.2012.2202320.

[95] S. Kvatinsky, E. G. Friedman, A. Kolodny, and U. C. Weiser, “TEAM: ThrEshold Adaptive Memristor Model,” *IEEE Trans. Circuits Syst. Regul. Pap.*, vol. 60, no. 1, pp. 211–221, Jan. 2013, doi: 10.1109/TCSI.2012.2215714.

[96] K. Fujiwara, T. Nemoto, M. J. Rozenberg, Y. Nakamura, and H. Takagi, “Resistance Switching and Formation of a Conductive Bridge in Metal/Binary Oxide/Metal Structure for Memory Devices,” *Jpn. J. Appl. Phys.*, vol. 47, no. 8, pp. 6266–6271, Aug. 2008, doi: 10.1143/JJAP.47.6266.

[97] D. Ielmini, “Modeling the Universal Set/Reset Characteristics of Bipolar RRAM by Field- and Temperature-Driven Filament Growth,” *IEEE Trans. Electron Devices*, vol. 58, no. 12, pp. 4309–4317, Dec. 2011, doi: 10.1109/TED.2011.2167513.

[98] Y. Yang, P. Gao, S. Gaba, T. Chang, X. Pan, and W. Lu, “Observation of conducting filament growth in nanoscale resistive memories,” *Nat. Commun.*, vol. 3, no. 1, p. 732, Jan. 2012, doi: 10.1038/ncomms1737.

[99] M. Arita, A. Takahashi, Y. Ohno, A. Nakane, A. Tsurumaki-Fukuchi, and Y. Takahashi, “Switching operation and degradation of resistive random access memory composed of tungsten oxide and copper investigated using in-situ TEM,” *Sci. Rep.*, vol. 5, no. 1, p. 17103, Dec. 2015, doi: 10.1038/srep17103.

[100] G. Bersuker *et al.*, “Metal oxide RRAM switching mechanism based on conductive filament microscopic properties,” in *2010 International Electron Devices Meeting*, Dec. 2010, p. 19.6.1-19.6.4. doi: 10.1109/IEDM.2010.5703394.

[101] T.-N. Fang *et al.*, “Erase mechanism for copper oxide resistive switching memory cells with nickel electrode,” in *2006 International Electron Devices Meeting*, Dec. 2006, pp. 1–4. doi: 10.1109/IEDM.2006.346731.

[102] D. Ielmini, “Resistive switching memories based on metal oxides: Mechanisms, reliability and scaling,” *Semicond. Sci. Technol.*, vol. 31, p. 063002, Jun. 2016, doi: 10.1088/0268-1242/31/6/063002.

[103] A. Sawa, “Resistive switching in transition metal oxides,” *Mater. Today*, vol. 11, no. 6, pp. 28–36, Jun. 2008, doi: 10.1016/S1369-7021(08)70119-6.

[104] A. Sawa, “Resistive Switching in Transition Metal Oxides,” *Mater. Today*, vol. 11, pp. 28–36, Jun. 2008, doi: 10.1016/S1369-7021(08)70119-6.

[105] C.-C. Hsu, Y.-S. Lin, C.-W. Cheng, and W.-C. Jhang, “Annealing Effect on the Performance of Copper Oxide Resistive Memory Devices,” *IEEE Trans. Electron Devices*, vol. 67, no. 3, pp. 976–983, Mar. 2020, doi: 10.1109/TED.2020.2968846.

[106] S. Zou, P. Xu, and M. C. Hamilton, “Resistive switching characteristics in printed Cu/CuO/(AgO)/Ag memristors,” *Electron. Lett.*, vol. 49, no. 13, pp. 829–830, Jun. 2013, doi: 10.1049/el.2013.1302.

[107] T. Shi, R. Wang, Z. Wu, Y. Sun, J. An, and Q. Liu, “A Review of Resistive Switching Devices: Performance Improvement, Characterization, and Applications,” *Small Struct.*, vol. 2, no. 4, p. 2000109, 2021, doi: 10.1002/sstr.202000109.

[108] Y. Crama and P. L. Hammer, *Boolean Functions: Theory, Algorithms, and Applications*. Cambridge University Press, 2011.

[109] R. O’Donnell, *Analysis of Boolean Functions*. Cambridge University Press, 2014.

[110] “The complexity of Boolean functions,” *Guide books*. https://dl.acm.org/doi/abs/10.5555/35517 (accessed Mar. 21, 2023).

[111] E. J. McCluskey, “Minimization of Boolean functions,” *Bell Syst. Tech. J.*, vol. 35, no. 6, pp. 1417–1444, Nov. 1956, doi: 10.1002/j.1538-7305.1956.tb03835.x.

[112] G. Papandroulidakis, A. Serb, A. Khiat, G. V. Merrett, and T. Prodromakis, “Practical Implementation of Memristor-Based Threshold Logic Gates,” *IEEE Trans. Circuits Syst. Regul. Pap.*, vol. 66, no. 8, pp. 3041–3051, Aug. 2019, doi: 10.1109/TCSI.2019.2902475.

[113] K. A. Ali, M. Rizk, A. Baghdadi, J.-P. Diguet, and J. Jomaah, “Hybrid Memristor–CMOS Implementation of Combinational Logic Based on X-MRL,” *Electronics*, vol. 10, no. 9, p. 1018, Apr. 2021, doi: 10.3390/electronics10091018.

[114] B. Gao *et al.*, “Memristor-based analogue computing for brain-inspired sound localization with in situ training,” *Nat. Commun.*, vol. 13, no. 1, p. 2026, Dec. 2022, doi: 10.1038/s41467-022-29712-8.

[115] L. Shi, G. Zheng, B. Tian, B. Dkhil, and C. Duan, “Research progress on solutions to the sneak path issue in memristor crossbar arrays,” *Nanoscale Adv.*, vol. 2, no. 5, pp. 1811–1827, 2020, doi: 10.1039/D0NA00100G.

[116] H. Li *et al.*, “Memristive Crossbar Arrays for Storage and Computing Applications,” *Adv. Intell. Syst.*, vol. 3, no. 9, p. 2100017, 2021, doi: 10.1002/aisy.202100017.

[117] A. Chen, “A Comprehensive Crossbar Array Model With Solutions for Line Resistance and Nonlinear Device Characteristics,” *IEEE Trans. Electron Devices*, vol. 60, no. 4, pp. 1318–1326, Apr. 2013, doi: 10.1109/TED.2013.2246791.

[118] J.-J. Huang, Y.-M. Tseng, W.-C. Luo, C.-W. Hsu, and T.-H. Hou, “One selector-one resistor (1S1R) crossbar array for high-density flexible memory applications,” in *2011 International Electron Devices Meeting*, Dec. 2011, p. 31.7.1-31.7.4. doi: 10.1109/IEDM.2011.6131653.

[119] S. Rehman, J.-H. Hur, and D. Kim, “Resistive Switching in Solution-Processed Copper Oxide (Cu $_x$ O) by Stoichiometry Tuning,” *J. Phys. Chem. C*, vol. 122, no. 20, pp. 11076–11085, May 2018, doi: 10.1021/acs.jpcc.8b00432.

[120] B. Fuchs, H.-P. Berlien, C. M. Philipp, and G. Müller, “Fundamentals of Nd:YAG Laser Applications,” in *Applied Laser Medicine*, H.-P. Berlien and G. J. Müller, Eds. Berlin, Heidelberg: Springer, 2003, pp. 199–203. doi: 10.1007/978-3-642-18979-1_6.

[121] J. Kwon *et al.*, “Flexible and Transparent Cu Electronics by Low-Temperature Acid-Assisted Laser Processing of Cu Nanoparticles,” *Adv. Mater. Technol.*, vol. 2, no. 2, p. 1600222, 2017, doi: 10.1002/admt.201600222.

[122] C. Chen *et al.*, “Size Distribution Control of Copper Nanoparticles and Oxides: Effect of Wet-Chemical Redox Cycling,” *Inorg. Chem.*, vol. 58, no. 4, pp. 2533–2542, Feb. 2019, doi: 10.1021/acs.inorgchem.8b03125.

[123] D. D. Ebbing and M. S. Wrighton, *General chemistry*. Boston: Houghton Mifflin Company Boston, Walter Lorraine Books, 1990.

[124] G. Katumba, B. Mwakikunga, and T. Mothibinyane, “FTIR and Raman Spectroscopy of Carbon Nanoparticles in SiO2, ZnO and NiO Matrices,” *Nanoscale Res. Lett.*, vol. 3, no. 11, p. 421, Nov. 2008, doi: 10.1007/s11671-008-9172-y.

[125] Puech *et al.*, “Analyzing the Raman Spectra of Graphenic Carbon Materials from Kerogens to Nanotubes: What Type of Information Can Be Extracted from Defect Bands?,” *C — J. Carbon Res.*, vol. 5, no. 4, p. 69, Nov. 2019, doi: 10.3390/c5040069.

[126] J. Bang, Y. Jung, H. Kim, D. Kim, M. Cho, and S. H. Ko, “Multi-Bandgap Monolithic Metal Nanowire Percolation Network Sensor Integration by Reversible Selective Laser-Induced Redox,” *Nano-Micro Lett.*, vol. 14, no. 1, p. 49, Dec. 2022, doi: 10.1007/s40820-021-00786-1.

[127] W. Jia, E. Reitz, H. Sun, B. Li, H. Zhang, and Y. Lei, “From Cu2(OH)3Cl to nanostructured sisal-like Cu(OH)2 and CuO: Synthesis and characterization,” *J. Appl. Phys.*, vol. 105, no. 6, p. 064917, Mar. 2009, doi: 10.1063/1.3097286.

[128] T. Öhlund, A. K. Schuppert, M. Hummelgård, J. Bäckström, H.-E. Nilsson, and H. Olin, “Inkjet Fabrication of Copper Patterns for Flexible Electronics: Using Paper with Active Precoatings,” *ACS Appl. Mater. Interfaces*, vol. 7, no. 33, pp. 18273–18282, Aug. 2015, doi: 10.1021/acsami.5b03061.

[129] PubChem, “Isopropyl Alcohol.” https://pubchem.ncbi.nlm.nih.gov/compound/3776 (accessed Mar. 21, 2023).

[130] PubChem, “Cupric nitrate.” https://pubchem.ncbi.nlm.nih.gov/compound/18616 (accessed Jul. 27, 2022).

[131] R. A. Rapp and F. Maak, “Thermodynamic properties of solid copper-nickel alloys,” *Acta Metall.*, vol. 10, no. 1, pp. 63–69, Jan. 1962, doi: 10.1016/0001-6160(62)90187-6.

[132] A. Khort, V. Romanovski, D. Leybo, and D. Moskovskikh, “CO oxidation and organic dyes degradation over graphene-Cu and graphene-CuNi catalysts obtained by solution combustion synthesis,” *Sci. Rep.*, vol. 10, p. 16104, Sep. 2020, doi: 10.1038/s41598-020-72872-0.

[133] D. Perello *et al.*, “Quantitative Experimental Analysis of Schottky Barriers and Poole–Frenkel Emission in Carbon Nanotube Devices,” *Nanotechnol. IEEE Trans. On*, vol. 8, pp. 355–360, Jun. 2009, doi: 10.1109/TNANO.2008.2008804.

[134] M. Winning, G. Gottstein, and L. S. Shvindlerman, “On the mechanisms of grain boundary migration,” *Acta Mater.*, vol. 50, no. 2, pp. 353–363, Jan. 2002, doi: 10.1016/S1359-6454(01)00343-3.